CATÓLICA
ESCOLA SUPERIOR DE BIOTECNOLOGIA
PORTO

FETALIX *IN VIVO* VALIDATION AND PROCESS SCALABILITY

by

Maria Leonor Lopes Leite Moreira de Sousa

(September, 2024)

CATÓLICA
ESCOLA SUPERIOR DE BIOTECNOLOGIA
PORTO

FETALIX *IN VIVO* VALIDATION AND PROCESS SCALABILITY

Thesis presented to Escola Superior de Biotecnologia of the Universidade Católica Portuguesa to fulfill the requirements of Master of Science degree in Biomedical Engineering

by

Maria Leonor Lopes Leite Moreira de Sousa

Supervisor: Joana Caldeira

Co-Supervisors: Raquel Gonçalves and Morena Fiordalisi

Tutor (University): Ana Leite de Oliveira

(September, 2024)

Dedico esta tese à minha bisavó São, Avó Nanda e Avô Zeca por todo o amor, dedicação e darem a sua vida para criar os três (bis)netos. São pilares essenciais na minha vida.

Resumo

A dor lombar (DL) é uma patologia musculoesquelética que afeta 80% da população. É causada, principalmente, pela degeneração do disco intervertebral (DIV), essencial para a mobilidade da coluna vertebral. Visto que as atuais terapias não proporcionam soluções a longo prazo, é urgente desenvolver novos tratamentos para restaurar um tecido funcional.

Previamente, o grupo mostrou que o núcleo pulposo (NP) fetal bovino, parte central do DIV, é rico em colagénio XII e XIV, duas proteínas pró-regenerativas que desaparecem com a idade. Além disso, NPs fetais descelularizados, co-cultivados com células de NP bovino, exibiram elevados níveis de agrecano e colagénio II e diminuíram a formação de novos vasos. Deste trabalho surgiu o Fetalix - o primeiro biomaterial de origem fetal para tratar a DL.

Esta tese pretendeu aferir o potencial do Fetalix *in vivo* por ressonância magnética (RM), histologia e análise comportamental, otimizar a produção escalonável e a injetabilidade.

Modificações nos protocolos de descelularização permitiram reduzir entre 6 e 8% a sua duração e aumentar a capacidade de processamento. Contudo, é necessário otimizá-los para obter uma redução de DNA dupla-hélice <50ng por mg de peso seco de matrix extracelular. Observou-se também uma redução expectável de glicosaminoglicanos. Quanto à produção e caraterização das partículas, o 4-Place Mini Bead Mill homogeniser foi escolhido por produzir partículas mais pequenas e porosas. Foram necessários 50 ciclos para obter uma solução injetável através de uma seringa de 30 G. O ensaio de injetabilidade revelou picos e forças médias de 200 g, indicando soluções facilmente injetáveis. O estudo *in vivo* mostrou concordância entre os resultados de RM (obtidos pelo algoritmo desenvolvido) e de histologia, à exceção do volume das hérnias. A administração de Fetalix induziu diminuição na altura, volume e brilho do DIV, em comparação com os outros grupos. Além disso, 2 de 3 animais exibiram volumes de hérnia e índices de degeneração mais elevados, exceto um animal que não apresentou hérnias. No teste de Von Frey, o grupo Fetalix apresentou uma sensibilidade semelhante ao naïve e reduzida em relação a animais lesionados, o que sugere que, contudo, estes foram capazes de recuperar a sua sensibilidade.

Em geral, os resultados mostraram que foi possível produzir o Fetalix como solução injetável. O estudo *in vivo* demonstrou que, apesar de não regenerar o DIV, a sua administração permitiu recuperar a sensibilidade para níveis semelhantes aos naïve.

Palavras-chave: Disco intervertebral, dor lombar, escalabilidade, estudo *in vivo*, Fetalix.

Abstract

Low back pain (LBP) is a musculoskeletal condition that affects over 80% of the population. It is mainly caused by degeneration of the intervertebral disc (IVD), a core element for spinal mobility. As current therapies do not provide long-term solutions, there is an urgent need to develop novel treatments to restore a functional tissue.

Our group has previously showed that fetal bovine nucleus pulposus (NP), the central part of the IVD, is enriched with collagen XII and XIV, two pro-regenerative proteins that disappear with age. Moreover, fetal decellularized NPs co-cultured with bovine NP cells, expressed higher levels of aggrecan and collagen II and reduced neovessel formation. From this work resulted Fetalix – the first fetal-inspired biomaterial to treat LBP.

Thus, the goal of this thesis was to assess Fetalix potential *in vivo* through magnetic resonance imaging (MRI), histology and behavioural assessment, while optimizing its scalable production and injectability.

Modified decellularization protocols enabled 6-8% time reduction and enabled an increase in processing capacity. However, further optimization is required to achieve a double-strand DNA reduction of <50ng per mg of extracellular matrix dry weight. As expected, glycosaminoglycans content was reduced. Regarding biomaterial's production and particle characterization, the 4-Place Mini Bead Mill homogeniser enabled the production of smaller and more porous particles, being selected for Fetalix production. 50 milling cycles were required to achieve an injectable solution. An injectability assay revealed peak and average forces around 200g, indicating easily injectable solutions. The *in vivo* study revealed that MRI (obtained through a developed algorithm) and histology results were consistent, expect hernias volume quantification. Fetalix administration induced decrease in IVD height, volume and brightness. Moreover, 2 out of 3 animals presented higher hernia volumes and degeneration scores, except one that did not have hernias. Von Frey test revealed that Fetalix group presented sensitivity similar to naïve and decreased compared to lesioned animals, suggesting that these animals were able to restore their sensitivity.

Overall, these results showed that it was possible to produce Fetalix as an injectable solution. The *in vivo* analysis demonstrated that, despite not regenerating the IVD, biomaterial's administration enabled sensitivity restoration to naïve levels.

Keywords: Fetalix, *in vivo* study, intervertebral disc, low back pain, scalability.

Agradecimentos

Esta dissertação é o resultado de cinco anos de muita aprendizagem, dedicação e crescimento profissional e pessoal. Ao longo deste percurso, tive o apoio de inúmeras pessoas que me marcam com a sua força e inspiração, às quais pretendo expressar o meu profundo agradecimento.

Gostaria de começar por agradecer à minha orientadora, Joana Caldeira, pela oportunidade de integrar a sua equipa, inicialmente para um estágio de verão, que se estendeu para a minha dissertação de mestrado. Sem dúvida que todo o seu apoio durante o último ano foi fulcral para o culminar deste trabalho. Agradeço, do fundo do coração, todo o carinho, aprendizagem, palavras de encorajamento e oportunidades. Gostaria, também, de agradecer às minhas co-orientadoras, Raquel Gonçalves e Morena Fiordalisi, por toda a ajuda, disponibilidade e carinho. Guardo todas as palavras de força e motivação que me deram. Morena, I know you understand Portuguese, but I just wanted to give you a special thank you in English. I won't forget all the hours we spent dissecting bovine tails together.

Um especial agradecimento a todos os elementos do grupo Biofabrication por me acolherem tão bem. Toda a vossa ajuda foi essencial para a realização desta dissertação, desde pequenas ajudas no laboratório a uma palavra amiga. Em particular, gostaria de agradecer ao Professor Pedro Granja por me receber no grupo e por toda a disponibilidade.

Gostaria de agradecer a todos aqueles que contribuíram, de alguma forma, para a realização deste trabalho, em particular, à Carla Cunha, ao Rui Simões, à Joana Paes de Faria e à Vânia Veloso.

Agradeço a todos os elementos do laboratório de Biomateriais do CBQF-ESB por me receberem tão bem nas suas instalações e por toda a ajuda prestada, em especial à Professora Ana Leite pela oportunidade e acesso a diversos equipamentos no decorrer deste projeto. Gostaria, também, de agradecer ao Professor João Costa, por todo o apoio e motivação, e à Inês Vasconcelos, por todo o carinho com que me recebeu e ajudou a realizar alguns ensaios.

A todos os meus amigos, um agradecimento do fundo do meu coração. Esta jornada não seria a mesma sem vocês do meu lado, sem todas as gargalhadas e lágrimas que passámos juntos.

Ao Rui, por me encorajar a embarcar nesta jornada sem nunca duvidar de que eu era capaz, quando eu própria duvidava. Não há palavras que descrevam todo o amor, companheirismo, força e entreajuda. Obrigada por puxares sempre o melhor de mim.

Por fim, agradeço do fundo do meu coração à minha família, por estarem sempre do meu lado e por todo o apoio incondicional ao longo destes 23 anos. Sei que sentem este marco como a vossa própria conquista.

Aos meus avós e bisavó, por todo o amor e valores que me transmitiram. Estiveram sempre do meu lado, em todas as etapas, a apoiar-me com orgulho. São grandes exemplos de força e resiliência para mim.

Por fim, aos meus pais e irmão, sem vocês do meu lado nada disto teria sido possível. Viveram comigo intensamente estes cinco anos e sei que as minhas alegrias e frustrações foram as vossas também. Agradeço todo o vosso amor, força, por me obrigarem a levantar a cabeça e enfrentar as adversidades. Esta conquista é reflexo dos valores que me transmitiram e de todo o vosso apoio. Obrigada por me darem todas as ferramentas necessárias para seguir os meus sonhos.

Para finalizar, tal como diria a avó São, “tudo valeu a pena”.

Contents

Table of figures

Table of abbreviations

AB	Alcian Blue
AB/PSR	Alcian blue/Picrosirius red
ADAMTS	A disintegrin and metalloproteinase with thrombospondin motifs
AF	Annulus fibrosus
CAM	Chorioallantoic membrane
CD	Chondrodystrophic
CEPs	Cartilaginous endplates
ChABC	Chondroitinase ABC
Co	Coccygeal
DAPI	4',6-diamidino-2-phenylindole
dECM	Decellularized extracellular matrix
DHI	Disc height index
DNA	Deoxyribonucleic acid
dNPs	Decellularized nucleus pulposus
ECM	Extracellular matrix
e.g.	For example
GAGs	Glycosaminoglycans
H&E	Hematoxylin and eosin
i.e.	That is
IL	Interleukin
IVD	Intervertebral disc
LBP	Low back pain
MMP	Matrix metalloproteinase
MRI	Magnetic resonance imaging
MSCs	Mesenchymal stem cells
NCD	Nonchondrodystrophic
NP	Nucleus pulposus
OCT	Optimal cutting temperature compound
PBS	Phosphate buffered saline
PEG	Polyethylene glycol
PGs	Proteoglycans
P/S	Penicillin/Streptomycin

PSR	Picrosirius red
RNA	Ribonucleic acid
RT	Room temperature
SD	Standard deviation
SDS	Sodium dodecyl sulfate
SEM	Scanning electron microscope
sGAGs	Sulfated glycosaminoglycans
SPARC	Secreted protein, acidic, rich in cysteine
TPU	Thermoplastic polyurethane
TRLs	Technology readiness levels
VEGF	Vascular endothelial growth factor
TIMP	Tissue inhibitors of metalloproteinase
TNF	Tumor necrosis factor
YLD	Years lived with disability

Chapter I - Introduction

1. Intervertebral disc: an overview

1.1. A healthy intervertebral disc

The intervertebral disc (IVD) is a soft tissue surrounded by the vertebral bodies. It enables spine movement, protects the spinal cord and nerve roots, and promotes load absorption (Shapiro et al., 2014). It is divided in three different regions, as shown in Figure 1.1: the nucleus pulposus (NP) – an inner soft and hydrated structure, the annulus fibrosus (AF) – a fibrocartilaginous tissue that surrounds the NP and the cartilaginous endplates (CEPs) – that cover the NP and AF superiorly and inferiorly (Shapiro et al., 2014; Bibby et al., 2001).

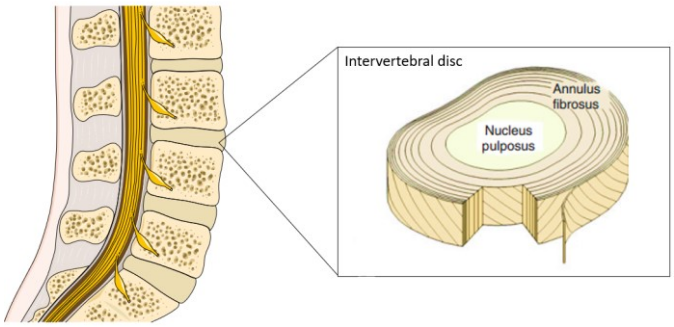

Figure 1.1 – The intervertebral disc. The NP is the inner part of the IVD, surrounded by a well-organized structure called AF. Adapted from (Shapiro et al., 2014).

1.1.1. Nucleus Pulposus

The NP is the central region of the IVD and it derives from the notochord (Taylor, 1975). During embryonic development, this tissue is enriched with notochordal cells. After birth, the number of cells decreases and, in adulthood, this tissue becomes mostly acellular (Shapiro et al., 2014; Taylor, 1975). It is acknowledged that notochordal cells play an essential role in maintaining IVD integrity (Erwin et al., 2011). In fact, species that do not present notochordal cells in adulthood (e.g humans) suffer with degeneration earlier in life (Bergknut et al., 2012). Nevertheless, adult NPs still contain chondrocyte-like cells (Errington et al., 1998).

This structure is mainly composed of water (Antoniou et al., 1996), proteoglycans (PGs) (Iatridis et al., 2007) and collagen type II (Antoniou et al., 1996). PGs are important and unique glycoproteins, whose core protein is covalently bound to sulphated glycosaminoglycans (GAGs) chains. The predominant PG in the NP is aggrecan, composed by chondroitin sulfate and keratan sulfate GAG chains (Silagi et al., 2018). This molecule has a major role in IVD

biomechanics considering that it provides the capacity to resist compressive loading (Shapiro et al., 2014).

The high aggrecan content in this structure results in cations' accumulation inside the NP, leading to a high osmotic pressure (Urban et al., 1981). This pressure is responsible for the NP's mechanical properties, crucial to force transmission, tissue stability and hydration (Shapiro et al., 2014).

1.1.2. Annulus fibrosus

The AF is a highly fibrous structure made up of 15-25 concentric layers, called lamellae, which enclose the NP (Inoue et al., 1975). Structurally, it can be divided in two regions: a central fibrocartilaginous region (inner AF) and a peripheral fibrous region (outer AF) (Tomaszewski et al., 2015).

The central region is rich in collagen type I and II (Eyre et al., 1976), PGs (Buckwalter, 1995) and water (Antoniou et al., 1996). It presents circular-shaped cells, morphologically similar to chondrocytes (Errington et al., 1998).

The peripheral region is enriched in collagen type I, that forms the lamellae, a well-organized structure (Eyre et al., 1976). Moreover, it presents elongated cells aligned with the tissue fibers (Errington et al., 1998) and lower water content, in comparison to the inner AF (Oshima et al., 1993).

Given the higher concentration of collagen (Singh et al., 2009), the AF presents higher tensile loading capacity, resulting in greater capacity to be stretched (Shapiro et al., 2014). In fact, the IVD's biochemical differences found along its structures (see Figure 1.2) (Bibby et al., 2001) have a major impact on tissue biomechanics (Singh et al., 2009).

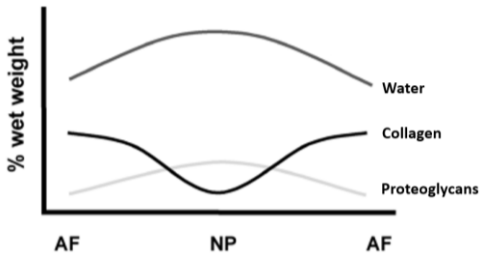

Figure 1.2 – Water and extracellular matrix content according to an IVD cross-section. The NP is a highly hydrated structure enriched in PGs, whereas the AF is a well-organized structure with superior collagen content. Adapted from (Bibby et al., 2001).

1.1.3. Cartilaginous endplates

The CEPs are hyaline cartilage structures (Roberts et al., 1989) that cover the NP and AF superiorly and inferiorly, providing an interface between the IVD and the bone (Tomaszewski et al., 2015). They have a crucial biomechanical role, by preventing the IVD from directly applying pressure into the bone (Shapiro et al., 2014). Chondrocytes found in these structures are key players, as they produce a matrix rich in collagen type II and PGs (Roberts et al., 1989). Moreover, this structure is crucial for nutrients diffusion, since the supply process is performed from the vertebrae to the CEPs, until it reaches the tissue's extracellular matrix (ECM) (Holm et al., 1981; Roberts et al., 1989; Urban et al., 2004).

1.1.4. IVD environment

Under normal physiological conditions, the IVD is predominantly avascular (Nerlich et al., 2007) and aneural (Bogduk et al., 1981), since blood vessels and nerves are only present in the peripheral part of the AF. Moreover, nutritive supply is scarce (Holm et al., 1981; Roberts et al., 1989; Urban et al., 2004).

As so, the IVD environment is considered harsh, given low oxygen, nutrients and pH. The latter is caused by lactic acid accumulation (Holm et al., 1981; Urban et al., 2004). However, during ageing, this tissue undergoes severe alterations becoming an even more hostile environment (Vo et al., 2016).

1.2 An aged and degenerated IVD

Ageing is a natural process in which cells and, consequently, their ECM undergoes several modifications. In the IVD, ageing involves alterations in cell morphology, density, and phenotype, as well as triggering cell death (Zhao et al., 2007). Consequently, ECM suffers structural and biochemical changes during this process, leading to alteration in its properties (Hwang et al., 2014).

IVD degeneration is a musculoskeletal condition, mainly caused by ageing (Novais et al., 2024). As average life expectancy is rising (United Nations, 2019), age is increasingly affecting the prevalence of this condition in the population (Novais et al., 2024). Nevertheless, as a multifactorial condition, there are other factors that contribute to tissue degeneration, namely obesity (Liuke et al., 2005), smoking (Uematsu et al., 2001), biomechanical stresses (Sward et al., 1991) and genetics (Kalichman et al., 2008; Martirosyan et al., 2016), among others.

It is well known that obesity is highly associated with narrowing of the IVD space and reduced magnetic resonance imaging (MRI) signal intensity. In fact, a correlation between

obesity and inflammatory mediators, particularly adipokines, has been reported to contribute to IVD degeneration (Segar et al., 2019).

Considering that most low back pain (LBP) patients are smokers, an *in vivo* study have focused on the effects of nicotine on the IVD (Uematsu et al., 2001). Animals exposed to nicotine exhibited inhibition of cell activity and ECM biosynthesis, as well as vascular constriction, thus contributing to IVD deterioration (Uematsu et al., 2001).

Another group has studied *in vivo* the effects of mechanical stress on IVD degeneration (Shi et al., 2022). Results showed that an increase in the mechanical stress decreased collagen type II expression and reduced cell viability, while increasing pro-inflammatory mediators. Additionally, an increase of NP stiffness was reported. All these features were indicative of IVD degeneration (Shi et al., 2022)

Regarding genetic influence, different research groups (Kalichman et al., 2008; Martirosyan et al., 2016) demonstrated that different genes contribute to an increased risk of tissue degeneration, namely collagen and aggrecan (Kalichman et al., 2008), as well as those coding for ECM degradating enzymes (Martirosyan et al., 2016).

IVD degeneration and ageing have similar physiological changes and, in most cases, the difference between these two pathomechanisms is not always clear (Galbusera et al., 2014). However, contrarily to age-related alterations that occur in the IVDs along the spine of each individual, the degenerative process may impact younger people, given its multifactorial nature, and occurs at an accelerated rate (Vo et al., 2016).

1.2.1 Cellular alterations

At the cellular level, nutrition deficiency is the major contributor to cell metabolic alterations and death, as they are crucial for survival (Buckwalter et al., 1993). During ageing, the tissue becomes less irrigated, due to a decrease in the number of blood vessels that supply the IVDs (Bernick et al., 1982). Noteworthy, with degeneration, a reverse effect is observed, in which new vessels (Salo et al., 2008) and nerves (Richardson et al., 2012) are formed. Additionally, CEPs undergo thinning and calcification (Bernick et al., 1982; Oda et al., 1988). This has a significant impact in water and solutes permeability and, consequently, in cell nutrition (Roberts et al., 1993) and pH levels, which decrease due to a rise in lactate content (Buckwalter, 1995). Such events further contribute to a reduction in cellularity, biofunctionality and biosynthesis (Buckwalter, 1995).

In parallel, cell senescence is an age-related process that may occur in the IVD, even without alterations in cell nutrition (Buckwalter, 1995), and is defined as a proliferation arrest (Gruber et al., 2007). In the context of IVD degeneration, there is an increase in senescent NP cells (S.-W. Jeong et al., 2014), which disturb matrix homeostasis (Ngo et al., 2017)

Despite viable, senescent cells present several phenotypic and genetic alterations (Gruber et al., 2007). In fact, researchers have demonstrated that cell senescence is highly associated with increased catabolism, expression of β-galactosidase and number of $p16^{ink4a}$ immune-positive cell, which are related to the upregulation of degrative enzymes, namely matrix metalloproteinase (MMP) - 13 and a disintegrin and metalloproteinase with thrombospondin motifs (ADAMTS) - 5 (Le Maitre et al., 2007). MMP expression, regulated by tissue inhibitors of metalloproteinases (TIMPs), is crucial for tissue remodelling (Vo et al., 2013). However, the upregulation of these enzymes has a negative impact on IVD degeneration (Bachmeier et al., 2009). In particular, MMP-13 degrades collagen type II (Mitchell et al., 1996), a predominant component in IVD's ECM composition, particularly in the NP and inner AF.

1.2.2 ECM changes

During ageing, PG levels, especially GAGs, decrease in the NP (Shapiro et al., 2014), constituting a major factor for the degenerative cascade (Ohnishi et al., 2020). In older individuals, these levels are similar to those of the AF (Antoniou et al., 1996). A study showed that PG content increases in the AF with degeneration, unlike in the NP, which led to conclude that AF presents a different response to ageing and degeneration (Singh et al., 2009).

Tissue dehydration is a result of PG content decrease, leading to an unclear differentiation between the NP and AF (Antoniou et al., 1996). It also results in decreased disc height and loss of mechanical properties (Galbusera et al., 2014).

Regarding collagen levels, there is a replacement of collagen type II by collagen type I in the NP and inner AF (Adams et al., 2006; Shapiro et al., 2014). Additionally, older IVDs are characterized by decreased ECM turnover, resulting in collagen crosslinking (Duance et al., 1998).

To better understand age-related ECM biochemical alterations, our research team focused on studying bovine NPs from three different ages: fetus (~7-8 months of gestation), young (~1 year old) and old (16-18 years old) individuals (Caldeira et al., 2017). The NP matrisome profile showed that fetal marices present increased levels of collagen type XII and XIV, two molecules with a known pro-regenerative role in other tissues (Nauroy et al., 2019; Wehner et al., 2017).

These molecules were absent in young and old bovine NPs. Additionally, NPs' ECM presented an enrichment in prolargin and fibronectin (proteins linked to fibrosis), a reduction in the number of collagen fibers and an increase in pore size (Caldeira et al., 2017).

1.2.3 Altered biomechanics

The biomechanical properties of the IVD are determined by interactions between its different structures and all the stimuli to which it is subjected. As a result of the events that occur with ageing and degeneration, this tissue experiences different biomechanical alterations (Shapiro et al., 2014).

One of the main features of a degenerated IVD is height decrease (Murata et al., 1994), which causes an increase in axial compression, resulting in a disorganization of the AF lamellar structure (O'Connell et al., 2011; O'Connell et al., 2007. Contrarily to degeneration, ageing does not significantly impact the structure's height (Frobin et al., 1997).

Furthermore, independently of ageing, a reduction in PGs content contributes to further IVD degeneration, resulting in increased stiffness (Ebara et al., 1996). Additionally, as a result GAGs loss that leads to dehydration, the NP undergoes decompression, which overloads the AF (Adams et al., 1996), resulting in spine instability (Mimura et al., 1994).

1.2.4 Inflammation

Throughout IVD degeneration, inflammation has a significant effect on tissue degradation, since pro-inflammatory cytokines promote dysregulation of ECM degradative enzymes (Cazzanelli et al., 2020). With the inflammatory cascade, there is an increase in inflammatory mediators, such as interleukin (IL)-1β and tumor necrosis factor (TNF)-α (Le Maitre, Hoyland, et al., 2007), particularly in the NP, comparatively with the AF (Bachmeier et al., 2007).

Additionally, there is also an increase in IL-2, -4, -10 and -14 (Akyol et al., 2010), which influence cell senescence and apoptosis (Lyu et al., 2021). A feedback mechanism has been identified, given senescent cells' contribution to the secretion of pro-inflammatory and catabolic mediators (Ngo et al., 2017).

1.2.5 Vascularization

A healthy IVD is mostly avascular, presenting vascularization only in the outer AF (Nerlich et al., 2007). However, during IVD degeneration, the tissue undergoes several alterations, including blood vessels ingrowth. A study focused on induced degeneration in porcine IVDs revealed that vascular endothelial growth factor (VEGF) receptors, mediators of the

angiogenesis process, were present in injured animals. Moreover, these animals showed blood and lymphatic vessels ingrowth (Salo et al., 2008).

p53 is a transcription factor that plays a key role in IVD homeostasis, since it controls cell metabolism and survival (Zhang et al., 2021), as well as neovascularization (Lu et al., 2013). However, the upregulation of this gene has a major impact on IVD degeneration, given the stimulation of NP cells apoptosis (Zhang et al., 2021). Considering the increased expression of VEGF and p53 in degenerated IVDs, there is a potential synergy between these two elements in enhancing blood vessels ingrowth (Lu et al., 2013).

1.2.6 Nerve ingrowth

An IVD under normal physiological conditions is almost aneural (Bogduk et al., 1981), which is not observed with ageing and degeneration. Richardson *et al.* (2012) have studied the input of healthy and degenerated NP cells on neural outgrowth, demonstrating their opposite effect. Degenerated NP cells promote nerve outgrowth and neoinnervation, whereas normal NP cells repress this process (Richardson et al., 2012).

Another group assessed the alterations in IVD innervation in secreted protein, acidic, rich in cysteine (SPARC)-null mice (Miyagi et al., 2014). SPARC is an important component for tissue remodelling (Miyagi et al., 2014), since it contributes to ECM maintenance (Whittal et al., 2021). SPARC-null mice present accelerated age-associated IVD degeneration (Miyagi et al., 2014; Whittal et al., 2021). These animals had increased nerve ingrowth and signs of pain, suggesting that enhanced innervation on degenerated IVDs may cause discogenic pain, namely LBP (Miyagi et al., 2014).

1.2.7 IVD degeneration phenotypes

To sum up, IVD degeneration is a process that mimics ageing at an accelerated pace. It is characterized by tissue dehydration, which leads to a decrease in NP pressure (Antoniou et al., 1996; Buckwalter, 1995), alterations in ECM composition, namely reduction in PGs content (Antoniou et al., 1996), replacement of collagen type II by I (Adams et al., 2006), collagen crosslinking (Duance et al., 1998; Sivan et al., 2006) and matrix degradation due to proteolytic enzymes (Bachmeier et al., 2009; Le Maitre et al., 2005; Novais et al., 2024). Figure 1.3 represents the IVD's degenerative features mentioned.

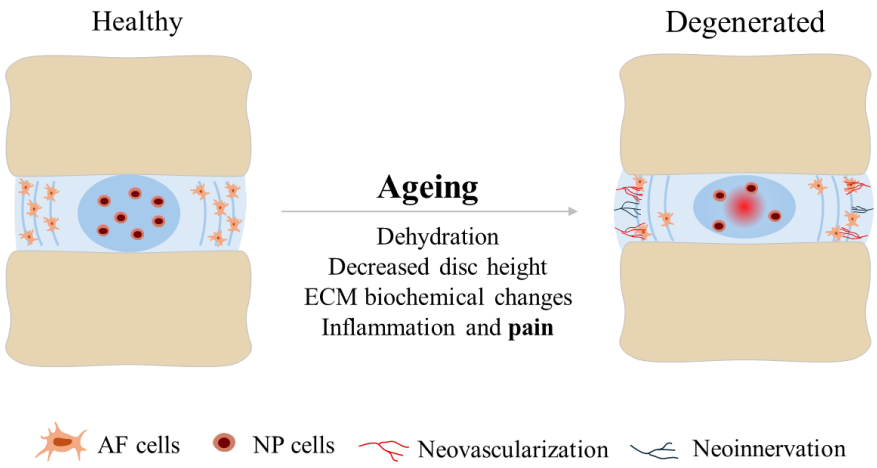

Figure 1.3 – IVD ageing and degeneration. The ageing and degenerative cascade are characterized by common biochemical, structural and biomechanical alterations that lead to pain.

Considering pathological heterogeneity, IVD degeneration has different phenotypes associated, namely calcification, fibrosis, herniation or a combination of these (Novais et al., 2024). IVD calcification is a process characterized by tissue mineralization (Hristova et al., 2011) associated with ageing (Chanchairujira et al., 2004) and degeneration severity (Shao et al., 2016). Fibrosis involves loss of viscoelasticity, due to a decrease in PGs content in the IVD's ECM, along with an increase in collagen content, resulting in a stiffer structure (Ohnishi et al., 2020; Yee et al., 2016). Finally, IVD herniation results in the protrusion of the NP towards the AF or the CEPs (Novais et al., 2024), due to the inflammatory cascade, ECM remodelling and biomechanical stresses (Ohnishi et al., 2020). This phenotype is one of the most common causes of painful IVDs, given the compression of the nerves that appear with degeneration (Ohnishi et al., 2020).

2. Low back pain

2.1. Epidemiology

LBP is a musculoskeletal disorder that affects over 80% of the population at least once in their lifetime, constituting the leading disorder regarding years lived with disability (YLD) and absence from work (Diwan et al., 2023; Molinos et al., 2023). This condition presents increased impact in the population, regarding YLD, when compared to diabetes and other chronic diseases (James et al., 2018). Alongside with the impact in patients' quality of life, LBP constitutes a major burden to hospitals and healthcare systems, regarding costs and resources (Diwan et al., 2023; Urits et al., 2019), associated with prolonged hospital stays, physical therapy and ambulatory care (Fatoye et al., 2023). It is estimated a total indirect cost ranging from 3.2

million to 13.2 billion dollars associated to LBP patients (Fatoye et al., 2023). In Portugal, these costs are around 738.85 million euros (Gouveia et al., 2011).

LBP can be classified into specific or non-specific. Non-specific LBP constitutes 80-90% of the cases (Fujii et al., 2019), affects people of all ages and does not have a recognized pathoanatomical cause (Maher et al., 2017). Therefore, treatment approaches are not clearly defined (Fujii et al., 2019). Regarding specific LBP, there are different types, namely nociceptive and neuropathic pain. Nociceptive pain is triggered by tissue damage associated to specific stimuli (e.g. heat/cold, mechanical pressure), as self-defence reaction, whereas neuropathic pain results from stimuli or diseases that directly affect the nervous system (Armstrong et al., 2024). Moreover, it is highly associated with other medical conditions, such as osteoarthritis, osteoporosis and muscle/fascia injuries (Fujii et al., 2019). LBP classification takes into account the duration of symptoms, being defined as acute in cases up to 4 weeks and as chronic up to 12 weeks (Atlas et al., 2001).

As previously mentioned in section 1, several factors can contribute to LBP, namely smoking (Shiri et al., 2010b), obesity (Shiri et al., 2010a), genetic predisposition (Postacchin et al., 1988), among others. However, IVD degeneration is the main cause of LBP (Cheung et al., 2009; Kjaer et al., 2005), being highly associated with nerve ingrowth towards the NP (Freemont et al., 1997; Miyagi et al., 2014).

2.2. Diagnosis

Imaging techniques are key for several types of clinical diagnosis, including LBP-associated IVD degeneration. Different methodologies can be used to diagnose IVD-related pathologies, namely radiography, computed tomography and MRI, but a correct diagnosis is crucial for an adequate treatment choice.

Radiography is a useful approach to assess CEPs morphological changes, disc height index (DHI), as well as some pathologies, such as scoliosis, facet hypertrophy and spondylolisthesis (Majumdar et al., 2011; P. H. Wu et al., 2020). However, this technology fails to detect early degenerative stages, IVD bulging and herniation (Majumdar et al., 2011).

Computed tomography is an imaging tool that contributes to diagnose prolapsed IVDs, as well as posterior osteophytes. However, besides poor contrast resolution given IVD's nature, patients are exposed to high doses of ionizing radiation, which led to the substitution of this procedure by MRI (Majumdar et al., 2011).

MRI is the gold standard approach to diagnose IVD conditions, enabling a radiation-free analysis according to different axis, with enhanced contrast and resolution (P. H. Wu et al., 2020). Moreover, it allows the assessment of IVD morphological changes (Majumdar et al., 2011). Some of the features extracted from MRI are related to IVD degeneration, as T1 and T2 weighted images (Majumdar et al., 2011). T1 mapping allows the digitalization of IVD's water content within the cartilaginous ECM, allowing the assessment of cartilage degeneration (Ogon et al., 2020). T2 mapping, in turn, can be correlated with ageing and degeneration grades, by inverse correlation with relaxation time (Marinelli et al., 2010; Pfirrmann et al., 2001).

Pfirrmann *et al.* (2001) developed a classification system for IVD degeneration using T2-weighted images, composed by five severity grades of progressive degeneration, from early to advanced stages (Pfirrmann et al., 2001).

Overall, MRI constitutes a key imaging technique to efficiently diagnose IVD degeneration in a minimally invasive way (Ogon et al., 2020). Moreover, it is an essential technique to assess the effectiveness of the therapies administered.

2.3. Current therapies

There are several strategies to treat LBP, according to the severity of the condition, including conservative or invasive approaches (Ying et al., 2023).

Conservative treatment is recommended in less severe cases before advancing for surgical and invasive therapies (P. H. Wu et al., 2020; Ying et al., 2023). It includes oral medication for pain relief (e.g. analgesics, non-steroidal anti-inflammatory drugs, opioids, etc), physical therapy, rest and pain-relieving injections (e.g. corticosteroids) (P. H. Wu et al., 2020). However, in most cases, these approaches are not efficient and the symptoms return (Hestbaek et al., 2003).

Invasive approaches are mainly considered when all the others fail to alleviate pain. In terms of surgical options for LBP, the most common are spinal fusion, microdiscectomy and disc replacement (Ying et al., 2023). Spinal fusion is a procedure to join two or more vertebrae (P. H. Wu et al., 2020), resulting in limited flexibility in order to prevent aggravation of the pathology (Woods et al., 2010; P. H. Wu et al., 2020). Moreover, it can place stress on the adjacent IVDs inducing further degeneration. Microdiscectomy is characterized by the removal of IVD fragments to avoid further compression, thus having a major impact on tissue biomechanics (Woods et al., 2010). Finally, as for disc replacement, the IVD is removed and replaced by a prothesis (P. H. Wu et al., 2020), aiming to maintain the biomechanical properties

of a healthy IVD (Woods et al., 2010). However, it often results in implant migration and the need for reoperations.

Both conservative and invasive approaches focus on alleviating pain and reducing spinal pressure, respectively, instead of addressing the pathophysiology of the problem (Ying et al., 2023). Considering that these therapies do not provide an effective and long-term solution to LBP patients (Woods et al., 2010; Ying et al., 2023), there is an urgent need to develop new regenerative therapies to functionally restore the IVD, or reverse the degenerative cascade, tackling this condition.

2.4. Future trends towards IVD regeneration

Considering the lack of therapies focused on the degenerative cues that enhance LBP, different groups have focused on tackling this problem (Samanta et al., 2023). Several regenerative strategies have been under study, namely using biological approaches (e.g cell-based, gene-based, growth factors, etc), biomaterials or the combination of both.

2.4.1. Cell-based therapies

With ageing and IVD degeneration, it is known that there is a decrease in the number of viable cells, concomitant with an increase in cell senescence, namely in the NP (Buckwalter, 1995; S.-W. Jeong et al., 2014). Therefore, the development of cell-based therapies aims to repopulate the tissue and restore the ECM environment, by increasing the number of cells and boosting ECM synthesis (van Uden et al., 2017).

Several potential cell types can be used, namely notochordal cells, NP cells, chondrocytes and mesenchymal stem cells (MSCs) (Woods et al., 2010). Moreover, cells can also be derived from different sources, such as autologous or allogenic (P. H. Wu et al., 2020).

Considering the harsh tissue environment (e.g. hypoxia and low pH and nutrition), it is noteworthy that, in order for this approach to be a viable strategy to tackle degeneration, transplanted cells need to succeed in homing and surviving in these conditions (Wu et al., 2020). Wuertz *et al.* (2008) demonstrated that, *in vitro*, IVD-like features, particularly low pH, have a negative impact on cell proliferation and biosynthesis (Wuertz et al., 2008). Moreover, an *in vi*vo study demonstrated that injected MSCs only survived for up to 2 weeks in the rat's IVDs (J. H. Jeong et al., 2009), evidencing the hostility of the degenerated IVD environment.

The combination of cell-based therapies with biomaterials may constitute a potential strategy to tackle cell's survival issue. In fact, it was demonstrated that 3D chitosan scaffolds

increased survival and differentiation of NP-like cells derived from human induced pluripotent stem cells, when compared to 2D Matrigel (Tang et al., 2024). An *in vivo* study in sheep revealed that IVDs administered with collagen scaffolds loaded with autologous adipose-derived MSCs presented height stabilization. In parallel, it reduced the frequency of degenerative features onset, thus revealing the potential of these therapies (Friedmann et al., 2021).

2.4.2. Gene editing

Gene therapy is increasingly becoming a field of interest to modulate the biological mechanisms of different tissues, namely the IVD (Wu et al., 2020). Through deoxyribonucleic acid (DNA) or ribonucleic acid (RNA) transfer, target cells can express the intended RNA and/or protein (Han, 2020). Considering that the insertion of unknown genetic material is not a positive factor for cell metabolism, local administration is conducted by using one of two types of vehicles: viral and non-viral vectors (Nishida et al., 2008). Viruses constitute a proper vehicle for gene-based therapies, given their ability to enter the target cells and constitutively express genes of interest (Nishida et al., 2008). However, this strategy may be highly toxic (Butt et al., 2022). On the other hand, non-viral vectors allow the delivery of genetic material using non-viral sources (e.g. electroporation, microinjections, polymer-based strategies, etc). However, despite its safety, this approach is unable to reach target genes expression levels as high as the other strategy (Butt et al., 2022).

Nishida *et al.* (1998) have demonstrated the *in vivo* potential of gene-based therapies to tack IVD degeneration. This study demonstrated that transfected cells expressed the lacZ gene, responsible for production of β-galactosidase, for up to 12 weeks, despite the harsh IVD's environment (Nishida et al., 1998).

Noteworthy, despite their potential to tackle the IVD degenerative cascade, gene-based therapies can have several associated risks, such as viral mutations or immune responses (Wu et al., 2020). Moreover, besides ethical concerns, the safety of these therapies must be ensured before clinical translation (Samanta et al., 2023).

2.4.3. Growth factors

Growth factors are proteins present in the human body that modulate several cellular and biological processes, such as cell proliferation, differentiation and repair, as well as ECM production. Considering these functionalities, researchers have focused on developing novel

therapies based on growth factors injection or transplantation of biomaterials with these proteins embedded (Masuda et al., 2004).

Different strategies regarding growth factors are being approached for IVD degeneration (Samanta et al., 2023). An *in vitro* study addressing the role of platelet derived growth factors revealed that this bioactive molecule promotes upregulation of collagen type II and aggrecan (Chen et al., 2006).

Additionally, an observation study in patients with LBP and cervical pain treated with infiltrations of plasma rich in growth factors showed a significant improvement in pain over the three and six months of observation, >30% and >87% respectively (Anitua et al., 2023). However, patients received 2-3 series of infiltration every two weeks, depending on their symptoms. This demonstrates one of the major drawbacks of these techniques, which is the need for multiple administrations in order to achieve a positive therapeutic outcome, increasing treatments costs and patient discomfort.

2.4.4. Biomaterials

Biomaterials are increasingly being explored to tackle degenerative diseases that often lead to pain (Gu et al., 2022). A biomaterial for tissue regeneration must provide a niche and stimulating environment, similar to the native, in order to promote cellular metabolism, particularly adhesion, proliferation and differentiation (Abdulghani et al., 2019; Liu et al., 2023).

There are different criteria that a biomaterial must fulfil, in order to constitute a suitable approach for tissue engineering (Mohd Isa et al., 2022). One of the main requirements is biocompatibility. Considering that biomaterials are not inert, biocompatibility is a determinant characteristic for the immune response. Biomaterial's presence *in situ* initiates several inflammatory responses, since it is recognized as a foreign object (Babensee et al., 1998; Zimmerli, 2011). Biodegradability is also an important feature, considering that the biomaterial must degrade along time, in order to allow cells to remodel the ECM. Furthermore, degradation by-products must be non-cytotoxic (Babensee et al., 1998). Finally, biomaterial's mechanical properties are crucial in the development of novel therapies, considering that they must match the anatomy and biomechanical requirements of the target tissue (O'Brien, 2011).

One of the most interesting features of biomaterials is the diversity and singularity of their properties, since different raw material components and manufacturing processes, for example, can lead to totally different cell responses (Liu et al., 2023; Wagner et al., 2020). In particular,

the macro and microarchitecture of the biomaterial has several implications in its performance, thus constituting a key feature in biomaterial design (O'Brien, 2011). A study using 3D printed scaffolds showed that geometry and architecture impact cell metabolism, affecting regeneration (Hallman et al., 2021). Moreover, it is known that ECM-based biomaterials affect cell interactions according to diverse matrix features, thus the need of choosing proper materials (Chaudhuri et al., 2020). For example, Caldeira *et al.* (2017) demonstrated that bovine NP's ECM from three different ages present structural and biochemical differences (Caldeira et al., 2017), which impact the properties of the biomaterials developed.

2.4.4.1. Decellularized extracellular matrix-based biomaterials

Native tissues are enriched with cells and ECM. The latter provides physical support for cell activity, since it is mainly composed by several structural biomolecules important for tissue maintenance and homeostasis (Brown et al., 2022; Yao et al., 2019). Moreover, it is known that ECM constitutes a key player in cell fate, since it regulates cell proliferation, differentiation and survival (Theocharis et al., 2019).

However, the application of a foreign object inside the body, such as an ECM-based biomaterial, triggers an immune response initiated by the recruitment of immune cells, namely macrophages and neutrophils (Kasravi et al., 2023). Thus, in order to minimize this inflammatory cascade, several research teams have employed a process named decellularization. It consists in the removal of cellular components, while preserving ECM structure and biochemical cues as much as possible (Kasravi et al., 2023; Yao et al., 2019). It is acknowledged that decellularized extracellular matrix (dECM) materials present higher biocompatibility than ECM-based biomaterials, as well as decreased rejection rates (Fishman et al., 2013; Kasravi et al., 2023).

To evaluate an efficient decellularization process, Crapo *et al.* (2011) defined that different criteria must be fulfilled, particularly <50ng dsDNA per mg ECM dry weight, < 200bp DNA fragment length and/or absence of nuclear material in tissues stained with 4',6-diamidino-2-phenylindole (DAPI) or Hematoxylin and Eosin (H&E) (Crapo et al., 2011). More recently, Kawecki *et al.* (2018) report complemented the previous criteria adding to the list the absence of intracellular membrane compartments and cell membrane elements, preservation of ECM elements (e.g. GAGs, collagen) and lack of cytotoxicity of the obtained ECM scaffolds (Kawecki et al., 2018).

Therefore, dECM-based biomaterials constitute promising therapeutic and regenerative strategies considering its composition and structure combined with low cytotoxicity (Taylor et al., 2018).

In the IVD field, several *in vitro* and *in vivo* studies highlight dECM-based biomaterials' capacity for regenerating the tissue and treat LBP, including their potential use as a delivery system for cell-based therapies, as reviewed elsewhere (M. Fiordalisi et al., 2020).

Multiple studies focused on dECM-based biomaterials have shown up-regulation of PGs, namely aggrecan, and collagen type II, which constitute positive indicators of healthy ECM restoration (Mercuri et al., 2013; Peng et al., 2021; Xu et al., 2019; Zhou et al., 2018). Moreover, crucial features for tissue regeneration have been observed, such as water content restoration (Peng et al., 2021) and disc height maintenance or recovery (Peng et al., 2021; Xu et al., 2019; Zhou et al., 2018). Additionally, other studies have shown promising results in tackling pain (Mohd Isa et al., 2018; Piening et al., 2022; Ura et al., 2021), a key feature to treat LBP.

In the development of dECM-based biomaterials, tissue donor age is a crucial aspect to be considered (M. Fiordalisi et al., 2020). It was already demonstrated by our team the impact of age in cellular, structural and biochemical features of bovine NP's ECM (Caldeira et al., 2017; Molinos et al., 2023). Interestingly, fetal bovine NPs present particular characteristics that may be key for IVD regeneration (Caldeira et al., 2017; M. F. Fiordalisi et al., 2022). Fiordalisi *et al.* (2022) assessed this with dECM from fetal bovive NPs, *in vitro* and *in ovo* using a chorioallantoic membrane (CAM) chick embryos assay (M. F. Fiordalisi et al., 2022). This study revealed that bovine NP cells cultured in fetal dECMs upregulate aggrecan and collagen II, pro-typical molecules of a healthy IVD environment. Notably, the CAM assay demonstrated that fetal matrices present the capacity to reduce neovascularization (M. F. Fiordalisi et al., 2022).

Several other strategies for IVD regeneration are currently in pre-clinical validation using diverse *in vivo* models. However, there is a considerable gap between bench and clinical research translation, which constitutes a major concern to develop novel therapies that can successfully achieve the market (Catoira et al., 2020). In particular, for dECM-based biomaterials, there is an urgent need to develop standard, scalable and automatized decellularization processes, using bioreactors, for example (Choudhury et al., 2020). Additionally, administration method, reproducibility, sterilization, safety and compliance with regulatory frameworks also need to be considered (L. Wang et al., 2022).

3. Pre-clinical models for IVD degeneration research

For validation of novel therapies, *in vitro* models enable the study of several pathobiological features. However, they lack to replicate the complexity and interactions of living systems (Ribitsch et al., 2020). In order to achieve more intricate systems, several teams have been developing organ-on-a-chip devices (Son et al., 2023) and dynamic co-culture systems (Dai et al., 2014). Other alternatives, include *ex vivo* (K. Wang et al., 2023) or *in silico* models (Baumgartner et al., 2021), that use tissue from different sources (e.g human, bovine, porcine, among other) and computational simulations, respectively, to assess physiological processes or diseases. However, there are numerous interactions that can not be replaced using these strategies (Bubak et al., 2015).

Thus, since these alternatives do not effectively mimic the complexity of *in vivo* systems, several research teams have focused on the development of diverse animal models to study IVD pathomechanims and the potential of novel regenerative solutions (Kroeber et al., 2002; Martin et al., 2013; Masuda et al., 2005. Considering that these models offer more complex and realistic systems when compared to humans, allowing more enlightening conclusions (Fusellier et al., 2020), worldwide regulatory frameworks require technologies to be validated in small and large animals models and, lastly, in human clinical trials, before market entry (Ribitsch et al., 2020).

3.1. Choice of a suitable *in vivo* model

To choose an appropriate animal model, many factors need to be considered (Mukherjee et al., 2022). First, it is essential to choose a model whose features resemble those of humans and of the pathophysiology to be assessed (Mukherjee et al., 2022; Ribitsch et al., 2020). Moreover, other factors may impact investigation and must be taken into account, such as age and sex, besides others related to the disease. In the development of a human therapy, the IVD characteristics of the animal model under study may affect the results, due to different mechanical properties, the presence of notochordal cells, among others (Fusellier et al., 2020). The occurrence of the pathology, whether natural or induced, can also interfere with the results, since spontaneous pathologies lead to increased inconsistency and variability (Fusellier et al., 2020).

Regarding IVD degeneration, there are rodent models, involving different mice and rat strains, rabbit experiments, and large animal studies, using pig, bovine, sheep and dog (some of them are referred in Table 1.1).

Table 1.1 – IVD degeneration *in vivo* models

Model		Methodology	Reference
Species	**Disease occurrence**		
C57BL/6 mice	Induced – Structural	Tail dorsal puncture using 26and 29 G needle at 1,75mm depth	(Martin et al., 2013)
SM/J mice	Spontaneous – Ageing	SM/J mice, known for poor regenerative potential, and LG/J mice, known as "super-healer"	(Choi et al., 2018)
Wistar Han rat	Induced – Structural	Tail dorsal puncture using 21- and 25 G needle at 5mm depth	(Cunha et al., 2017)
Sprague Dawley rat	Induced - Structural	Nucleotomy using ventral puncture with microsurgical drill (equivalent to 25 G and 21 G) at 2 mm depth	(Kim et al., 2011)
	Induced – Structural	Tail dorsal puncture using 20 G needle at 5mm depth vs. whole disc	(Han et al., 2008)
	Induced - Mechanical	Static shear load of up to 4N for 1 and 2 weeks	(Kim et al., 2012)
Rabbit	Induced - Structural	Transverse stab incision + needle puncture using 16,18 and 21 G at 5mm depth	(Masuda et al., 2005)
	Induced – Mechanical	Axial dynamic stress by an implanted device applying a compressive force of 2,4 MPa	(Kroeber et al., 2002)
Dog	Spontaneous – Ageing	Evaluation of CD and NCD dogs	(Bergknut et al., 2012)
Sheep	Induced – Structural and mechanical	Subtotal nucleotomy + ChABC injection over a range of	(Gullbrand et al., 2017)

		dosages (0,1U; 1U or 5U) using a 22G needle	
Goat	Induced - Mechanical	ChABC injection (0,2; 0,25; 0,30 and 0,35 U/mL) using a 29 G needle	(Hoogendoorn et al., 2007)

CD – chondrodystrophic; ChABC - chondroitinase ABC; NCD - nonchondrodystrophic

Rodents have an IVD geometry and ECM composition analogous to humans (Fusellier et al., 2020). Moreover, normalised values show that rat's IVD biomechanical properties are similar to humans, despite being quadrupeds (Showalter et al., 2012). However, one of its major drawbacks is the presence of notochordal cells in the NP during adulthood, which are absent in humans since childhood (Fusellier et al., 2020). This may have a critical impact in animal experiments, considering that notochordal cells have the ability to protect the tissue and prevent early onset degeneration (Erwin et al., 2011). Thus, it may lead to misinterpretation of data.

Several large animal models, namely goat and sheep, also present similar ECM composition to the human IVD (Fusellier et al., 2020), namely in terms of collagen and NP water content (Beckstein et al., 2008; Showalter et al., 2012). Regarding GAGs levels (Beckstein et al., 2008), this similarity is seen in goat and pig, alongside with rat and rabbit. Additionally, goat, bovine and sheep present similar torsion biomechanics compared to the human spine (Showalter et al., 2012).

Dogs have also been largely used in IVD degeneration and herniation studies, considering they also suffer from this disorder (Bergknut et al., 2012). They can be classified in two classes: chondrodystrophic (CD) and nonchondrodystrophic (NCD). The former is highly associated with IVD degeneration in early stages of life, commonly caused by genetics, causing NP ECM modifications and long bones ossification (Smolders et al., 2013). The latter suffers from degeneration later on, mainly due to trauma and deterioration (Bergknut et al., 2012). Considering the condition's onset and its resemblance to the degenerative progression in human IVDs (Fusellier et al., 2020), these animals are commonly used as a large animal model of this disease.

Some of the models take advantage of spontaneous degeneration (Bergknut et al., 2012; Choi et al., 2018), as chondrodystrophic dogs and SM/J mice whose regenerative potential is weak (Choi et al., 2018). In contrast, there are other types of models with induced degeneration, from mechanical induction associated with static (Kim et al., 2012) and dynamic (Kroeber et

al., 2002) forces, to chemonucleolysis caused by enzymatic lysis using chondroitinase ABC injections into the NP (Gullbrand et al., 2017; Hoogendoorn et al., 2007). There are also studies using intradiscal needle puncture (Cunha et al., 2017; Han et al., 2008; Masuda et al., 2005), particularly in mice and rats, given the accessibility to the coccygeal IVDs (Barcellona et al., 2022),

Laboratory animals, mostly rodents, are often preferred over large model organisms due to the ease of handling and manipulation, cost-effectiveness given the low husbandry cost, and diversity in genetic variants (Mern et al., 2021). Even though spontaneous models have natural occurrence of the diseases and their complexity, these models lack standardization. Thus, induced models are generally used (Ribitsch et al., 2020).

3.2. Ethical concerns

In biomedical research, the application of animal models raises several ethical questions. Currently, the regulatory agencies (e.g. European Medicines Agency, USA Federal Food and Drug Administration, National Agencies) require the validation of therapies through different models, from laboratory science animals to larger ones (Mukherjee et al., 2022; Ribitsch et al., 2020). Considering this, at the European level, restrict legislation was established regarding animal housing and handling, procedures and their welfare. The description of these procedures must be integrated at national law-decrees, in order to guarantee safety and well-being to all animals (European Parliament and of the Council of the European Union, 2010). Another important issue in animal experimentation is the establishment of humane endpoint before the beginning of the study, in order to guarantee that welfare is prioritised over the experiment and the results (Denayer et al., 2014). Finally, there is a huge effort by veterinaries and caregivers to ensure appropriate training and supervision (Bubak et al., 2015).

The 3R's principle – Reduce, Refine and Replace – is a general principle recognised by several authorities that aims to ensure that animals rights and welfare are met throughout the studies (Petetta et al., 2021). Reduction in animal experimentation stands for the necessity to reduce as much as possible the number of animals per study, while providing reliable outcomes (Kiani et al., 2022). Refinement involves a series of procedures that improve overall animal welfare (Petetta et al., 2021), namely enriched husbandry conditions (e.g. add different bedding materials or shelters) (Mate et al., 2022; Ratuski et al., 2022, proper handling procedures (e.g. handling through observation tunnel or cupping) (Davies et al., 2022) and providing analgesia (Berke et al., 2022). Finally, replacement means the substitution, whenever possible, of *in vivo*

models for other, such as *in vitro* or *in silico* (Petetta et al., 2021). Moreover, there are other possibilities, namely using tissue harvested from patients' biopsies or abattoir byproducts (Arck, 2019). Some researchers have proposed the inclusion of another R related to responsibility of animal experimentation (Kiani et al., 2022).

Overall, animal studies are essential before entering clinical trials, playing a crucial role in translating novel therapies into the market and benefiting both human and veterinary patients.(Mukherjee et al., 2022).

Chapter II - Aim of the thesis

The prevalence of LBP and IVD degeneration is rising over the years, causing a tremendous socio-economic impact worldwide. Given the lack of long-term effective approaches to address this condition, there is an urgent need to design novel regenerative therapies to restore tissue's properties and improve patients' quality of life.

To develop an effective therapy that can successfully reach the market, *in vivo* proof-of-concept in a small animal (e.g rodents) is a prerequisite before proceeding to large animal models and human clinical trials. In parallel, it is necessary to consider process scalability, ensuring a safe, reproducible and efficient manufacturing process.

Our group demonstrated the potential of fetal bovine NPs, as they are enriched in collagen types XII and XIV, two molecules that disappear with ageing. Additionally, it was showed that bovine fetal decellularized NPs (dNPs), co-cultured with bovine NP cells, exhibited higher aggrecan and collagen type II expression, as well as reduced neovessel formation. These results culminated in the foundation of FetalDisc, a spin-off from i3S, which developed Fetalix. This product is the first fetal-inspired biomaterial to treat LBP and consists of an injectable fetal dNP-based particle solution.

Therefore, the main goal of this thesis was to conduct a pre-clinical validation of Fetalix in a rat model, while assessing decellularization process scalability. The specific objectives were the following:

1. To evaluate the efficiency of modifications in the standard decellularization protocol that could potentially improve process scalability;
2. To investigate Fetalix injectability through a 30 G needle;
3. To assess the therapeutic effect of Fetalix in an *in vivo* rat model of IVD degeneration.

Overall, this work aims to contribute for the development of a novel and efficient solution to restore a functional IVD and tackle LBP by slowing or reversing the degenerative cascade. The knowledge herein generated will be of utmost importance to improve future experimental designs, as well as to refine manufacturing process efficiency.

Chapter III - Materials and methods

1. Biomaterial production

1.1 Tail dissection and IVD isolation

A protocol previously established by the team was performed, as described elsewhere (M. F. Fiordalisi et al., 2022). Fetal (~7 months of gestation) bovine tails were collected from a local slaughterhouse (PEC Nordeste, Portugal) under the approval of the Portuguese National Authority for Animal Health (DGAV). After washing and disinfecting, fetal bovine tails were dissected under sterile conditions. Following skin, muscle and ligaments removal, IVDs were isolated, placed in optimal cutting temperature compound (OCT) and snap frozen with 2-methylbutane cooled in liquid nitrogen, as previously optimized. Samples were stored at -20ºC, until further use.

1.2 Small scale NP decellularization

For standard NP decellularization, a previously established protocol was followed (M. F. Fiordalisi et al., 2022). Briefly, fetal IVDs obtained in 1.1 were thawed at room temperature (RT) and washed in phosphate buffered saline (PBS) to remove the excess of OCT. Upon CEPs removal, NPs were isolated from the central region of the IVD using a 4 mm biopsy punch. The small cylinders obtained were transversally cut in half and placed in 24 well-plates with PBS. Afterwards, samples were immersed in PBS supplemented with 10% Penicillin/Streptomycin (P/S) and 1% Amphotericin B for 15 min. Next, NPs were placed in Hypotonic Buffer A (pH 7.8, 10 mM Tris, 0.1% EDTA) for 18h and then washed three times in PBS (1h/wash). After the PBS washes, samples were incubated in 0,1% sodium dodecyl sulfate (SDS) solution (pH 7.8, 10mM Tris) for 1h and washed three times (20min/wash) with Hypotonic Buffer B solution (pH 7.8, 10mM Tris). Finally, NPs were placed in DNAse treatment solution (pH 7.8, 20 mM Tris, 2mM $MgCl_2$, 50 U/mL DNAse) for 3 h at 37ºC, followed by three washes (20 min/each) in PBS. All steps of the protocol were conducted under agitation (165 rpm) and at RT (24ºC), except the DNAse treatment step, as described (M. F. Fiordalisi et al., 2022). Moreover, all the solutions were supplemented with 1% P/S, 0.5% Amphotericin B and 0.1% Gentamicin. In the end, dNPs were either frozen at -80ºC and lyophilized at -50ºC for 72h for biomaterial's production or placed in 10% neutral buffered formalin overnight at 4ºC for histology processing. Native samples were kept as control and stored as previously mentioned.

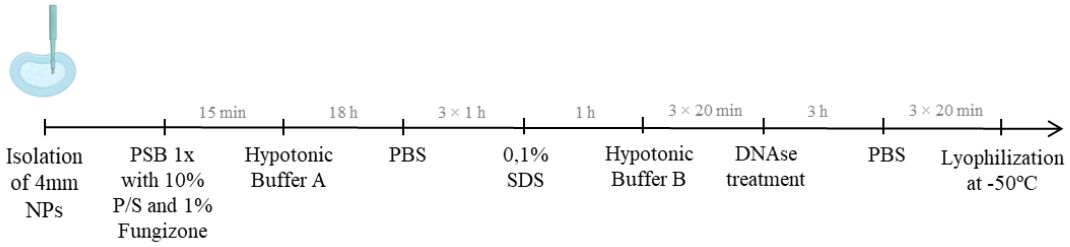

Figure 3.1 – Schematic timeline of the standard decellularization protocol. This protocol was performed in 4mm NP scaffolds in a 24-well plate.

1.3. Modified decellularization protocols

In addition to the standard decellularization protocol abovementioned (Chapter 3, section 1.2), two other alternative protocols were tested aiming to improve process scalability: a shortened version of the procedure used (M. F. Fiordalisi et al., 2022) and a vacuum-assisted decellularization protocol to be used with several large tissue pieces (multiple whole NPs) simultaneously.

For the shortened procedure, after the incubation in Hypotonic Buffer A, NPs were washed in PBS three times for 20 min/each, instead of 1h/each. All the previous and subsequent steps remained unchanged. Samples for DNA and GAGs quantification were stored at -20ºC and lyophilized at -50ºC for 72h. Native samples were kept as control and stored as described.

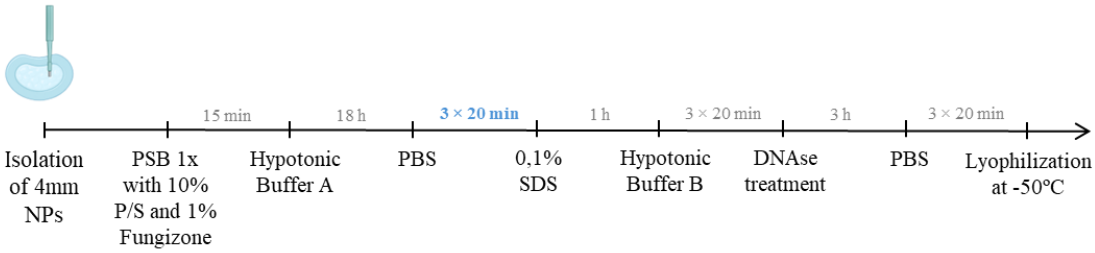

Figure 3.2 - Schematic timeline of the shortened decellularization protocol. This protocol was performed in 4mm NP scaffolds in a 24-well plate. The alterations are presented in bold blue letters.

A vacuum-assisted decellularization protocol was also performed following an adaptation of the standard procedure. In brief, upon CEPs removal and isolation of the whole NP, samples were transferred intact into a 50 mL falcon tube placed inside a desiccator, which was connected to a vacuum pump. The process was performed under agitation (~400rpm) and at RT. Due to technical limitations, the DNAse treatment step was performed without vacuum, at 37ºC, under agitation (~400rpm). Samples for DNA and GAGs quantification were stored at -20ºC and

further lyophilized at -50ºC for 72h. For histology purposes, dNPs were placed for 24h in 10% neutral buffered formalin overnight at 4ºC. Native samples were kept as control and stored as described.

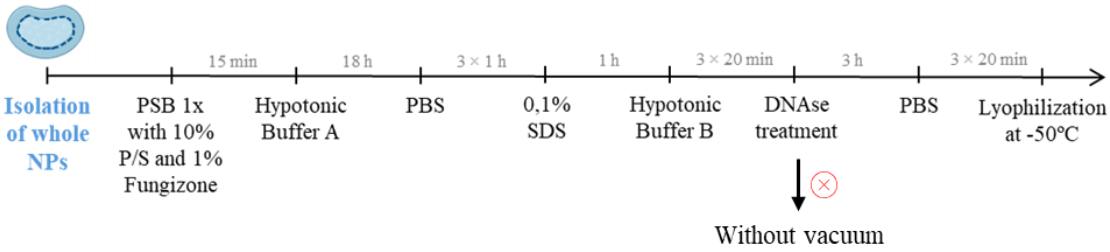

Figure 3.3 - Schematic timeline of the vacuum-assisted decellularization protocol. This protocol is performed in whole NP scaffolds in a 50mL falcon under vacuum. The alterations are presented in bold blue letters.

2. Optimization of an injectable solution

2.1 Milling process optimization

Lyophilized dNPs were further processed using three different milling equipment: Pulverisette 23 (Fritsch), Analytical Mill A10 basic (IKA) and 4-place Mini Bead Mill homogeniser (VWR). For the latter one, dNPs were also resuspended at 10 mg/mL in 0.9% NaCl solution.

For the Pulverisette 23, milling was performed by processing dry dNPs for 1 min at 50s^{-1} of oscillation. Regarding the Analytical Mill A10 basic, the milling was conducted in 4 cycles of 15s at 20000 rotations per minute. Finally, the 4-Place Mini Bead Mill homogeniser was used to mill resuspended dNPs in 1-minute cycles, at speed 5, intercalated with ice periods. Before milling process, lyophilized dNPS were pre-cut using scissors.

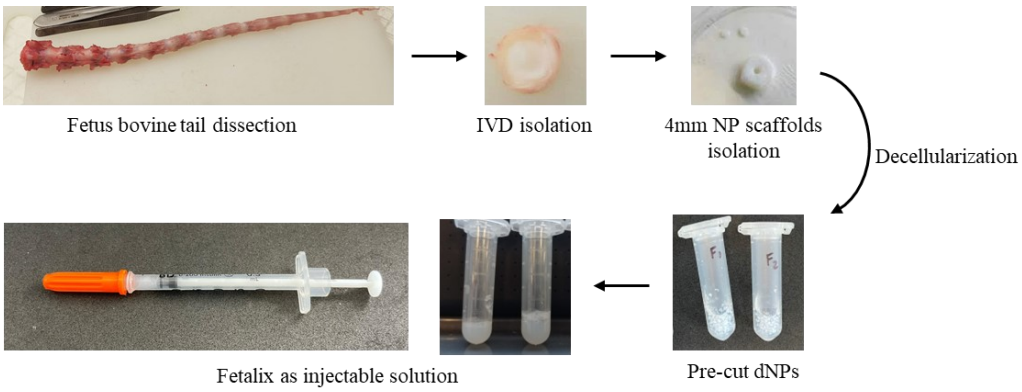

Figure 3.4 – Fetalix's production steps. Each image exhibits each step of Fetalix's production process.

2.2 Particles characterization

Particles resuspended in 0.9% NaCl solution were analysed by brightfield microscopy for the different procedures understudy. Images were obtained at a 4X magnification. Particles' size was measured using ImageJ. Lyophilized samples were analysed using scanning electron microscope (SEM). For that, samples had to be coated with Au/Pd in the SC7640 sputter coater (Polaron, UK) at 20 mV prior to examination on a PhenomTM Pro Desktop SEM (ThermoScientificTM, US). Morphology visualization was performed at 10kV. Images were obtained at 300X, 1000X and 5000X magnification.

2.3 Injectability tests

A preliminary injectability test for the particles obtained in the 4-place Mini Bead Mill homogeniser (VWR) was conducted. dNPs pre-cut with scissors were resuspended 0.9% NaCl solution, according to 10 mg/mL of concentration. Injectability was evaluated by applying manual pressure using different needle sizes (21-, 25-, 27- and 30-G), in descending order of diameter and after the milling cycles.

An injectability test to measure the resistant force of the injection phases for both Analytical Mill A10 basic (IKA) and 4-place Mini Bead Mill homogeniser (VWR) resuspended particles was conducted by mechanical compression using a Texture Analyzer TA.XTplus (Stable Micro Systems, Godalming, Surrey) according to the literature (Robinson et al., 2020). Two different needle sizes were tested (20 and 30 G) with a 5kg load cell. For the compression assay, conditions were the following: pre-test and post-test speed of 10mm/s, test speed of 5 mm/s and trigger force of 0.005kg. To perform the test, Figure 3.5 shows the apparatus set up in which the probe presses the syringe barrel. Force (g)/strain (%) curves were obtained.

Figure 3.5 – Injectability assay set up. The syringe is placed in the clamps allowing the plunger to be pressed by the probe and the biomaterial to be injected.

For this test, saline solution and the particles obtained from the two equipment were tested, in which a stress/strain (MPa/%) curve was obtained. For the 30 G needle, Fetalix (i.e resuspended particles obtained in the 4-Place Mini Bead Mill homogeniser) was also injected in a thermoplastic polyurethane (TPU) 3D-printed block (see Figure 3.6), in order to add resistance and better mimic and injection within the IVD. The block's properties were evaluated with a 30kg load cell. A stress/strain (MPa/%) curve was also obtained.

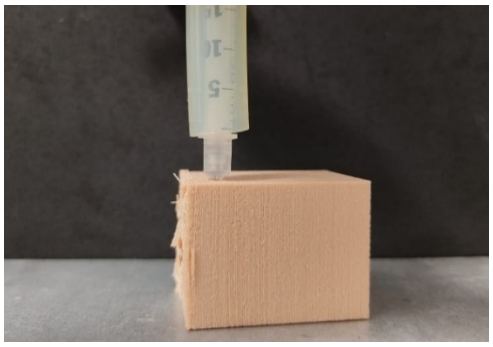

Figure 3.6 – Fetalix injection in a TPU block. By injecting Fetalix into the block, there will be resistance, which mimics the real conditions of injecting the resuspended solution into a patient.

2.4 Process' yield

To determine the process' yield of Fetalix production, 4mm punches were extracted from the NP and cut in half, thereby constituting two dNP scaffolds. After lyophilization at -50ºC, dNPs were weighted. Considering a concentration of 10mg/mL and a volume of 100 µL/IVD is required for human administration, the number of injections produced using a fetal bovine tail was estimated.

3. *In vivo* tests

3.1 Fetalix production

For the *in vivo* administration, NPs were decellularized, according to the standard protocol, lyophilized, resuspended at 10mg/mL (dry weight) in 0.9% NaCl and milled using the 4-Place Mini Bead Mill homogeniser under sterile conditions.

3.2 Experimental design

Animal experimentation was conducted at i3S' animal facility (Porto, Portugal), in accordance with European Legislation on Animal Experimentation through the Directive 2010/63/UE and approved by the i3S Animal Welfare and Ethics Review Body (license n° 2023-23).

The IVD degeneration by rat caudal needle puncture model was used (Cunha et al., 2017). Briefly, male Wistar Han rats with 14-16 weeks old (298 ± 22 g) were anesthetized via inhalation with 5% of isoflurane and 1L/min of O_2. After confirmation of loss of reflexes by paw pinch method, animals were weighted and placed in prone position on top of a heating pad and under 2.5% of isoflurane and 0.2L/min of O_2 anaesthesia. The lesion was performed in three different groups: lesion, saline and Fetalix (n=5/group). For each animal, three consecutive coccygeal (Co) IVDs (Co 5/6, Co 6/7, and Co 7/8) were identified by digital palpation and an intradiscal needle puncture was performed with a 21G needle at 5 mm depth using a needle cap device (see Figure 3.7). Naïve animals (n=4) were kept as control group.

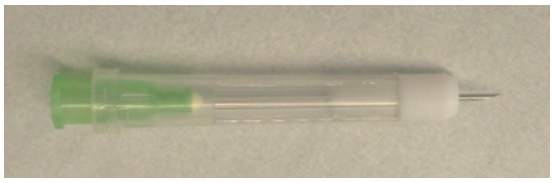

Figure 3.7 – Home-made needle cap device. This apparatus was kindly provided by Dr. Carla Cunha. Image obtained from (Cunha et al., 2017).

Two weeks postinjury, animals were prepared as before and administered, using a 30G needle at 5 mm depth, with 10µL of Fetalix or with 10µL vehicle (i.e 0.9% saline solution). Lesioned-only animals were kept as control group for the injury.

Four weeks post-administration, animals were humanely sacrificed by CO_2 inhalation (5 min of induction and 1 min of dwell time), according to the Standard Operating Procedure nº85 established by the Institute's Animal Facility and following the American Veterinary Medical Association recommendations of 2020.

The timeline for the *in vivo* study is shown in Figure 3.8.

Figure 3.8 – *In vivo* timeline. Timing for each experiment, as well as parameters evaluated at each timepoint.

Animals were kept in a 12h-light/dark cycle, with controlled temperature and humidity and provided with food and water *ad libitum* (i.e without restrictions). Type III cages, that housed 2-3 animal of the same group, were covered with corn cob and enriched with soft paper tissue and a cardboard tunnel. Animals were properly handled and restrained during all the procedures and monitored without signs of pain and/or distress.

3.3 MRI scanning and tail processing

After sacrifice, 2D T2-weighted MRI data was acquired with a turbo-RARE pulse sequence (17 slices per tail, with a thickness of 0.5 mm and no gap) on a Bruker Maxwell BioSpec 3 Tesla scanner, running ParaVision 360 v3.5. An automated algorithm was used to extract IVD's height, area and brightness. Volume was obtained through the sum of each area multiplied by slice's thickness.

Afterwards, the tail was processed. NP of Co 5/6 was isolated, placed in TRYzol and stored at -20ºC for future analysis. Each spinal unit corresponding to Co 6/7 and 7/8 was placed in 10% neutral buffered formalin for one week. Then, the tissue was placed in EDTA-glycerol decalcifying solution under agitation (60 rpm) that was changed twice a week for approximately 2 months. Decalcification of the tail vertebrae was assessed with a 25 G needle puncture. Once decalcification was achieved, the tails were processed for histological analysis.

3.4 Behavioural assay

Before sacrifice, all animals underwent three non-consecutive habituation days with a blinded experimenter, in order to conduct the Von Frey test. On the sacrifice day, animals were mechanically stimulated in each of the four paws by vertically applying Von Frey monofilaments (Semmes-Weinstein, Ugo Basile) into the plantar surface (Deuis et al., 2017). A positive response was defined when paw withdrawal, licking or limb shaking was observed at the stimulation moment or immediately after it (Deuis et al., 2017). The test was performed until three positive responses were received for the same filament.

4. Histological analysis

Samples for histological analysis were further processed and paraffin embedded. Regarding NP samples from decellularization protocols, sequential transversal 3 μm sections were obtained using a microtome (Microm HM335E). Concerning the rat's IVDs, transversal 5 μm sections were provided by i3S' Histology and Electron Microscopy Service.

For H&E staining, sections were incubated in Gill's Hematoxylin dye (3min), washed in tap water, incubated with Eosin solution (4min), washed in ethanol, cleared and mounted with

Entellan. Concerning Alcian Blue/Picrosirius Red (AB/PSR) staining, sections were incubated in AB solution (pH=2.5, 30 min), rinsed in tap water (5 min), incubated in PSR (1h) and rinsed in acidified water (0.01% HCl, 1min). Finally, samples were dehydrated, cleared and mounted with Entellan. For the NP samples, an extra step of Gill's Hematoxylin (3min) was conducted. Regarding DAPI staining, sections were incubated in DAPI solution (1:1000, in PBS 1X) for 10 min and mounted with Entellan.

Finally, samples stained with H&E and AB/PSR with Hematoxylin were analysed in a brightfield microscope (Leica DM2000 LED) with a digital camera 4X, 10X and 20X magnification. Samples stained with DAPI were analysed in the ZOE Fluorescent Cell imager.

Tail's sections were stained with H&E, in order to select the herniated regions. Afterwards, herniated areas stained with AB/PSR were scanned by PhenoImager HT. For each tail's sections, hernias were delineated manually using the freehand selection tool of ImageJ. Hernia volume for each IVD was determined from the sum of the areas of each individual section, according to (Cunha et al., 2017).

IVDs were submitted to a histological grading score, that assesses tissue's degeneration (B. Han et al., 2008). This grading system considers AF and NP's cellularity and morphology, as well as the interface between the two structures, scoring each parameter in a scale between 1 (healthy) and 3 (severely degenerated). IVD samples were only evaluated according to AF's morphology and cellularity and the remaining border between this structure and the NP.

5. DNA quantification

DNA quantification of native and decellularized NPs was assessed by using the PureLink Genomic DNA mini kit (Invitrogen) for DNA extraction and the Quant-iT PicoGreen dsDNA kit (Invitrogen), according to manufacturer's instructions. Briefly, samples were milled using a scalpel and digested for 4h at 55ºC with PureLink Genomic Digestion Buffer and Proteinase K. Supernatant was treated with RNAse A and master mix of PureLink® Genomic Lysis/Binding Buffer with 96-100% ethanol. Afterwards, washing and elution steps were performed, in order to collect samples' DNA. Two standard curves were set: a low-range (6.25 pg/mL to 25 ng/mL) and a high-range (1 ng/mL to 2 µg/mL). Fluorescence was measured in a black 96 well-plate at 480nm of excitation and 520nm of emission using Synergy™ Mx multi-mode microplate reader (BioTek). Values were normalized by dry weight (mg) and data expressed as ng DNA/mg dry weight.

6. sGAGs quantification

Sulfated GAGs (sGAGs) were quantified in native and decellularized NPs using the Blyscan Sulfate GAGs Assay (Biocolor). Briefly, samples were milled using a scalpel and digested overnight at 55ºC with Papain Extraction Reagent, supplemented by papain crystallized suspension. Afterwards, blyscan dye reagent supplementation was followed by centrifugations and an incubation with dissociation reagent. A standard curve was set (0.30 to 5µg/mL). Absorbance was measured in a 96 well-plate at 656 nm using Synergy™ Mx multi-mode microplate reader (BioTek). Values were normalized by dry weight (mg) and data expressed as µg sGAGs/mg dry weight

7. Statistical analysis

Statistical analyses were performed using GraphPad Prism 8.4.0 software. Normality tests were applied. For DNA and GAGs quantification, as well as for injectability through mechanical assay, two-way ANOVA followed by Sidak's multiple comparisons test was used. As for the remaining data, Kruskal-Wallis test was used followed by Dunn's multiple comparison test.

Chapter IV - Results and discussion

1. Modified decellularization protocols

To develop a product that reaches the market, scalability of the production process is a key step that must be considered in early technology readiness levels (TRLs) - a system that aims to evaluate the state of technological maturity according to nine levels (Cobos et al., 2021).

Considering that the team's startup is currently at TRL 4, i.e. the technology is being validated at lab scale, it was important to consider further scalability of Fetalix's production. Therefore, two modified decellularization protocols were tested, one concerning optimization of protocol duration and another aiming to improve handling capacity (i.e processing a greater amount of tissue simultaneously). In the former, PBS washing time was reduced by 2 hours. In the latter, decellularization was conducted in whole fetal NPs, instead of using 4 mm scaffolds cut transversally in two thinner pieces. Additionally, 24-well plates were replaced by 50 mL falcons and the solutions were changed by decantation instead of pipetting. These alterations reduced the time required to exchange solutions and the total manual procedure, while increasing processing capacity. To increase system performance, a vacuum pump was included to enhance the diffusion of detergents within the samples. The time required for each protocol, including the standard, is shown in Figure 4.1.

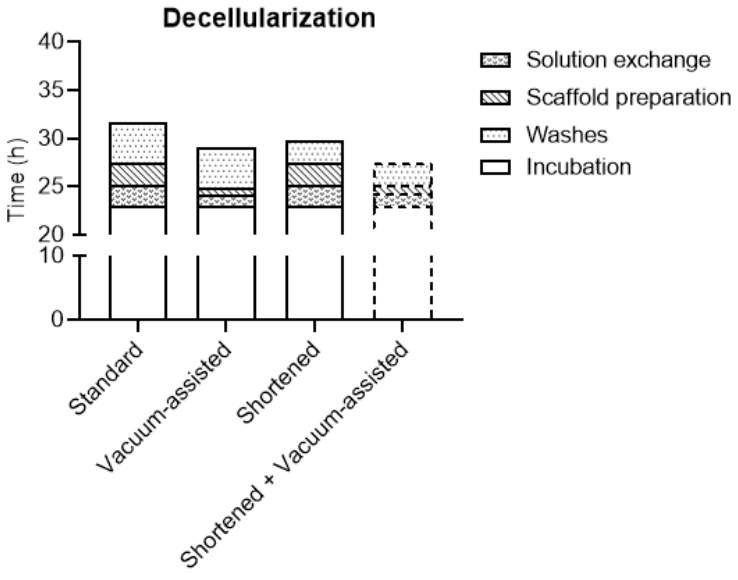

Figure 4.1 – Duration of different decellularization protocols. Evaluation of procedure time according to detergent incubation, PBS washes, preparation of samples and exchanging solutions steps (i.e. pipetting or decanting the solution for its removal and adding the following one). Dashed line indicates expected time as the combination of both protocols was not tested.

Results revealed an 8% reduction in total processing time with the vacuum-assisted protocol, compared to the standard (29.17 h *vs* 31.75 h) and a 6% decrease regarding the shortened process (29.75 h *vs* 31.75 h). Therefore, the vacuum-assisted protocol, besides allowing the decellularization of multiple whole NPs simultaneously and incrementing the amount of starting tissue, resulted in a higher reduction in the protocol duration, even though the difference between both modified protocols was only 40 minutes.

In the future, further refinements and optimization of both protocols to be combined, could result in a reduction of washing time and increase in the number of samples to be processed. As so, the protocol would take a total of 27.17 h, enabling a 14% decrease compared to the standard small-scale protocol.

To evaluate process efficiency of the modified decellularization protocols, both DNA and sGAGs content were assessed. Results are shown in Figure 4.2

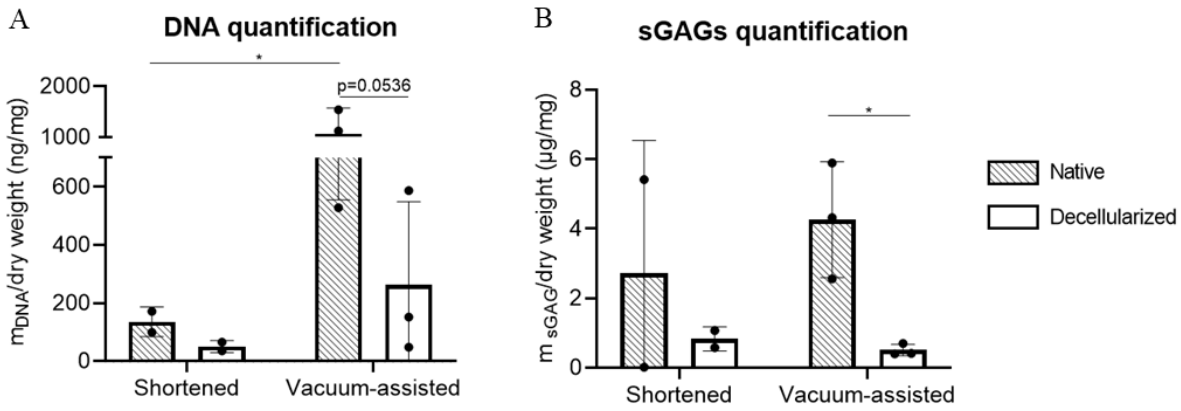

Figure 4.2 – Assessment of modified protocols efficiency. (A) DNA and (B) sGAGs quantification of native and decellularized samples. Two-way ANOVA followed by Sidak's multiple comparisons test. *$p < 0.05$. Error bars represent mean ± SD (n=2-3).

In the shortened decellularization protocol, there was a 63% decrease in DNA content (135.40 ± 51.16 ng/mg of native tissue vs. 50.49 ± 20.92 ng/mg of decellularized tissue). Regarding sGAGs content, there was a 69% reduction (2.72 ± 3.28 µg/mg of native tissue vs. 0.83 ± 0.35 µg/mg of decellularized tissue).

For the vacuum-assisted decellularization protocol, there was a 75% decrease in DNA content (1063.00 ± 508.30 ng/mg of native tissue vs. 262.50 ± 285.90 ng/mg of decellularized tissue). Moreover, the sGAGs quantification revealed an 88% reduction (4.26 ± 1.67 µg/mg of native tissue vs. 0.51 ± 0.17 µg/mg of decellularized tissue).

Considering decellularization efficiency criteria (Crapo et al., 2011), the shortened protocol was slightly above the indicated value of <50ng/mg of dry tissue. Despite one of the samples being within the cut-off value established, this result was not expected, considering that only the PBS washing time was reduced relatively to the previously optimized standard protocol (M. F. Fiordalisi et al., 2022). Performing DAPI on these samples would also be useful to validate the protocol efficacy by a different technique. If this outcome is confirmed, the reduction of PBS washing time may compromise the removal of DNA residues entrapped in the tissue, thereby impairing the viability of this protocol.

With the vacuum-assisted protocol, decellularized samples' DNA content was considerably higher than the decellularization criteria, even though one of the samples presented DNA content within the cut-off.

Of note, there were statistically significant differences when comparing native samples' total DNA levels of each of the protocols tested (135.40 ± 51.16 ng/mg *vs* 1063.00 ± 508.30 ng/mg, for shortened and vacuum-assisted procedures respectively). Samples decellularized following the vacuum-assisted protocol presented an almost 10-fold increase in DNA content. This may reflect inter-animal variability or differences in DNA content between IVDs of different spinal levels, as can be seen from the individual values of native samples, which may affect cell number, negatively impacting solutions diffusion and as a result, protocol efficiency. Additionally, histological analysis of the vacuum-assisted protocol (see Supplementary Figure 6.1) revealed that the NPs were not correctly isolated from the AF. Considering that the AF has a superior cell density, compared to the NP (Pattappa et al., 2012), the presence of this structure alongside animal variability contributed for the difference observed in terms of native samples' DNA content.

In addition, during the implementation of the vacuum-assisted protocol, the incubation with DNAse was not performed under vacuum due to technical limitations. Considering that it was targeted to decellularize whole fetal NPs and that this enzyme is key to break the DNA present in the tissue, any compromise in the solutions' diffusion into the samples may jeopardize DNA removal from the tissue.

Regarding sGAGs content, the reduction observed in both protocols is in line with the previously published data from (M. F. Fiordalisi et al., 2022) using the small-scale protocol. In fact, the sGAGs decrease observed with the modified protocols was not so marked as with the

standard one. In addition, these differences are not even evident in the histological analysis (Supplementary Data 6.1).

In the future, apart from increasing sample number when testing both modified protocols, it would be essential to quantify DNA and sGAGs content when using the standard small-scale decellularization protocol. This would enable the quantitative comparison of the protocols against the control. This add-on would be extremely important, given that the study only analysed the samples' DNA content per wet weight due to different hydration status of samples from distinctive aged donors (M. F. Fiordalisi et al., 2022), contrary to the assay herein performed. Furthermore, there is also variability intrinsic to the operator conducting the protocol, hence the importance of performing the standard protocol.

Despite the variable efficacy of the decellularization procedures, with some refinement and further optimization, the vacuum-assisted protocol combined with the shortened version, may provide a suitable methodology to scale up Fetalix production. In order to understand the viability of the method, future works should focus on repeating NP dissection under the stereomicroscope to ensure total AF removal and controlling samples' height to guarantee proper detergent diffusion and decreased process variability. Moreover, the DNAse treatment should be performed under vacuum, with a pre-heated solution. This can potentially improve DNA removal as a result of more effective tissue diffusion.

2. Biomaterial injectability and particles characterization

Injectability is a key feature to be evaluated, considering the proposed biomaterial's route of administration. As so, prior to the *in vivo* study, it was necessary to ensure a reproducible method to produce a Fetalix formulation passible to be injected through a 30 G needle and, therefore, to be delivered into rat's IVDs.

For that, several ECM griding have been described, namely pestle and mortar-based sample crushing in liquid nitrogen (Bobrova et al., 2022), cryogenic ball milling through impact and friction with the samples (Klak et al., 2021), blade (Aubeux et al., 2016) or burr (Oropeza et al., 2022) grinding, rotatory cutting (T. W. Gilbert et al., 2005), among others.

Fetal NP scaffolds were decellularized, according to the standard protocol, and lyophilized, in order to test different equipment for the milling process, namely Analytical Mill A10 Basic (blade grinder), Pulverisette 23 (ball miller) and 4-Place Mini Bead Mill homogeniser (bead miller). From the equipment tested, only the Analytical Mill A10 Basic and the 4-Place Mini Bead Mill homogeniser were able to mince the samples, considering that Pulverisette 23 was

not able to mill the scaffold, neither dry nor following resuspension in NaCl 0.9% solution (i.e. vehicle). In fact, some samples became flattened and black during the process, which could indicate that the friction between the grinding balls and the samples was too harsh, possible causing sample sintering. As so, these results invalidated the use of this equipment further material characterization.

Particles produced in the Analytical Mill A10 Basic and the 4-Place Mini Bead Mill homogeniser were evaluated by brightfield microscope after resuspension in 0.9% saline solution (see Supplementary Figure 6.2). Results regarding particle's size are shown in Figure 4.3.

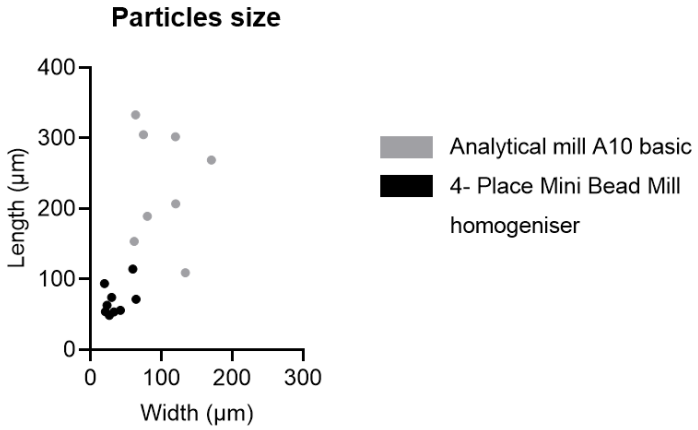

Figure 4.3 – Size analysis of particles produced with two different milling devices. Length and width analysis was conducted using ImageJ, in particles obtained following Analytical mill A10 basic or 4-Place Mini Bead Mill homogenisation.

Brightfield microscopy analysis of the resuspended particles processed with each device revealed that the 4-Place Mini Bead Mill Homogeniser mainly produced particles within 100 µm of width and length, whereas the particles produced in the Analytical Mill A10 basic presented up to 200 µm in width and 350 µm in length. Moreover, the latter produced more heterogeneous particles in size, when compared to the 4-Place Mini Bead Mill homogeniser, as shown by the dispersion presented in the graph.

As so, it was possible to conclude that the 4-Place Mini Bead Mill homogeniser allowed the production of smaller and more homogeneous particles in terms of size. Wu et al. (2020) revealed that heterogeneous particle sizes and irregular geometries lead to inconsistencies in fluidity (Z. Wu et al., 2020). In addition, the 30 G needle to be used for the *in vivo* assay has an inner diameter of 159 µm (Hamilton, n.d.), meaning that resuspended particles should be

smaller than that to avoid clogging, which was only possible with the 4-Place Mini Bead Miller homogeniser.

In parallel, milled lyophilized samples were topographically evaluated by SEM (Figure 4.4).

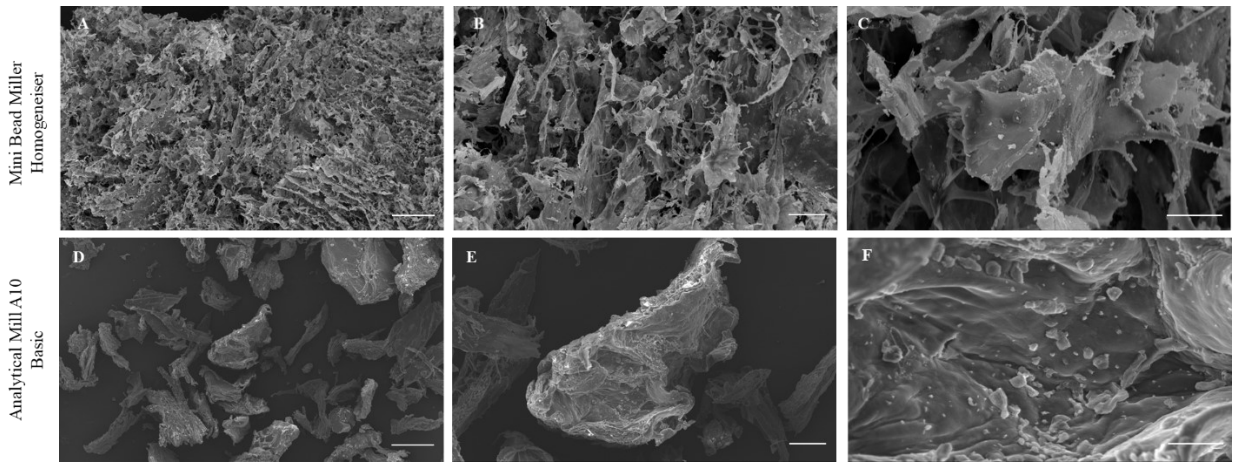

Figure 4.4 – SEM analysis of the particles produced in two different milling devices. (A-C) Particles obtained in the 4-Place Mini Bead Mill Homogeniser. (D-F) Particles obtained in the Analytical Mill A10 Basic. (A and D): 4X, scale bar 200µm; (B and D): 1000X, scale bar 50µm; (C and F): 5000X, scale bar 15µm.

Results showed that the particles produced with the 4-Place Mini Bead Mill homogeniser created a compact structure upon freeze-drying. Moreover, these particles presented a more fibrous and porous structure, a key feature for cell infiltration, adhesion and proliferation (Tanzli et al., 2024). Regarding the use of Analytical Mill A10 Basic, particles were milled dry, thus avoiding agglomerate formation (Figure 4.4D). Such particles exhibited a less porous and blunt morphology, as result from blade milling. As so, despite having a more conserved topography when compared to fetal NPs (Caldeira et al., 2017), these particles presented a less advantageous surface for scaffold repopulation.

Besides the size and morphology obtained by using different methodologies, the 4-Place Mini Bead Mill homogeniser allowed the milling of small quantities of dECM (~5mg), contrarily to the Analytical Mill A10 Basic. Although the aim of this study was to scale up the process, in order to minimize raw material waste, it was decided to use the 4-Place Mini Bead Mill homogeniser for the production of Fetalix, as small quantities of biomaterial were needed for the *in vivo* studies.

After choosing the milling procedure, a preliminary injectability test was performed to determine the number of cycles required to obtain a particle solution injectable through a 30 G needle, considering it was the needle size chosen to perform Fetalix's administration *in vivo*.

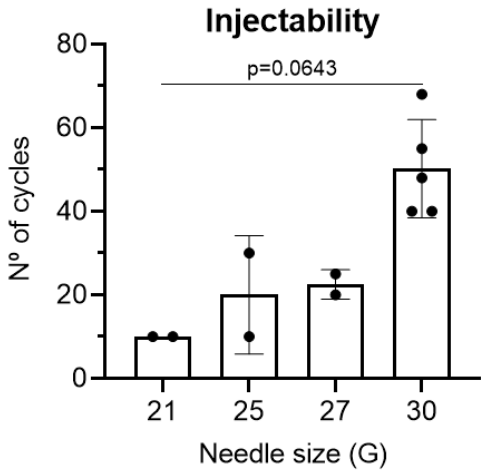

Figure 4.5 – Preliminary injectability assay. The effect of increasing milling cycles on injectability through different needle sizes was explored to determine the number of cycles required to obtain a 30 G injectable solution. Kruskal-Wallis test was used followed by Dunn's multiple comparison test. Error bars represent mean ± SD (n=2-5).

This assay revealed that, by incrementing the number of cycles in the 4-Place Mini Bead Mill Homogeniser, the solution became injectable through smaller needle sizes. Overall, it was possible to achieve a 30G injectable solution with an average of 50 milling cycles. Moreover, during the assay, it was noticed that higher volumes (e.g 800µL vs. 1200 µL) of particle's suspension increased the number of cycles required to achieve injectability (data not shown).

A mechanical compression assay was performed to measure the peak and average forces for injection. These properties are key for injectable biomaterials (Cilurzo et al., 2011), considering that increased injection forces and duration negatively affect patient compliance (Watt et al., 2019). Peak force was extracted from the first peak of the force/strain curves presented in Supplementary Figures 6.3 and 6.4. Average force was obtained by mean force from the strain range 20-60% from the curves, in which the force applied establishes a plateau. Results are shown in Figure 4.6.

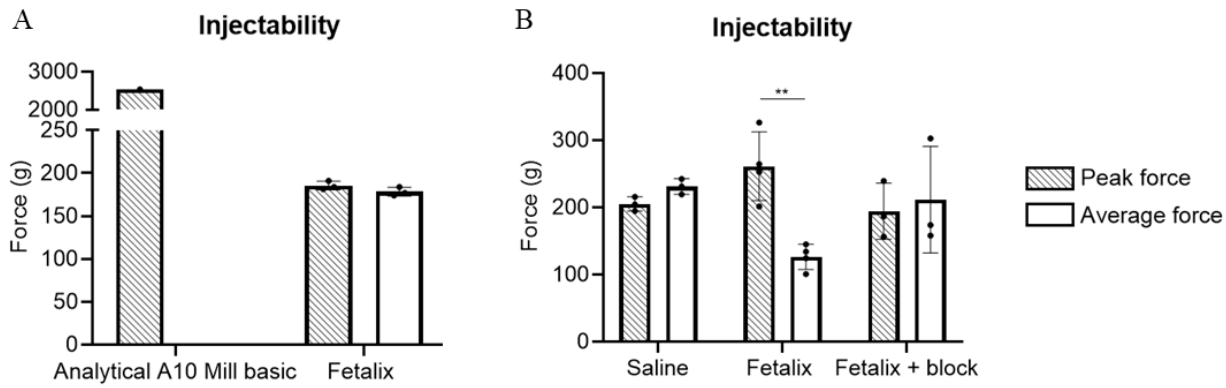

Figure 4.6 – Injectability assay by mechanical compression. (A) 20 G and (B) 30 G needles. In this assay, particles obtained from Analytical A10 Basic mill and 4-Place Mini Bead Mill homogeniser (Fetalix), as well as saline solution, were injected to determine peak and average forces. Fetalix was also injected into a TPU block. Two-way ANOVA followed by Sidak's multiple comparisons test. ** $p < 0.01$. Error bars represent mean ± SD (n=1-4).

Results showed that, in the 20 G needle, the Analytical A10 basic particles clogged and exploded the syringe with an applied force of 2533g, not constituting an injectable particle solution. In contrast, Fetalix was injected through the 20 G needle with a force of 185.5 ± 5.0g and an average force of 178.3 ± 5.0g.

Regarding the 30 G needle, the peak forces obtained were 205.1 ± 10.6g for saline, 261.3 ± 51.3g for Fetalix and 194.3 ± 41.9g for Fetalix in the TPU block. For average forces, the values obtained were 231.1 ± 11.6g, 126.2 ± 18.8g and 211.6 ± 79.4g, respectively.

These results revealed that Fetalix injection with the 30 G needle, in contrast to that with the 20 G, presented a significantly higher peak force than the average force. Since the 30 g needle has a smaller diameter, the biomaterial particles could initially create some resistance to the injection. Given that the 20 G needle has a larger diameter, there was no evidence of particle resistance, as reflected by the similarity between average and peak forces.

Moreover, this pattern was not observed in saline solution, the vehicle used to produce the biomaterial, since the average force was slightly higher than the peak force, despite not statistically significant. This suggests that the force applied during the injection was greater than the force that initiated it. This trend was not expected, since the peak force is generally higher (Cilurzo et al., 2011).

Finally, when Fetalix was injected into the TPU block, the average force was slightly superior than the peak force, despite no statistical differences. This trend was contrary to Fetalix

injection into the air. This suggests that, after initiating the injection, a greater resistance was found, possibly due to particles friction and clogging inside the block.

In Supplementary Figure 6.4A, it was possible to observe a plateau phase in the saline solution injection, suggesting a stable injection force. However, in all the conditions tested for Fetalix, this was not observed, given that several peaks were observed in the expected plateau zone, possibly caused by heterogeneity in particle size or presence of agglomerates. Nevertheless, more instability was observed with the 30 G needle, compared to the 20 G, an expected result given the needle's smaller diameter and inversely proportional resistance. However, the most unstable injection was Fetalix's into the TPU block, given force variations and increased number of peaks. Since the injection was performed into the block, more resistance was found during the administration, unlike the other runs, hence explaining the result.

Several groups have been studied injectability (Cilurzo et al., 2011; Prasetyono et al., 2019; Robinson et al., 2020; Schneider et al., 2018). Robinson *et al.* (2020) revealed that injection forces below 12N, equivalent to ~ 1223g, represent easily injectable materials (Robinson et al., 2020). So, according to this estimate, saline and Fetalix were easily injected through the two needles and, in the case of the latter, as well as into the TPU block.

To assess the mechanical properties of the block and understand whether they resemble those of the rat IVD, a mechanical compression test was conducted. Results are shown in Supplementary Figure 6.4D. From the slopes of the curves, it was possible to obtain two young modulus values, one at an earlier stage of compression (5-10% strain) and one at a final stage (60-70% strain). Values obtained were 36.95 ± 14.60kPa and 259.44 ± 33.33kPa, respectively. Considering that TPU is an elastomer presenting high flexibility (Arnold et al., 2019), it was expected not to have a constant young's modulus (Arnold et al., 2019), as shown in Supplementary Figure 6.4D.

Ho *et al.* (2006) focused on studying the mechanical properties of the rat tail IVDs. In this study, the average young's modulus for the intact IVD was ~160kPa (Ho et al., 2006). Considering that the biomaterial's administration is performed transversally, by puncturing the AF dorsally and then the NP, assessing the mechanical properties as a whole tissue was appropriate. By comparing the values obtained with those found in the literature, it was possible to recognise that the IVD young's modulus was within the range obtained for the TPU block.

Therefore, it was possible to infer that the force applied in Fetalix's administration in the IVD should be within the range obtained for the block. Furthermore, an injured IVD, such as in this study, has a loss of hydrostatic pressure, which facilitates the administration process. So, according to the values described in the literature (Robinson et al., 2020), the injection would be considered easy to administer. In humans, if the range of forces is identical, the biomaterial is also expected to be easily administered. Additionally, as the force applied is reduced, it reduces patient perception, thereby contributing to minimally invasive administration (Watt et al., 2019).

In the future, it would be important to repeat this assay with more replicates, in order to achieve more consistent conclusions. Moreover, it would also be key to conduct a saline injection using 20 G and 30 G needles in the block, as performed for Fetalix, to assess whether the instability pattern is maintained. Additionally, it would also be interesting to assess the injection in a bovine IVD *ex vivo* model.

Lastly, regarding Fetalix production's yield, it was estimated that 3 dNPs are needed for a single injection, considering the mean dry weight (1.16 ± 0.67 mg) (see Supplementary Data Figure 6.5) and pre-processing losses. Therefore, considering that a tail provides 12 dNP scaffolds, in average, an entire tail supplies raw material for 4 human injections.

3. *In vivo* tests

3.1. Histological analysis

After optimization of biomaterial's production, it was possible to proceed with the *in vivo* study. NPs were isolated from fetal IVDs, decellularized according to the standard small-scale protocol and milled to produce a Fetalix's batch to administer *in vivo*. As quality control, native and decellularized samples were paraffin-embedded and sections were evaluated by DAPI staining (for nuclei detection) and AB/PSR with Hematoxylin staining (for PGs, collagen and nuclei identification). This analysis assessed the efficacy of the decellularization procedure in eliminating nuclear components, as well as in preserving or removing ECM components. Results are shown in Figure 4.7.

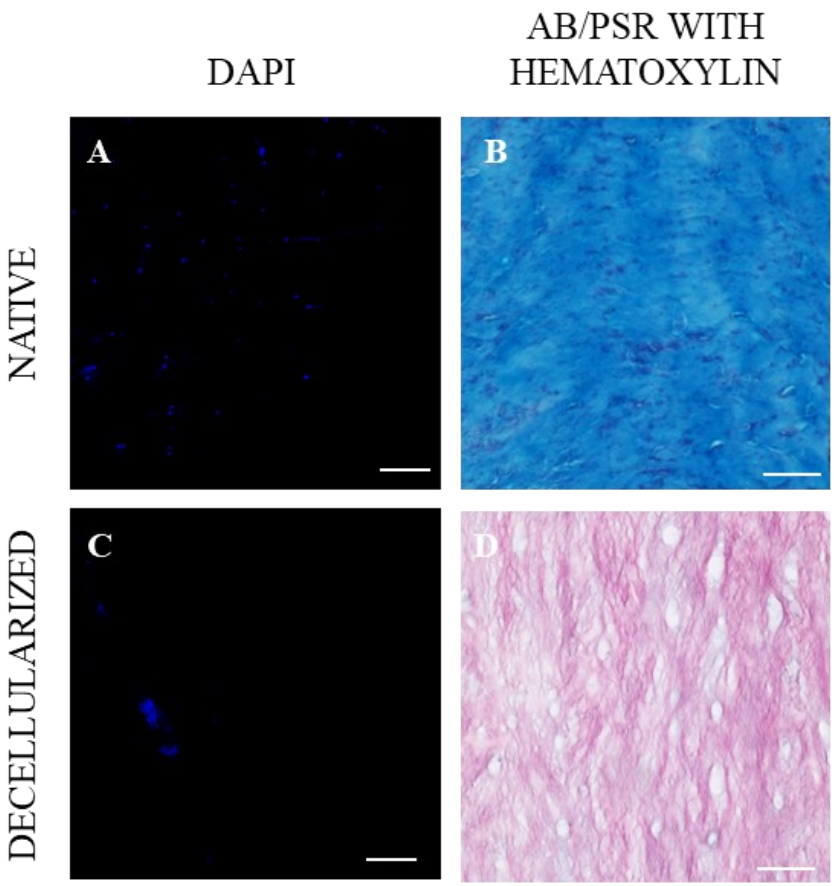

Figure 4.7 – Decellularization efficiency evaluation by histological analysis of native and decellularized NP samples. (A and C): scale bar 100 μm; (B and D): scale bar 25 μm. Red: collagen; blue: GAGs; purple: cell nuclei.

DAPI staining (Figure 4.7 A/C) revealed the presence of nuclei (blue) in native samples, whereas in decellularized scaffolds, there was minimal nuclei content stained in blue, demonstrating the efficacy of the decellularization process in these samples. Noteworthy most of the blue content present in Figure 4.7C is tissue background. Additionally, results shown in Figure 4.7 B/D, regarding AB/PSR with Hematoxylin staining, corroborated these obtained with DAPI. Native samples presented nuclei content, visible in purple, whereas decellularized scaffolds did not show any signs of intact nuclear components. Efficient DNA removal is key to translate a dECM-based biomaterial into the market, considering that DNA residues may contribute to cytotoxicity and adverse effects (Crapo et al., 2011). Therefore, the decellularized samples' quality control assessment revealed that the viability of using these scaffolds for *in vivo* administration.

Regarding ECM components, native samples presented intense blue staining, revealing higher GAG content, an expected result considering NP's composition (Silagi et al., 2018).

Decellularized samples only presented faint red staining, revealing the collagen present in the dECM. This demonstrates that the decellularization protocol used decreased GAG content, while preserving the collagen present in the matrix. This reduction has been reported in literature (Fernandez et al., 2016) as a potential consequence of the use of detergents, considering that SDS is known for damaging collagen integrity and inducing GAGs removal (T. Gilbert et al., 2006). Such effect was expected, considering previous results of the protocol used (M. F. Fiordalisi et al., 2022). Despite a more widely open network compared with that of the native tissue, maintenance of the collagen content was observed constituting a positive outcome, considering that it is a main component of IVD's ECM (Aladin et al., 2010). On the other hand, GAGs loss in decellularized matrices can have a negative impact on the scaffolds' properties, considering that PGs have a major role in hydration and maintenance of osmotic pressure, thereby affecting mechanical properties (X. Liu et al., 2018). However, as previously showed (M. F. Fiordalisi et al., 2022), it is anticipated that endogenous NPs cells that repopulate Fetalix dNP particles will restore GAG expression *in situ*.

Considering the major removal of nuclei content revealed in the histological analysis, it was possible to conclude that the decellularization process was efficient, thus moving forward with the administration of this batch for *in vivo* administration.

3.2. MRI assessment of rat IVDs

In the *in vivo* experiment, rat's IVDs were lesioned and, in two of the groups, administered with Fetalix or saline solution. It is well known that this type of IVD lesion triggers several alterations in the tissue, namely DHI decrease, occurrence of hernias, ECM alterations, increase of inflammatory players, among others (Cunha et al., 2017). In order to assess tissue's features, after sacrifice, MRI scans from rat tails were obtained *ex vivo*, in order to assess IVD's morphology and brightness and extract height and volume metrics. Scans are presented in Figure 4.8.

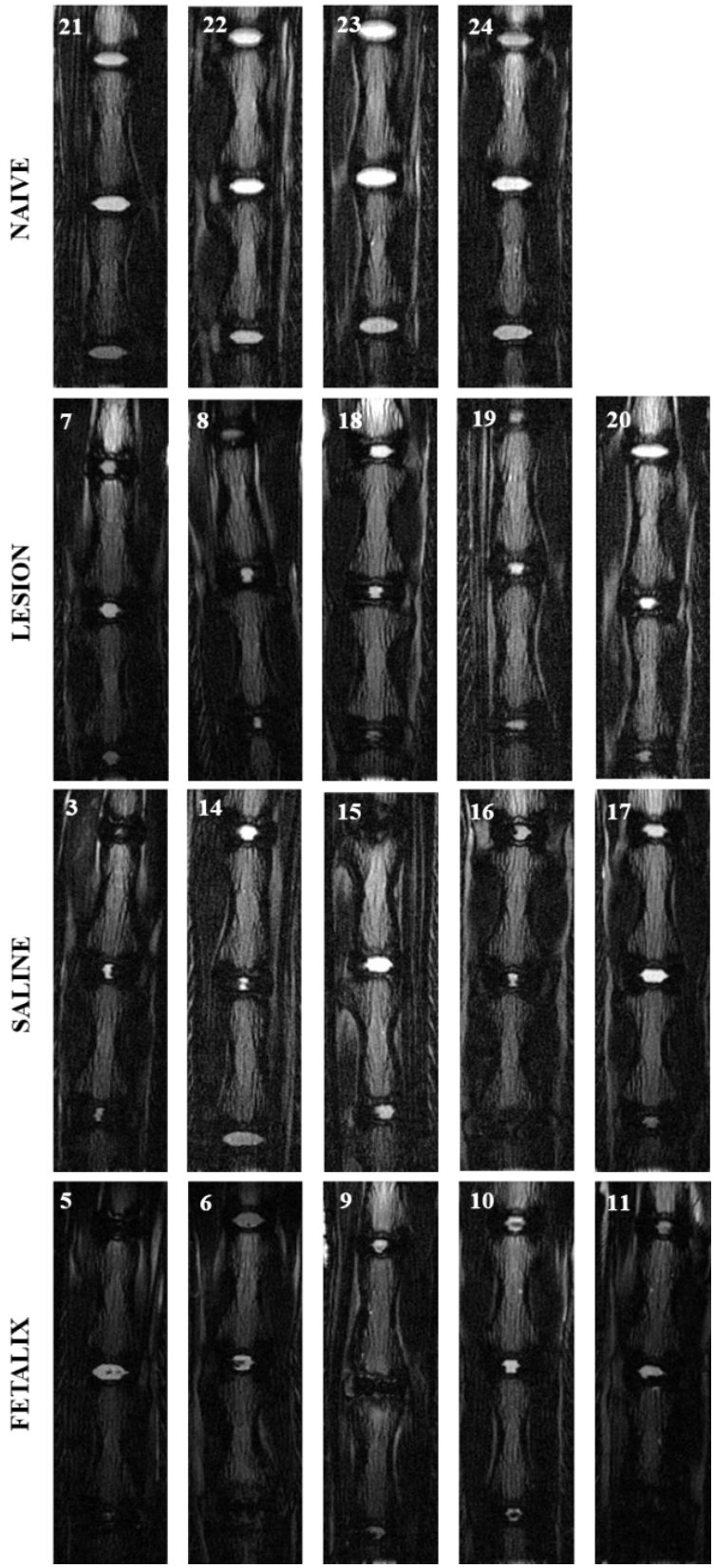

Figure 4.8 – *Ex vivo* rat tails MRI scans. Images represent the IVD, in white. Each scan, from a representative slice, shows three different IVDs, of which top one is Co5/6, the middle is Co6/7 and the bottom one is Co 7/8. The number indicate the animal's ID.

In MRI scans, healthy IVDs appear as hyperintense elliptical structures (da Costa et al., 2020), in which the brightness intensity correlates with high water and PGs content (Pearce et al., 1991) - major NP components. In degenerative stages, characterized by dehydration and PG loss, IVDs appear with decreased intensity in T2 weighted MRI scans (da Costa et al., 2020). Besides brightness decrease, there is also a reduction in IVD's size, as shown elsewhere (Qian et al., 2019).

Our scans revealed it was possible to acquire data from the *ex vivo* tails, despite variability in the acquisition, given the surrounding tissues and anatomical differences between animals. This can be seen, for instance, in naïve animals that were not submitted to any type of procedure. However, in some cases, it appears that on the edges, signal was less intense, affecting IVDs and bones' brightness. Therefore, since it affected both structures, it could be inherent to the acquisition, which hinders an objective brightness' analysis.

All groups in general, compared to naïve, visually exhibited decreased brightness and volume, apart from specific cases in the lesion (animal #20) and saline (animal #15) groups. This suggests that, in general, despite treatment or vehicle administration, animals were negatively impacted by intradiscal lesion executed. Moreover, some cases in the saline and Fetalix groups showed that these animals were even more affected with the administration received, given the particularly reduced IVD volume and brightness, compared to lesion. Noteworthy, there were some black IVDs in the scans, more present in Fetalix (animals #5, 6, 9 and 11), but also in the saline group (animals #15 and 16). Considering that lesion and naïve groups did not present this feature, it suggests that some IVDs were, possibly, severely degenerated following treatment administration.

In parallel, animal #20 (lesion) presented one IVD (Co 5/6) with similar brightness and elliptical morphology comparatively to naïve animals. This suggests that, in this case, the lesion may not have been properly executed. However, in order to verify this, it would be necessary to conduct histological analysis. As this IVD was stored in TRYzol for future experiments, it was not possible to assess it histologically. Interestingly, CO 6/7 from animal #15 (saline) also presented hyperintense brightness, similar to naïve animals, despite not fully preserving its elliptical shape

Considering that MRI scans can present artifacts inherent to the acquisition (Krupa et al., 2015), macroscopic observations can only be corroborated through metrics extraction regarding IVD's height and volume, as well as through histological analysis.

To extract maximum height and area features from rat IVDs in MRI images, an automated analysis algorithm was developed (unpublished data). This enabled the analysis of all MRI slices from each IVD. Despite overall algorithm's accuracy (~ 90%) (see Figure 4.9A and Supplementary Table 6.1), there were slices in which the assessment of two independent evaluators did not match the algorithm's segmentation. As so, those cases were performed manually via ImageJ. Volume values were obtained as described in the Materials and Methods section. Results are shown in Figure 4.9.

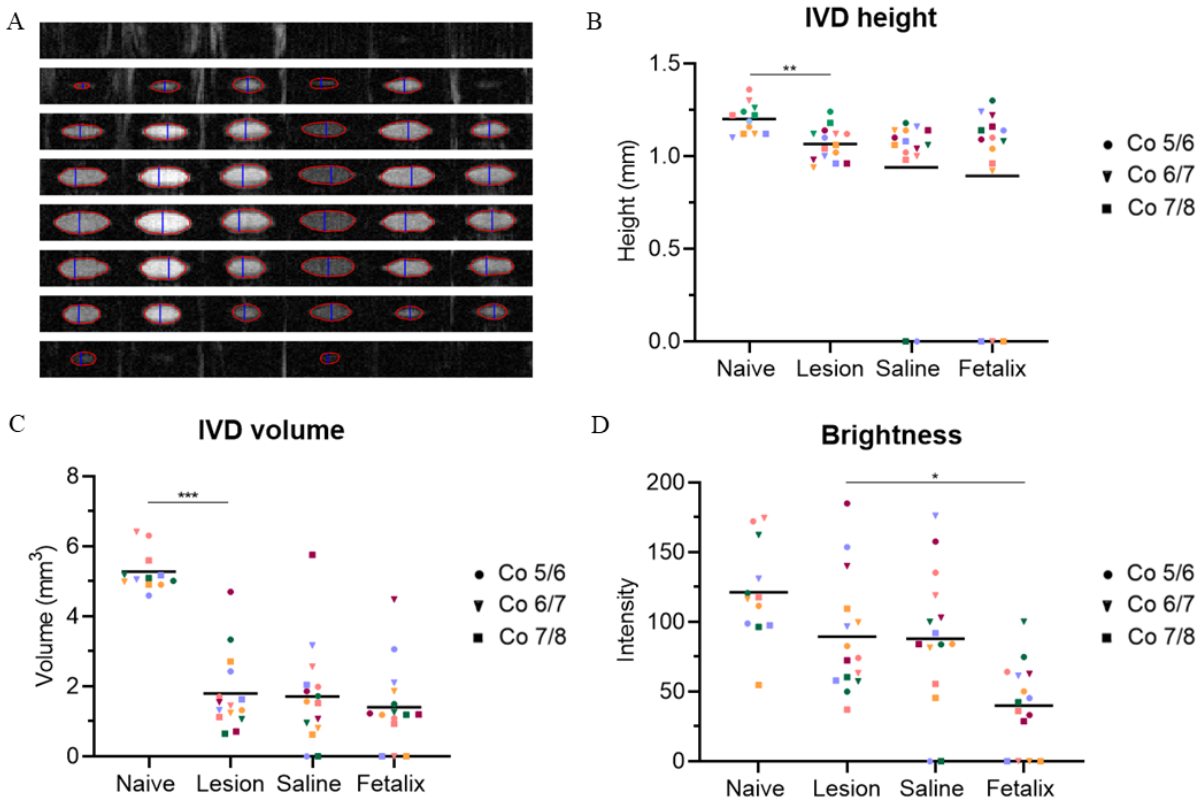

Figure 4.9 – Intervertebral disc's segmentation and metrics extraction. (A) segmentation of IVD's area (red) and height (blue). Each line represents the segmentation in each slice, whereas each column represents an independent IVD. (B) Maximum height, (C) volume and (D) brightness segmentation. Each symbol represents an IVD and each colour indicates a different animal. Kruskal-Wallis test was used followed by Dunn's multiple comparison test. *$p < 0.05$; ** $p < 0.01$; *** $p < 0.001$. Line represents mean (n=12-15).

Results showed that IVD height in the spinal units Co 5/6-7/8 was 1.20 ± 0.08 mm for naïve, which is in line with reference values, thus validating the algorithm. In fact, Sprague Dawley rats described in the literature presented a decreased height of 0.94 ± 0.09 mm for Co 9/10 (Beckstein et al., 2008). This was expected considering that its location is inferior

relatively to the ones evaluated in the study herein presented. Lesioned animals (1.07 ± 0.09 mm) displayed a statistically significant decrease in height, compared to naïve. Both treatment groups (saline, 0.94 ± 0.39 mm and Fetalix, 0.89 ± 0.47 mm) did not exhibit statistically significant differences compared to lesion despite a lower height average, as a result of presenting completely dark discs with no measurable height values.

A similar trend was obtained for volume analysis, with a statistically significant decrease for the lesion (1.80 ± 1.09 mm^3) compared to naïve (5.28 ± 0.56 mm^3), but no statistically significant differences between lesion and treatment (saline, 1.71 ± 1.42 mm^3 and Fetalix, 1.41 ± 1.18 mm^3) groups.

Regarding brightness analysis, naïve animals presented an intensity of 121.20 ± 34.99. Despite a visible intensity decrease in all groups compared to naïve, namely lesion (89.37 ± 42.09), saline (87.92 ± 49.77) and Fetalix (39.99 ± 30.63). The only statistically significant difference observed was between Fetalix treated and lesioned animals, the latter having increased brightness.

Moreover, results showed that most of lesioned animals maintain the tendency of upper IVDs (Co 5/6) being morphologically higher and larger than lower ones (Co 7/8) (see Supplementary Figure 6.6). Interestingly, animals administered with saline solution did not show this pattern. In fact, they exhibited a different trend for height and volume. Finally, Fetalix group showed the former trend for height (higher Co 5/6), but not for volume (larger Co 7/8).

It was possible to conclude that the lesion induced, as well as the administrations, had more impact in the IVDs' volume (66-73% difference compared to naïve), than in their height (11-26% difference compared to naïve), which corroborates macroscopic evaluation of the MRI scans. Moreover, results also revealed that Fetalix had a more adverse effect in the IVD compared to the lesioned group, particularly in terms of brightness decay, suggesting dehydration and PGs loss. Thus, the biomaterial was not capable of restoring the IVD structural features and hydration status, presenting a more severe degenerative state.

MRI scans also unveiled the presence of hernias (Figure 4.10).

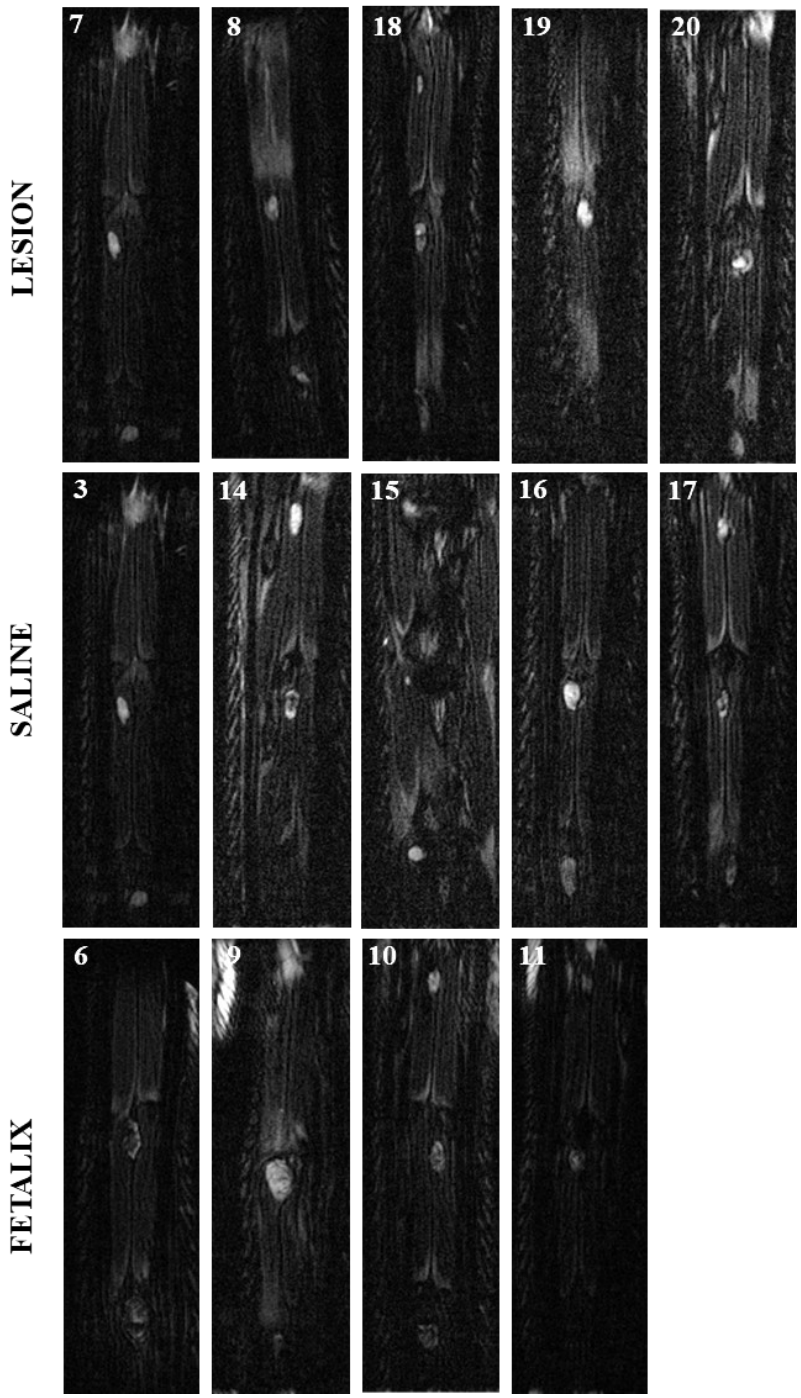

Figure 4.10 – Hernias visible in MRI scans. Each image shows a representative slice per hernia. The numbers indicate the animal's ID.

MRI scans presented hernias in the first slices acquired. Considering that the acquisition was conducted in the dorsal to the ventral region of the tail, the hernias were observed in dorsal part. Since it is known that needle punctures damages AF's structure (Cunha et al., 2017; B. Han et al., 2008) and both injury and administration were performed in that region, hernia presence was anticipated.

Upon analysing the images, no naïve animals exhibited hernias, a result in accordance with the expectations considering that these were healthy non-intervened animals. On the other hand, all injured and administered animals presented hernias, despite their morphological and incidence differences. However, there is an exception. Interestingly, one animal treated with Fetalix (animal #5) did not present any hernia. Given disparity between hernias morphology, histological analysis would be important for a better comprehension of the hernia's content and shape.

In contrast to IVDs, hernias' volume was quantified manually by identifying the region of interest on ImageJ, since the algorithm was developed to identify IVDs. Results are shown in Figure 4.11.

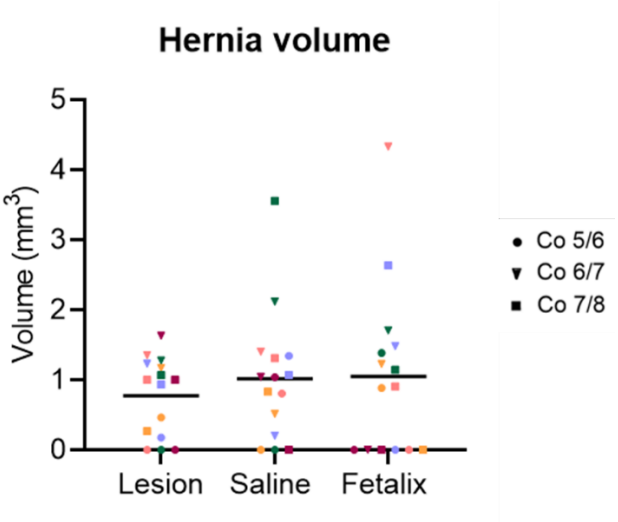

Figure 4.11 – Hernias' volume through MRI assessment. Each symbol represents an IVD and each colour represent an animal. Kruskal-Wallis test was used followed by Dunn's multiple comparison test. Line represents mean (n=15).

All three groups, lesion (0.77 ± 0.56 mm^3), saline (1.02 ± 0.93 mm^3) and Fetalix (1.05 ± 1.22 mm^3), presented widely disperse hernia volumes. Although the lesion and saline groups showed, in general, smaller hernias, the group treated with Fetalix presented a decreased hernia incidence, as only 9 hernias were detected, whereas 12 were detected in the other groups. Interestingly, it was possible to observe that there was an increase in hernia incidence (14 hernias out of 15 IVDs) in the central zone (Co 6/7), followed by Co 7/8 with (12 hernias out of 15 IVDs) and 5/6 with (7 hernias out of 15 IVDs).

Of note, when comparing the IVDs and hernias' volumes, animals treated with Fetalix, which showed reduced IVD volume, presented bigger hernias. As these animals were

administered with biomaterial, hernia volume could be taking into account not only NP extrusion but also the biomaterial injected.

Hernia volume results obtained for the lesioned group are notably higher comparatively with literature values (Cunha et al., 2017). This suggests that either the procedure performed in this assay led to the occurrence of bigger hernias or it was a technical bias. Due to artifacts and differences in hernia content and shape, hernia volume extracted from MRI scans should be validated by histology.

Cunha *et al.* (2017) revealed that hernias spontaneously regress over time by presenting a reduction in hernia volume from 2 to 6 weeks post-lesion, as well as in degeneration severity (Cunha et al., 2017). This suggests that, in our study, the administration was performed in a highly severe state of injury, since it was performed at 2 weeks post-lesion. Nevertheless, as only one time point was evaluated and tail images were only acquired after sacrifice, it was not possible to follow hernia regression with time. Therefore, a longitudinal study with different administration timepoints would be key to understand hernia resorption and the effects of Fetalix at different degeneration stages.

3.3. Histological analysis

Histological assessment of IVD sections was performed, in order to analyse tissue's morphology and composition, as well as to validate MRI results regarding hernia volume, and to conduct histological grading score assessment. Unfortunately, due to constraints in the histology service and time limitations, it was only possible to obtain sections of 7 IVDs, namely #3 Co 7/8 (saline), #5 Co 6/7 (Fetalix), #7 Co 6/7 (lesion), #9 Co 6/7 (Fetalix), #11 Co 7/8 (Fetalix), #14 Co 7/8 (saline) and #23 Co 6/7 (naïve). This set of samples comprised more animals from the saline and Fetalix groups, as naive and lesioned animals have been already well described in the literature (Cunha et al., 2017). As so, preference was given to the administered groups.

Sections were stained with AB/PSR, in order to assess the tissue's structure, ECM composition, as well as to identify the hernias present and quantify volume. Results are shown in Figure 4.12.

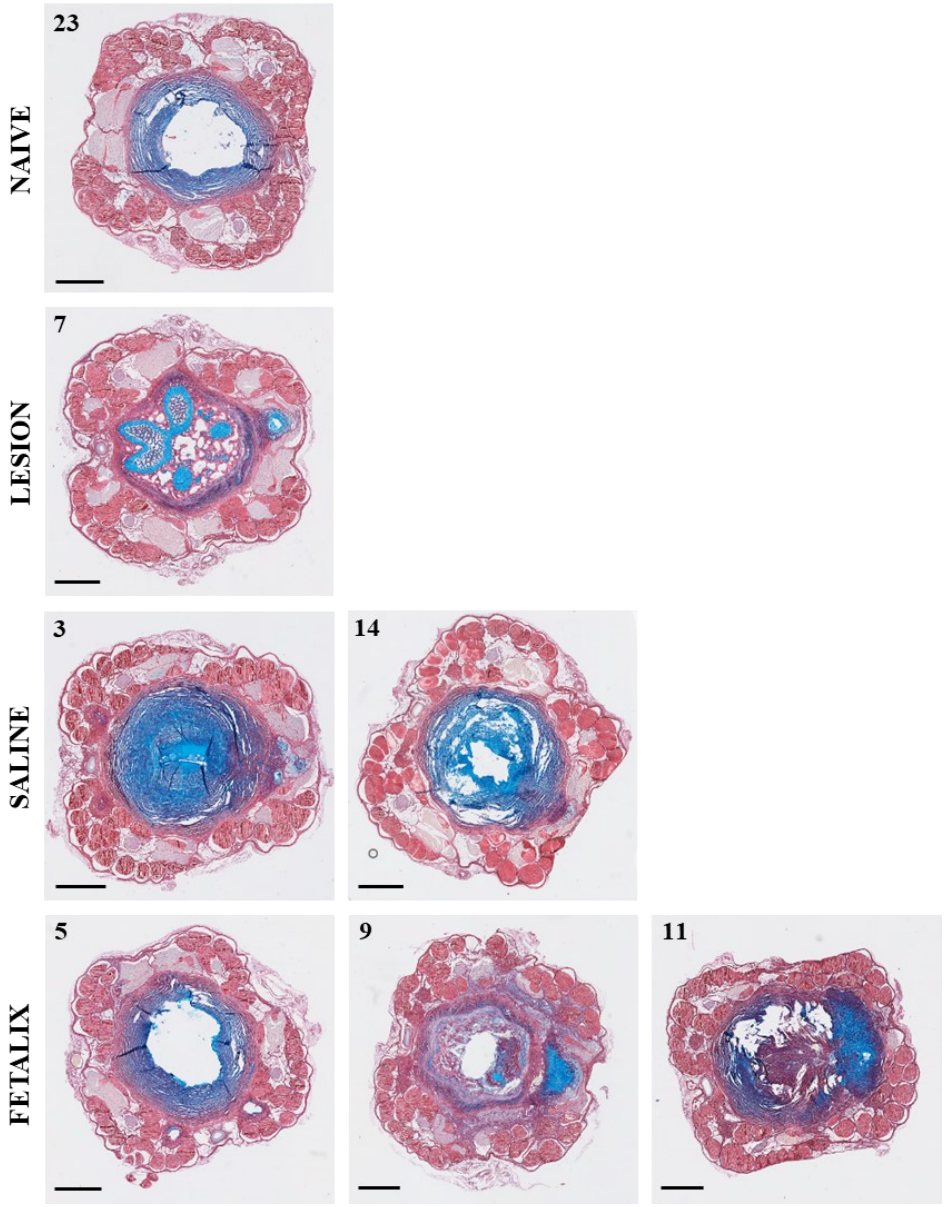

Figure 4.12 – Rat tails' cross section. AB/PSR histological images of a representative section of the tail, presenting the IVDs, muscle and hernias. The number indicate the animal's ID. Scale bar: 800 μm.

Problems were faced when sectioning most samples from the paraffin blocks. For that, some portions of the NP material are absent from several sections, which is especially evident in the naïve NP, which was expected to have an intact structure, given that this animal did not undergo any procedure. Moreover, all sections from animal #7 (lesion) presented remnants of bone's growth plate.

Nevertheless, all animals except #23 (naïve) and #5 (Fetalix) presented hernias. Despite being an expected result for naïve samples, histological data from the group administered with Fetalix validated MRI information, which also indicated hernia absence in animal #5.

In turn, hernia size was different between animals. Qualitative data suggests that sections from lesion and saline hernias presented similar areas. Despite sections' poor quality, results showed an AF and NP disruption (particularly in animals #9 and 11), suggesting NP extrusion, likewise in the lesioned IVD. Overall, hernias presented morphological similarities with literature (Cunha et al., 2017).

Hernia volumes were quantified manually by ImageJ in all the section obtained from the histology service. Results regarding hernia volume quantification are shown in figure 4.13.

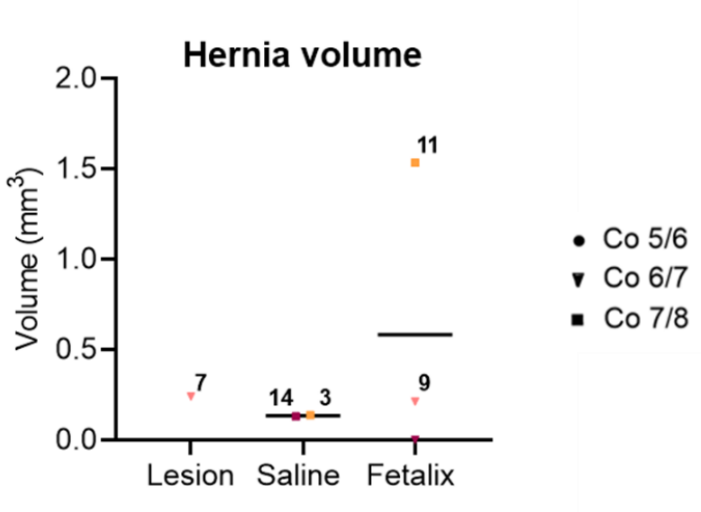

Figure 4.13 – Hernias' volumes obtained through histological analysis. Each symbol represents an IVD and each colour represent an animal. Numbers indicate the animal's ID. Kruskal-Wallis test was used followed by Dunn's multiple comparison test. Line represents mean (n=1-3).

Hernia volumes calculated from histological sections were of 0.241 mm^3 for lesion, 0.135 ± 0.005 mm^3 for saline and 0.583 ± 0.832 mm^3 for Fetalix treated IVDs. All animals displayed similar volumes, except for animal #11 that presented a much larger hernia volume (0.1.535 mm^3). Rat #5 did not present hernia.

Comparing these values to those obtained from MRI quantification, there was a considerable disparity between both evaluations. Considering that the IVDs' height was around 1 mm and only a few 5 µm slides were extracted from the IVDs, these results were not representative of the whole IVD and a big portion of it must have been lost, potentially biasing

hernia volume analysis. Nevertheless, these values are within literature reports (Cunha et al., 2017). However, as described above, the hernias of these animals were macroscopically larger, but only a few slides were analysed, decreasing the quantification accuracy.

Besides this quantification, degeneration grading score was performed according to criteria previously established (B. Han et al., 2008). Given the sectioning issues reported above, on some slides the NP was not present. As so, it was not possible to evaluate its cellularity and morphology. The IVDs were scored according to the AF and the remaining border between this structure and the NP. As they were only evaluated in three out of five categories, the minimum score is 3 (healthy) and the maximum is 9 (severely degenerated). Results are shown in Figure 4.14.

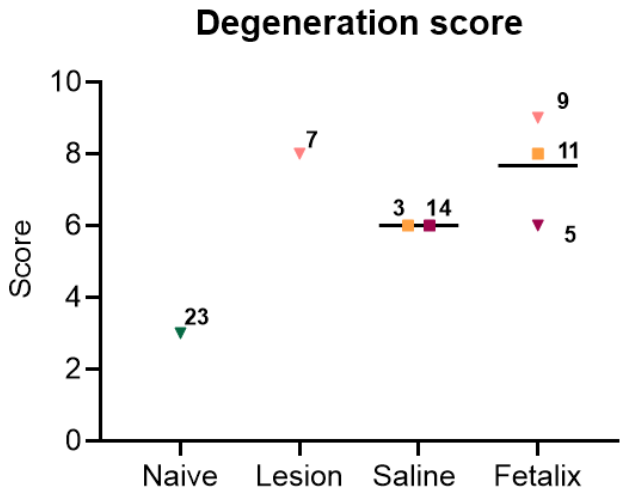

Figure 4.14 – IVD's degeneration grading score. The score attributed was according to AF's cellularity and morphology and the NP/AF interface. Numbers indicate the animal's ID. Kruskal-Wallis test was used followed by Dunn's multiple comparison test. Line represents mean (n=1-3).

The average degeneration scores attributed were 3 for naïve, 8 for lesion, 6 for saline and 7.67 ± 1.53 for Fetalix. The minimum score was given to naïve and represented a healthy IVD. The remaining animals presented higher scores, compared to naïve.

None of the animals, except #23, was scored with 1 (lowest score) in, at least, one of the categories. This means all other IVDs were scored with 2 or 3, indicating alterations in the features evaluated. Animal #7 (lesioned) did not present maximum degenerative score within the features evaluated, as previously described (Cunha et al., 2017). In fact, animal #9 (Fetalix) was the only one attributed with maximum score.

The two evaluated samples from the saline group (#3 and 14) presented a lower score, compared to lesion and Fetalix, thus suggesting less severe degeneration states. Some IVD reports suggest that saline solution's administration may contribute to dilute the inflammatory mediators (Gilbert et al., 2016), thereby neutralizing the environment and slowing down the degenerative cascade (Fukusaki et al., 1998).

Interestingly, the three animals treated with Fetalix herein evaluated by histology (#3, 9 and 11) exhibited differences in the grading score, suggesting variations in the degenerative state. Moreover, only animal #9 achieved maximum score, indicating severe IVD degeneration. This result was in line with MRI scan, in which this IVD appeared black, corroborating previously analysis.

In parallel, animals #5 Co 6/7 and #14 Co 7/8, which presented the same grading score, had also been reported to have similar morphology and brightness on the MRI scans, further validating the data.

These results reveal that 2 of the 3 animals assessed by histology, from Fetalix treatment group, were not capable of slowing or reversing the degenerative cascade. Nevertheless, one of the animals in the group did not exhibit herniation and presented lower degenerative score when compared to the lesioned animal.

Several limitations were identified in this part of the study: sectioning was imperfect, only 7 IVDs were evaluated corresponding to 15% of the total discs to analyse. As so, these preliminary conclusions should be taken cautiously, given that data might not be representative.

Overall, despite hernia volume quantification, MRI results were validated by histological analysis, thereby supporting the previously stated conclusions. In the future, it would be interesting to test different treatment timepoints and concentrations, as well as a new formulation of Fetalix, namely as an injectable hydrogel, not only to deliver the fetal NP dECM with pro-regenerative cues but also to provide mechanical properties to the tissue, while promoting increased tissue hydration. Eventually, it could be also combined with MSCs to potentiate their effect and promote cell survival.

3.4. Behavioural assay

IVD degeneration is characterized by an increase in the number of nociceptive receptors, which are sensitive to mechanical stimulation. The presence of inflammatory mediators also stimulates them (Diwan et al., 2023). So, considering that the main goal of this work was to

investigate Fetalix's potential to restore the IVD in order to tackle LBP, a pain assessment was key to understand the therapeutic outcome of the fetal-inspired biomaterial.

For that, before sacrifice, animals were submitted to a Von Frey behavioural assay. This test is based on hindpaw mechanical pressure for assessing LBP (Mosley et al., 2017) and is commonly used in IVD degeneration models (Evashwick-Rogler et al., 2018; Lai et al., 2015). Results are shown in Figure 4.15.

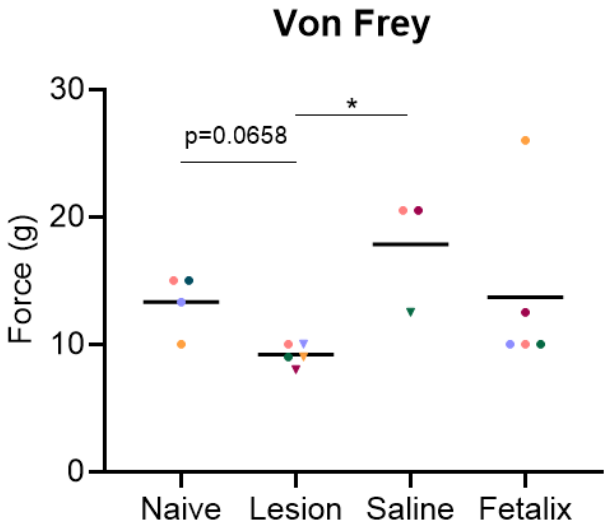

Figure 4.15 – Behavioural assay by Von Frey. Triangles represent animals with less habituation. Caliber of the filament represented in grams (g). Kruskal-Wallis test was used followed by Dunn's multiple comparison test. *p<0.05. Line represents mean (n=3-5).

Results showed that naïve animals that did not undergo any type of procedure presented a sensitivity to mechanical stimuli of 13.33 ± 2.36g. Lesioned animals responded to filaments of smaller calibre (9.20 ± 0.34g), indicating more sensitivity to mechanical pressure, compared to naïve. Regarding the group administrated with saline solution, animals responded positively to larger calibre filaments (17.83 ± 4.62g), compared to both naïve and lesion, thus suggesting an even minor sensitivity to mechanical stimuli than naïve animals. Finally, animals administered with Fetalix reacted positively to filaments similar to naïve (13.70 ± 6.96g), presenting decreased sensitivity to mechanical pressure compared to lesion. Nevertheless, the only statistically significant difference in sensitivity reported was between lesioned and saline.

Contrarily to lumbar models, there is lack of information regarding pain assessment in caudal IVD degeneration, since the tissue is almost aneural (Barcellona et al., 2022). Despite not being described as painful or invasive model (Cunha et al., 2017), the force applied value

in the lesioned group (i.e sensitivity to mechanical stimuli) was expected, considering that the animals were submitted to a caudal injury with a 21G needle, inducing some level of discomfort. Kim *et al.* (2011) showed that rats that undergone lumbar puncture with microsurgical drills (equivalent to 21 G and 25 G needles) presented pressure hyperalgesia, evaluated by the vocalization thresholds in applied pressure assays (J.-S. Kim et al., 2011). Despite using a different behavioural assay and in another spinal region, this study provides information regarding pain in this type of models, corroborating the result obtained. Moreover, since no pain tests had previously been conducted in this model, this study provided the first behavioural results, showing that the model induces some degree of sensitivity in lesioned animals compared to naïve, as they became more susceptible to pain.

Regarding the group administered with saline solution, not only did animals respond to larger calibre filaments than lesion but also seem higher than naïve, indicating that, despite lesion induction, they presented less sensitivity to mechanical stimuli than the baseline. Pain relief (up to 3 months) with saline injection compared to other treatments has previously been reported in osteoarthritis studies, potentially due to cooling or elution (Colen et al., 2012; Rosseland et al., 2004). Considering that saline solution may neutralize the harsh environment typical of degeneration (Fukusaki et al., 1998; Gilbert et al., 2016), intradiscal saline administration may contribute to reduced sensitivity to mechanical pressure stimuli due to washing out key players of inflammation. A possible reason for the hypoalgesia of the saline group compared to naïve may have been what happens when a needle injects medication too quickly, eventually causing nerve damage. In fact, this has been shown with anaesthetic injection (Farber et al., 2013; Lim et al., 2015; Rayan et al., 1985).

Finally, the group administered with Fetalix presented sensitivity to pressure stimuli similar to naïve animals, which suggests that, despite not restoring IVD structure, these animals were able to restore their sensitivity within four weeks of administration, a positive outcome for a therapy directly towards LBP patients. Interestingly, animal #11, that presented a larger hernia, showed less sensitivity to mechanical stimuli and reacted positively to the test in larger calibre filaments, compared to the other animals in the group.

Some additional assays must be performed in the future to clarify the mechanism behind Fetalix, namely immunohistochemistry to identify neural ingrowth by nerve fiber marker (e.g PGP9.5) (Miyagi et al., 2014) and neovessel formation (e.g VEGF-1). Moreover, considering that there is one IVD still stored per animal, it is possible to conduct high throughput analysis

(either transcriptomics and proteomics) in the IVDs, in order to check for the effect on pain or axon formation pathways. Indeed, unpublished data suggests that fetal collagens present in Fetalix might be able to modulate axonal projection.

The behavioural effect observed may have a similar mechanics to ozone therapy, a treatment described for IVD herniation. When administered at lower concentrations, it alleviates the inflammatory cascade (Elmounedi et al., 2024), decrease IVD volume due to dehydration (Murphy et al., 2016), caused by GAGs fragmentation. In this case, decreased volume results in reduction of intradiscal pressure, alleviating pain by nerves decompression (Murphy et al., 2016). Considering that IVDs treated with Fetalix had a reduced volume, lower tissue pressure could alleviate pain, as animals' sensitivity to mechanical stimuli was similar to naïve animals.

Overall, these results led to the reflection, already raised by the scientific community (Mekhail et al., 2021), of whether saline solution is a proper vehicle for this assay, given the elution of the degenerative mediators that could lead to misinterpretation of the results.

Chapter V – General conclusion

As the prevalence of LBP in the population is growing, mostly caused by IVD degeneration, and given the lack of effective solutions, there is an urgent need to develop novel strategies to slow or halt the degenerative cascade of the tissue. Therefore, this thesis aimed to validate the potential of Fetalix – the first fetal-inspired biomaterial to treat LBP – in an *in vivo* rat model. Additionally, it intended to assess the biomaterial production process's scalability, a crucial step towards reaching the market.

The modified decellularization protocols (shortened and vacuum-assisted version) aimed at process scalability, achieved an 8% and 6% total time reduction, respectively, compared to the standard procedure. Nevertheless, there is also room for improvement in terms of maintenance of product properties and performance, as well as reproducibility. In fact, concerning DNA removal, further optimization is needed to achieve a systematic reduction of <50ng dsDNA per mg ECM dry weight. Concerning GAGs decrease, despite already described in the literature (M. F. Fiordalisi et al., 2022), several strategies can be envisioned to overcome this issue. Nevertheless, cells (either exogenous or endogenous) seeded on the dECM-based scaffolds are expected to produce GAGs *in situ,* thus compensating for their loss with decellularization, as our group has shown with NP cell repopulation (M. F. Fiordalisi et al., 2022).

As for the biomaterial's production through dNP grinding and particle characterization, both 4-Place Mini Bead Mill homogeniser and Analytical Mill A10 Basic were able to mill dECM scaffolds. Despite resulting in less conserved and more irregular topography, the 4-Place Mini Bead Mill homogeniser enabled the production of smaller but more porous particles, favouring injectability and cell infiltration, thus being chosen for Fetalix production. 50 milling cycles were required to obtain an injectable solution on a 30 G needle, a crucial step to enable Fetalix's administration in the rat model of IVD degeneration understudy.

A mechanical compression assay was adapted to obtain quantitative injection force measurements. Values around 200g extrapolated from this test were way below those representing easily injectable forces (< 1223 g) (Robinson et al., 2020), independently of injecting it into the TPU block (with analogous biomechanical properties to the rat IVD) or not.

Due to several still unanswered issues regarding the modified protocols, for the *in vivo* study, NPs were decellularized according to the standard small-scale protocol. dNP histological

analysis was performed as a quality control and revealed an efficient decellularization process, indicating that scaffolds were viable for *in vivo* administration.

MRI analysis and the automated algorithm developed to extract rat IVD's height and area were validated by histology (in the limited samples analysed), in spite of discrepancy in (larger) hernia volume and technical issues in paraffin sectioning. Fetalix administration induced a reduction in IVD height, volume and brightness, compared to the other groups. However, despite displaying larger hernia compared to lesion and saline groups, possibly due to NP protrusion alongside biomaterial extravasation, animals administered with Fetalix, presented decreased hernia incidence. This was in line with the trend observed by histological analysis of the few selected samples and of the possible measurable features. In fact, 2/3 Fetalix injected IVDs presented a similar or higher grading score than the lesioned one, but 1/3 (animal #5), which did not show signs of herniation, had a lower score than lesion.

Von Frey behavioural test showed that animals administered with Fetalix presented mechanical sensitivity levels similar to naïve and decreased compared to lesioned animals. This suggests these animals were able to restore sensitivity and alleviate pain, despite having a less obvious effect on tissue regeneration. In fact, ozone therapy, a proposed IVD therapy has been shown to act by breaking down GAGs, thus dehydrating the NP, reducing disc volume and subsequently relieving nerve root compression (Murphy et al., 2016). Unexpectedly, animals treated with saline solution, reduced sensitivity to mechanical stimuli compared to all groups (including naïve), potentially due to a neutralizing effect in the inflammatory environment (Fukusaki et al., 1998; H. T. J. Gilbert et al., 2016), suggesting this might not be an adequate control.

Overall, the main objectives of the thesis were achieved. Nevertheless, there are some limitations to this work, including the number of samples in the decellularization, the absence of some important conditions in the injectability test and the impossibility to assess all the histological samples.

In conclusion, this thesis enabled the development of an easily injectable formulation of Fetalix and the first steps towards scalable production. Furthermore, despite not slowing or reversing IVD degeneration, it allowed restoration of sensitivity levels similar to naive, constituting a positive therapeutic outcome. Therefore, it was possible to obtain the first *in vivo* data regarding Fetalix, thereby enabling formulation refinements and a more comprehensive *in vivo* study to be conducted in the future.

Chapter VI – Future work

This thesis assessed key aspects regarding Fetalix development, namely its characterization, production, scalability of the decellularization process and the *in vivo* potential to regenerate the IVD and tackle LBP. All the knowledge obtained will be fundamental for further optimizing both formulation and process scalability. Importantly, some of the animals treated with the biomaterial showed normal sensitivity levels, a positive therapeutic outcome that should be more thoroughly explored hereafter. As so, future studies will be necessary to answer some core questions.

First of all, regarding the modified decellularization protocols, it would be necessary to optimize and refine the procedures, in order to achieve a systematic DNA removal. Besides increasing the number of samples and comparing quantitatively with the standard protocol, future work should focus on a) standardizing NP isolation with no AF fragments attached; b) controlling samples' height to guarantee proper detergent diffusion and decreased process variability; c) performing DNAse treatment under vacuum to boost decellularization efficacy. These accomplishments represent a relevant advance towards automation and standardization envision industrial scale production in large bioreactors. To surpass GAG decrease, a possible strategy could be to supplement dECM with chondroitin sulphate, as described by (Zhou et al., 2018).

As for injectability, it would be crucial to add some important conditions, particularly saline solution through a 20 G needle and 30G needle into the TPU block, in order compare Fetalix to adequate controls. Additionally, it would be of interest to test injectability using a bovine or human IVD *ex vivo*, a relevant environment for the study. Syringeability (solution aspiration) studies would also be valuable, considering that if the product reaches the market, it must be aspirated in order to be administered to the patient.

Finally, regarding the *in vivo* study, future work should focus on: a) completing the IVDs histological analysis; b) assessing biomaterial biocompatibility through kidney, liver and spleen analysis; c) investigating vascularization and innervation and d) performing highthroughput transcriptomic or genomic analysis on the collected tissue to unveil the mechanism behind the observed effect. *In vivo* study, it would be advantageous to conduct a longitudinal assessment to understand the efficacy of Fetalix treatment over time and at different disease stages. Importantly, different Fetalix concentrations should be tested, as well assessing biomaterial's preventive effect.

Chapter VI - Supplementary data

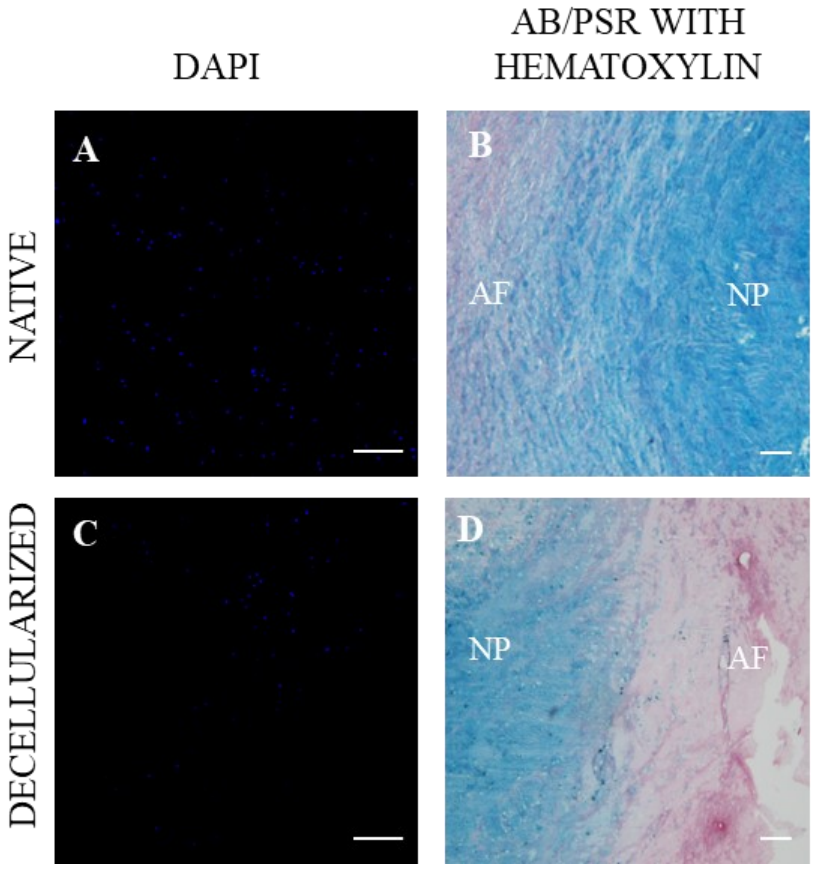

Figure 6.1 – Histological analysis of the vacuum-assisted decellularization protocol. (A and C): scale bar 100 µm; (B and D): scale bar 50 µm. NP: nucleus pulposus; AF: annulus fibrosus.

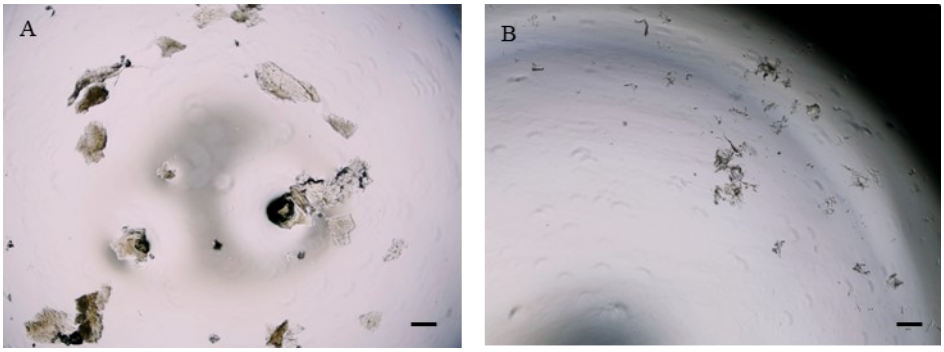

Figure 6.2 – Microscopic images of particles obtained in two different milling equipment. (A) Analytical A10 Basic mill and (B) 4-Place Mini Bead Mill homogeniser. Scale bar 200 µm.

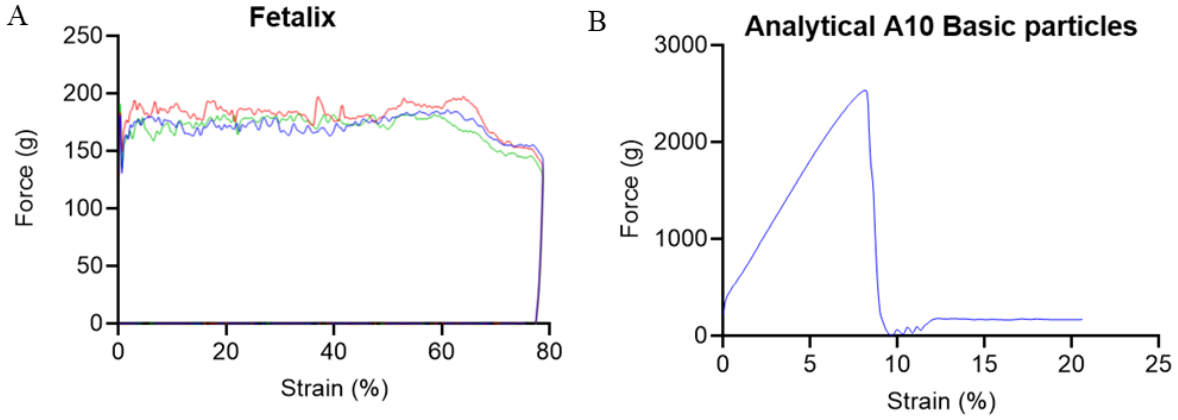

Figure 6.3 – Injectability assay through a 20G needle. (A) Fetalix and (B) Analytical 10 Basic particles force/strain curves.

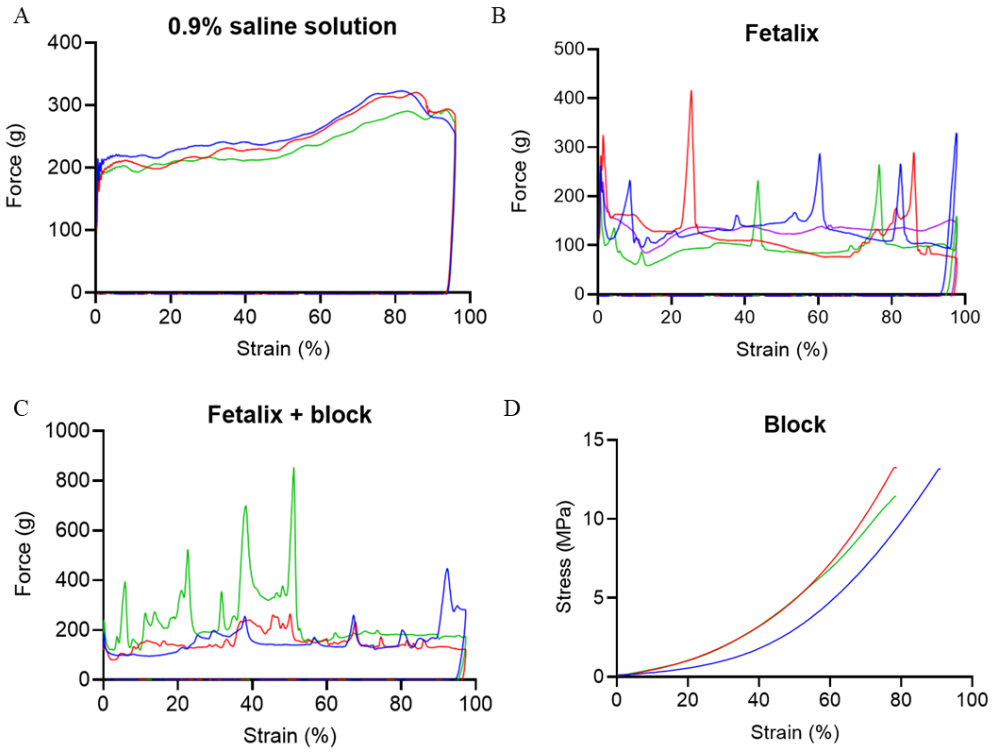

Figure 6.4 – Injectability assay through a 30G needle. (A) Saline, (B) Fetalix and (C) and Fetalix injected into TPU block force/strain curves. (D) Block's mechanical properties evaluation by stress/strain curve.

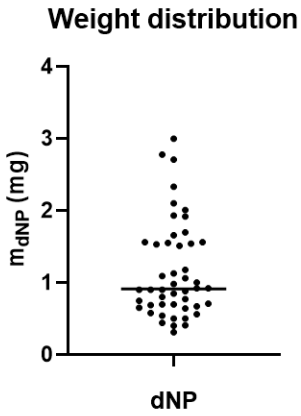

Figure 6.5 – Assessment of dNP scaffolds dry weight distribution. Line represents mean (n=48).

Table 6.1 – Algorithm's efficiency in extracting IVD's metrics

		Mean Accuracy (%)	Standard Deviation (%)
Evaluator A	Group 1	90.00	8.12
	Group 2	94.17	3.73
	Group 3	91.67	5.10
	Group 4	85.00	2.28
	Group 5	89.58	7.98
	Total	90.08	3.36
Evaluator B	Group 1	90.83	5.43
	Group 2	92.50	5.43
	Group 3	90.83	5.43
	Group 4	87.50	4.17
	Group 5	88.54	8.59
	Total	90.04	2.00
Overall Accuracy		90.06 ± 0.03 %	

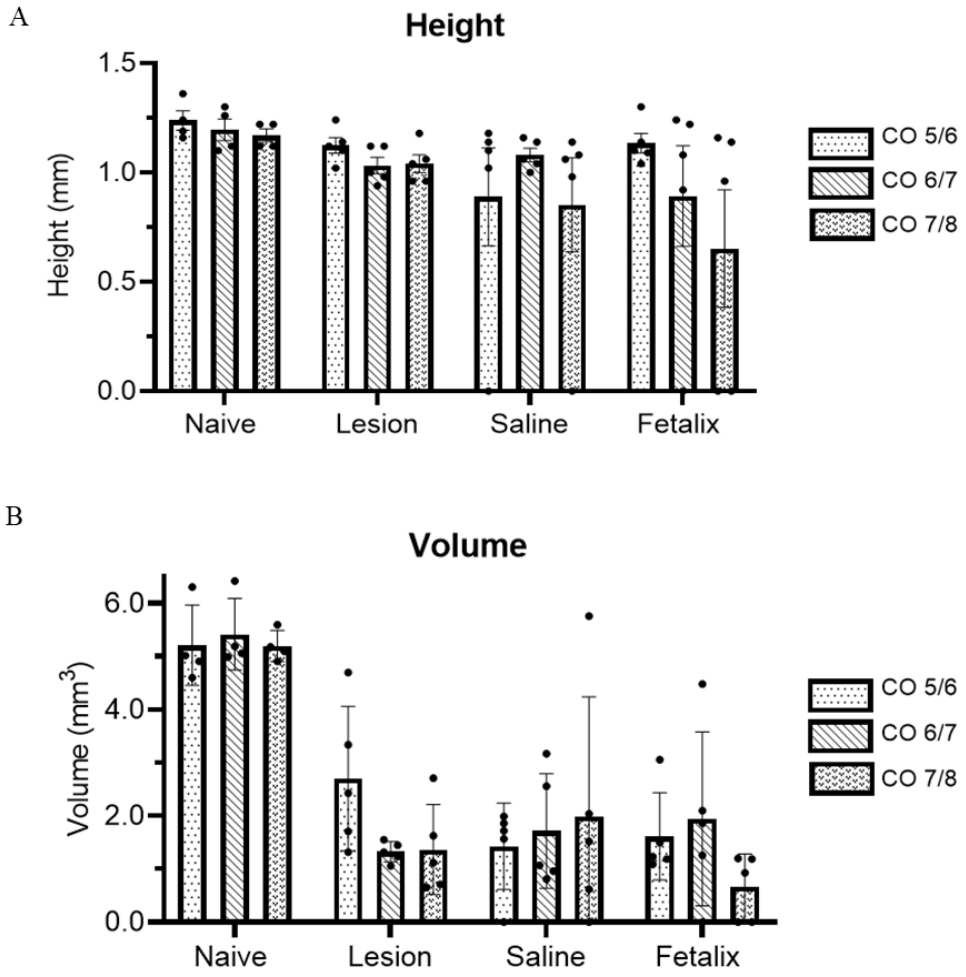

Figure 6.6 – Intervertebral disc's metric extraction. (A) Height and (B) volume quantification. Each point represents one animal. Error bars represent mean ± SD (n=12-15).

References

Abdulghani, S., & Mitchell, G. (2019). Biomaterials for In Situ Tissue Regeneration: A Review. *Biomolecules*, *9*(11), 750. doi: 10.3390/biom9110750

Adams, M. A., McMillan, D. W., Green, T. P., & Dolan, P. (1996). Sustained Loading Generates Stress Concentrations in Lumbar Intervertebral Discs. *Spine*, *21*(4), 434–438. doi: 10.1097/00007632-199602150-00006

Adams, M. A., & Roughley, P. J. (2006). What is Intervertebral Disc Degeneration, and What Causes It? *Spine*, *31*(18), 2151–2161. doi: 10.1097/01.brs.0000231761.73859.2c

Akyol, S., Senel Eraslan, B., Etyemez, H., Tanriverdi, T., & Hanci, M. (2010). Catabolic cytokine expressions in patients with degenerative disc disease. *Turkish Neurosurgery*. doi: 10.5137/1019-5149.JTN.3394-10.1

Aladin, D. M. K., Cheung, K. M. C., Ngan, A. H. W., Chan, D., Leung, V. Y. L., Lim, C. T., Luk, K. D. K., & Lu, W. W. (2010). Nanostructure of collagen fibrils in human nucleus pulposus and its correlation with macroscale tissue mechanics. *Journal of Orthopaedic Research*, *28*(4), 497–502. doi: 10.1002/jor.21010

Anitua, E., Milani, I., Martinez, A., Cabello, F., Prado, R., Padilla, S., & Sanado, L. (2023). Plasma Rich in Growth Factors (PRGF) in the Treatment of Patients With Chronic Cervical and Lumbar Pain: A Prospective Observational Clinical Study. *Pain Physician*, *26*(6), E725–E736.

Antoniou, J., Steffen, T., Nelson, F., Winterbottom, N., Hollander, A. P., Poole, R. A., Aebi, M., & Alini, M. (1996). The human lumbar intervertebral disc: evidence for changes in the biosynthesis and denaturation of the extracellular matrix with growth, maturation, ageing, and degeneration. *Journal of Clinical Investigation*, *98*(4), 996–1003. doi: 10.1172/JCI118884

Arck, P. C. (2019). When 3 Rs meet a forth R: Replacement, reduction and refinement of animals in research on reproduction. *Journal of Reproductive Immunology*, *132*, 54–59. doi: 10.1016/j.jri.2019.03.004

Armstrong, S. A., & Herr, M. J. (2024). *Physiology, Nociception*.

Arnold, F. J., & Maran, F. S. (2019). Young's modulus determination of elastomeric materials using capacitance measurement. *European Journal of Physics*, *40*(5), 055002. doi: 10.1088/1361-6404/ab1f1f

Atlas, S. J., & Deyo, R. A. (2001). Evaluating and managing acute low back pain in the primary care setting. *Journal of General Internal Medicine*, *16*(2), 120–131. doi: 10.1111/j.1525-1497.2001.91141.x

Aubeux, D., Beck, L., Weiss, P., Guicheux, J., Enkel, B., Pérez, F., & Simon, S. (2016). Assessment and Quantification of Noncollagenic Matrix Proteins Released from Human Dentin Powder Incorporated into a Silated Hydroxypropylmethylcellulose Biomedical Hydrogel. *Journal of Endodontics*, *42*(9), 1371–1376. doi: 10.1016/j.joen.2016.05.019

Babensee, J. E., Anderson, J. M., McIntire, L. V., & Mikos, A. G. (1998). Host response to tissue engineered devices. *Advanced Drug Delivery Reviews*, *33*(1–2), 111–139. doi: 10.1016/S0169-409X(98)00023-4

Bachmeier, B. E., Nerlich, A. G., Weiler, C., Paesold, G., Jochum, M., & Boos, N. (2007). Analysis of Tissue Distribution of TNF-α, TNF-α-Receptors, and the Activating TNF-α–Converting Enzyme Suggests Activation of the TNF-α System in the Aging Intervertebral Disc. *Annals of the New York Academy of Sciences*, *1096*(1), 44–54. doi: 10.1196/annals.1397.069

Bachmeier, B. E., Nerlich, A., Mittermaier, N., Weiler, C., Lumenta, C., Wuertz, K., & Boos, N. (2009). Matrix metalloproteinase expression levels suggest distinct enzyme roles during lumbar disc herniation and degeneration. *European Spine Journal*, *18*(11), 1573–1586. doi: 10.1007/s00586-009-1031-8

Barcellona, M. N., McDonnell, E. E., Samuel, S., & Buckley, C. T. (2022). Rat tail models for the assessment of injectable nucleus pulposus regeneration strategies. *JOR SPINE*, *5*(3). doi: 10.1002/jsp2.1216

Baumgartner, L., Reagh, J. J., González Ballester, M. A., & Noailly, J. (2021). Simulating intervertebral disc cell behaviour within 3D multifactorial environments. *Bioinformatics*, *37*(9), 1246–1253. doi: 10.1093/bioinformatics/btaa939

Beckstein, J. C., Sen, S., Schaer, T. P., Vresilovic, E. J., & Elliott, D. M. (2008). Comparison of Animal Discs Used in Disc Research to Human Lumbar Disc. *Spine*, *33*(6), E166–E173. doi: 10.1097/BRS.0b013e318166e001

Bergknut, N., Rutges, J. P. H. J., Kranenburg, H.-J. C., Smolders, L. A., Hagman, R., Smidt, H.-J., Lagerstedt, A.-S., Penning, L. C., Voorhout, G., Hazewinkel, H. A. W., Grinwis, G. C. M., Creemers, L. B., Meij, B. P., & Dhert, W. J. A. (2012). The Dog as an Animal Model for

Intervertebral Disc Degeneration? *Spine*, *37*(5), 351–358. doi: 10.1097/BRS.0b013e31821e5665

Berke, M. S., Colding-Jørgensen, P., Hestehave, S., Kalliokoski, O., Jensen, H. E., Sørensen, D. B., Hau, J., & Abelson, K. S. P. (2022). Effects of buprenorphine on acute pain and inflammation in the adjuvant-induced monoarthritis rat model. *Heliyon*, *8*(11), e11554. doi: 10.1016/j.heliyon.2022.e11554

Bernick, S., & Cailliet, R. (1982). Vertebral End-Plate Changes With Aging of Human Vertebrae. *Spine*, *7*(2), 97–102. doi: 10.1097/00007632-198203000-00002

Bibby, S. R. S., Jones, D. A., Lee, R. B., Yu, J., & Urban, J. P. G. (2001). The pathophysiology of the intervertebral disc. *Joint Bone Spine*, *68*(6), 537–542. doi: 10.1016/S1297-319X(01)00332-3

Bobrova, M., Safonova, L., Efimov, A., Lyundup, A., Mozheiko, N., Agapova, O., & Agapov, I. (2022). Scaffolds Based on Silk Fibroin with Decellularized Rat Liver Microparticles: Investigation of the Structure, Biological Properties and Regenerative Potential for Skin Wound Healing. *Pharmaceutics*, *14*(11), 2313. doi: 10.3390/pharmaceutics14112313

Bogduk, N., Tynan, W., & Wilson, A. S. (1981). The nerve supply to the human lumbar intervertebral discs. *Journal of Anatomy*, *132*(Pt 1), 39–56.

Brown, M., Li, J., Moraes, C., Tabrizian, M., & Li-Jessen, N. Y. K. (2022). Decellularized extracellular matrix: New promising and challenging biomaterials for regenerative medicine. *Biomaterials*, *289*, 121786. doi: 10.1016/j.biomaterials.2022.121786

Bubak, A. N., Elsworth, J. D., & Sladek, J. R. (2015). Animal models in regenerative medicine. In Stem Cells in Regenerative Medicine (pp. 301–316). Wiley. doi: 10.1002/9781118846193.ch16

Buckwalter, J. A. (1995). Aging and Degeneration of the Human Intervertebral Disc. *Spine*, *20*(11), 1307–1314. doi: 10.1097/00007632-199506000-00022

Buckwalter, J. A., Woo, S. L., Goldberg, V. M., Hadley, E. C., Booth, F., Oegema, T. R., & Eyre, D. R. (1993). Soft-tissue aging and musculoskeletal function. *The Journal of Bone & Joint Surgery*, *75*(10), 1533–1548. doi: 10.2106/00004623-199310000-00015

Butler, C. R., Hynds, R. E., Crowley, C., Gowers, K. H. C., Partington, L., Hamilton, N. J., Carvalho, C., Platé, M., Samuel, E. R., Burns, A. J., Urbani, L., Birchall, M. A., Lowdell, M. W., De Coppi, P., & Janes, S. M. (2017). Vacuum-assisted decellularization: an accelerated protocol to

generate tissue-engineered human tracheal scaffolds. *Biomaterials*, *124*, 95–105. doi: 10.1016/j.biomaterials.2017.02.001

Butt, M., Zaman, M., Ahmad, A., Khan, R., Mallhi, T., Hasan, M., Khan, Y., Hafeez, S., Massoud, E., Rahman, M., & Cavalu, S. (2022). Appraisal for the Potential of Viral and Nonviral Vectors in Gene Therapy: A Review. *Genes*, *13*(8), 1370. doi: 10.3390/genes13081370

Caldeira, J., Santa, C., Osório, H., Molinos, M., Manadas, B., Gonçalves, R., & Barbosa, M. (2017). Matrisome Profiling During Intervertebral Disc Development And Ageing. *Scientific Reports*, *7*(1), 11629. doi: 10.1038/s41598-017-11960-0

Catoira, M. C., González-Payo, J., Fusaro, L., Ramella, M., & Boccafoschi, F. (2020). Natural hydrogels R&D process: technical and regulatory aspects for industrial implementation. *Journal of Materials Science: Materials in Medicine*, *31*(8), 64. doi: 10.1007/s10856-020-06401-w

Cazzanelli, P., & Wuertz-Kozak, K. (2020). MicroRNAs in Intervertebral Disc Degeneration, Apoptosis, Inflammation, and Mechanobiology. *International Journal of Molecular Sciences*, *21*(10), 3601. doi: 10.3390/ijms21103601

Chanchairujira, K., Chung, C. B., Kim, J. Y., Papakonstantinou, O., Lee, M. H., Clopton, P., & Resnick, D. (2004). Intervertebral Disk Calcification of the Spine in an Elderly Population: Radiographic Prevalence, Location, and Distribution and Correlation with Spinal Degeneration. *Radiology*, *230*(2), 499–503. doi: 10.1148/radiol.2302011842

Chaudhuri, O., Cooper-White, J., Janmey, P. A., Mooney, D. J., & Shenoy, V. B. (2020). Effects of extracellular matrix viscoelasticity on cellular behaviour. *Nature*, *584*(7822), 535–546. doi: 10.1038/s41586-020-2612-2

Chen, W. -H., Lo, W. -C., Lee, J. -J., Su, C. -H., Lin, C. -T., Liu, H. -Y., Lin, T. -W., Lin, W. -C., Huang, T. -Y., & Deng, W. -P. (2006). Tissue-engineered intervertebral disc and chondrogenesis using human nucleus pulposus regulated through TGF-β1 in platelet-rich plasma. *Journal of Cellular Physiology*, *209*(3), 744–754. doi: 10.1002/jcp.20765

Cheung, K. M. C., Karppinen, J., Chan, D., Ho, D. W. H., Song, Y.-Q., Sham, P., Cheah, K. S. E., Leong, J. C. Y., & Luk, K. D. K. (2009). Prevalence and Pattern of Lumbar Magnetic Resonance Imaging Changes in a Population Study of One Thousand Forty-Three Individuals. *Spine*, *34*(9), 934–940. doi: 10.1097/BRS.0b013e3181a01b3f

Choi, H., Tessier, S., Silagi, E. S., Kyada, R., Yousefi, F., Pleshko, N., Shapiro, I. M., & Risbud, M. V. (2018). A novel mouse model of intervertebral disc degeneration shows altered cell fate and matrix homeostasis. *Matrix Biology*, *70*, 102–122. doi: 10.1016/j.matbio.2018.03.019

Choudhury, D., Yee, M., Sheng, Z. L. J., Amirul, A., & Naing, M. W. (2020). Decellularization systems and devices: State-of-the-art. *Acta Biomaterialia*, *115*, 51–59. doi: 10.1016/j.actbio.2020.07.060

Cilurzo, F., Selmin, F., Minghetti, P., Adami, M., Bertoni, E., Lauria, S., & Montanari, L. (2011). Injectability Evaluation: An Open Issue. *AAPS PharmSciTech*, *12*(2), 604–609. doi: 10.1208/s12249-011-9625-y

Cobos, M. P., Quezada, V. F., Morloy, L. I. Z., Alvarez, P. V., & Gonzalez, S. P. (2021). A model based on the Technology Readiness Level (TRL) scale to measure the maturity level of research projects that can become spinoffs in Higher Education Institutions. *2021 Congreso Internacional de Innovación y Tendencias En Ingeniería (CONIITI)*, 1–6. doi: 10.1109/CONIITI53815.2021.9619667

Colen, S., van den Bekerom, M. P. J., Mulier, M., & Haverkamp, D. (2012). Hyaluronic Acid in the Treatment of Knee Osteoarthritis. *BioDrugs*, *26*(4), 257–268. doi: 10.1007/BF03261884

Crapo, P. M., Gilbert, T. W., & Badylak, S. F. (2011). An overview of tissue and whole organ decellularization processes. *Biomaterials*, *32*(12), 3233–3243. doi: 10.1016/j.biomaterials.2011.01.057

Cunha, C., Lamas, S., Gonçalves, R. M., & Barbosa, M. A. (2017). Joint analysis of IVD herniation and degeneration by rat caudal needle puncture model. *Journal of Orthopaedic Research*, *35*(2), 258–268. doi: 10.1002/jor.23114

da Costa, R. C., De Decker, S., Lewis, M. J., & Volk, H. (2020). Diagnostic Imaging in Intervertebral Disc Disease. *Frontiers in Veterinary Science*, *7*. doi: 10.3389/fvets.2020.588338

Dai, J., Wang, H., Liu, G., Xu, Z., Li, F., & Fang, H. (2014). Dynamic compression and co-culture with nucleus pulposus cells promotes proliferation and differentiation of adipose-derived mesenchymal stem cells. *Journal of Biomechanics*, *47*(5), 966–972. doi: 10.1016/j.jbiomech.2014.01.023

Davies, J. R., Purawijaya, D. A., Bartlett, J. M., & Robinson, E. S. J. (2022). Impact of Refinements to Handling and Restraint Methods in Mice. *Animals*, *12*(17), 2173. doi: 10.3390/ani12172173

Denayer, T., Stöhr, T., & Roy, M. V. (2014). Animal models in translational medicine: Validation and prediction. *European Journal of Molecular & Clinical Medicine*, *2*(1), 5. doi: 10.1016/j.nhtm.2014.08.001

Deuis, J. R., Dvorakova, L. S., & Vetter, I. (2017). Methods Used to Evaluate Pain Behaviors in Rodents. *Frontiers in Molecular Neuroscience*, *10*, 284. doi: 10.3389/fnmol.2017.00284

Diwan, A. D., & Melrose, J. (2023). Intervertebral disc degeneration and how it leads to low back pain. *JOR SPINE*, *6*(1). doi: 10.1002/jsp2.1231

Duance, V. C., Crean, J. K. G., Sims, T. J., Avery, N., Smith, S., Menage, J., Eisenstein, S. M., & Roberts, S. (1998). Changes in Collagen Cross-Linking in Degenerative Disc Disease and Scoliosis. *Spine*, *23*(23), 2545–2551. doi: 10.1097/00007632-199812010-00009

Ebara, S., Iatridis, J. C., Setton, L. A., Foster, R. J., Mow, V. C., & Weidenbaum, M. (1996). Tensile Properties of Nondegenerate Human Lumbar Anulus Fibrosus. *Spine*, *21*(4), 452–461. doi: 10.1097/00007632-199602150-00009

Elmounedi, N., Bahloul, W., Kharrat, A., Horchani, M., Ben Jannet, H., Racem Guidara, A., & Keskes, H. (2024). Ozone therapy (O2-O3) alleviates the progression of early intervertebral disc degeneration via the inhibition of oxidative stress and the interception of the PI3K/Akt/NF-κB signaling pathway. *International Immunopharmacology*, *129*, 111596. doi: 10.1016/j.intimp.2024.111596

Errington, R. J., Puustjarvi, K., White, I. R., Roberts, S., & Urban, J. P. (1998). Characterisation of cytoplasm-filled processes in cells of the intervertebral disc. *Journal of Anatomy*, *192 (Pt 3)*(Pt 3), 369–378. doi: 10.1046/j.1469-7580.1998.19230369.x

Erwin, W., Islam, D., Inman, R. D., Fehlings, M. G., & Tsui, F. W. L. (2011). Notochordal cells protect nucleus pulposus cells from degradation and apoptosis: implications for the mechanisms of intervertebral disc degeneration. *Arthritis Research & Therapy*, *13*(6), R215. doi: 10.1186/ar3548

European Parliament and of the Council of the European Union. (2010). Directive 2010/63/EU of the European Parliament and of the Council of 22 September 2010 on the protection of animals used for scientific purposes. *Official Journal of the European Union*.

Evashwick-Rogler, T. W., Lai, A., Watanabe, H., Salandra, J. M., Winkelstein, B. A., Cho, S. K., Hecht, A. C., & Iatridis, J. C. (2018). Inhibiting tumor necrosis factor-alpha at time of induced

intervertebral disc injury limits long-term pain and degeneration in a rat model. *JOR SPINE*, *1*(2). doi: 10.1002/jsp2.1014

Eyre, D. R., & Muir, H. (1976). Types I and II collagens in intervertebral disc. Interchanging radial distributions in annulus fibrosus. *Biochemical Journal*, *157*(1), 267–270. doi: 10.1042/bj1570267

Farber, S. J., Saheb-Al-Zamani, M., Zieske, L., Laurido-Soto, O., Bery, A., Hunter, D., Johnson, P., & Mackinnon, S. E. (2013). Peripheral Nerve Injury After Local Anesthetic Injection. *Anesthesia & Analgesia*, *117*(3), 731–739. doi: 10.1213/ANE.0b013e3182a00767

Fatoye, F., Gebrye, T., Ryan, C. G., Useh, U., & Mbada, C. (2023). Global and regional estimates of clinical and economic burden of low back pain in high-income countries: a systematic review and meta-analysis. *Frontiers in Public Health*, *11*. doi: 10.3389/fpubh.2023.1098100

Fernandez, C., Marionneaux, A., Gill, S., & Mercuri, J. (2016). Biomimetic nucleus pulposus scaffold created from bovine caudal intervertebral disc tissue utilizing an optimal decellularization procedure. *Journal of Biomedical Materials Research Part A*, *104*(12), 3093–3106. doi: 10.1002/jbm.a.35858

Fiordalisi, M. F., Ferreira, J. R., Pinto, M. L., Ribeiro-Machado, C., Teixeira Pinto, M., Oliveira, M. J., Barbosa, M. A., Madeira Gonçalves, R., & Caldeira, J. (2022). The impact of matrix age on intervertebral disc regeneration. *Biomaterials Advances*, *143*, 213192. doi: 10.1016/j.bioadv.2022.213192

Fiordalisi, M., Silva, A. J., Barbosa, M., Gonçalves, R., & Caldeira, J. (2020). Decellularized Scaffolds for Intervertebral Disc Regeneration. *Trends in Biotechnology*, *38*(9), 947–951. doi: 10.1016/j.tibtech.2020.05.002

Fishman, J. M., Lowdell, M. W., Urbani, L., Ansari, T., Burns, A. J., Turmaine, M., North, J., Sibbons, P., Seifalian, A. M., Wood, K. J., Birchall, M. A., & De Coppi, P. (2013). Immunomodulatory effect of a decellularized skeletal muscle scaffold in a discordant xenotransplantation model. *Proceedings of the National Academy of Sciences*, *110*(35), 14360–14365. doi: 10.1073/pnas.1213228110

Freemont, A. J., Peacock, T. E., Goupille, P., Hoyland, J. A., O'Brien, J., & Jayson, M. I. V. (1997). Nerve ingrowth into diseased intervertebral disc in chronic back pain. *The Lancet*, *350*(9072), 178–181. doi: 10.1016/S0140-6736(97)02135-1

Friedmann, A., Baertel, A., Schmitt, C., Ludtka, C., Milosevic, J., Meisel, H.-J., Goehre, F., & Schwan, S. (2021). Intervertebral Disc Regeneration Injection of a Cell-Loaded Collagen Hydrogel in a Sheep Model. *International Journal of Molecular Sciences*, *22*(8), 4248. doi: 10.3390/ijms22084248

Frobin, W., Brinckmann, P., Biggemann, M., Tillotson, M., & Burton, K. (1997). Precision measurement of disc height, vertebral height and sagittal plane displacement from lateral radiographic views of the lumbar spine. *Clinical Biomechanics*, *12*, S1–S63. doi: 10.1016/S0268-0033(96)00067-8

Fujii, K., Yamazaki, M., Kang, J. D., Risbud, M. V., Cho, S. K., Qureshi, S. A., Hecht, A. C., & Iatridis, J. C. (2019). Discogenic Back Pain: Literature Review of Definition, Diagnosis, and Treatment. *JBMR Plus*, *3*(5). doi: 10.1002/jbm4.10180

Fukusaki, M., Kobayashi, I., Hara, T., & Sumikawa, K. (1998). Symptoms of Spinal Stenosis Do Not Improve After Epidural Steroid Injection. *The Clinical Journal of Pain*, *14*(2), 148–151. doi: 10.1097/00002508-199806000-00010

Fusellier, M., Clouet, J., Gauthier, O., Tryfonidou, M., Le Visage, C., & Guicheux, J. (2020). Degenerative lumbar disc disease: in vivo data support the rationale for the selection of appropriate animal models. *European Cells and Materials*, *39*, 17–48. doi: 10.22203/eCM.v039a02

Galbusera, F., van Rijsbergen, M., Ito, K., Huyghe, J. M., Brayda-Bruno, M., & Wilke, H. J. (2014). Ageing and degenerative changes of the intervertebral disc and their impact on spinal flexibility. *European Spine Journal*. doi: 10.1007/s00586-014-3203-4

Gilbert, H. T. J., Hodson, N., Baird, P., Richardson, S. M., & Hoyland, J. A. (2016). Acidic pH promotes intervertebral disc degeneration: Acid-sensing ion channel -3 as a potential therapeutic target. *Scientific Reports*, *6*(1), 37360. doi: 10.1038/srep37360

Gilbert, T., Sellaro, T., & Badylak, S. (2006). Decellularization of tissues and organs. *Biomaterials*. doi: 10.1016/j.biomaterials.2006.02.014

Gilbert, T. W., Stolz, D. B., Biancaniello, F., Simmons-Byrd, A., & Badylak, S. F. (2005). Production and characterization of ECM powder: implications for tissue engineering applications. *Biomaterials*, *26*(12), 1431–1435. doi: 10.1016/j.biomaterials.2004.04.042

Gouveia, M., & Augusto, M. (2011). Custos indirectos da dor crónica em Portugal. *Revista Portuguesa de Saúde Pública*, *29*(2), 100–107.

Gruber, H. E., Ingram, J. A., Norton, H. J., & Hanley, E. N. (2007). Senescence in Cells of the Aging and Degenerating Intervertebral Disc. *Spine*, *32*(3), 321–327. doi: 10.1097/01.brs.0000253960.57051.de

Gu, X., Carroll Turpin, M. A., & Romero-Ortega, M. I. (2022). Biomaterials and Regenerative Medicine in Pain Management. *Current Pain and Headache Reports*, *26*(7), 533–541. doi: 10.1007/s11916-022-01055-5

Gullbrand, S. E., Malhotra, N. R., Schaer, T. P., Zawacki, Z., Martin, J. T., Bendigo, J. R., Milby, A. H., Dodge, G. R., Vresilovic, E. J., Elliott, D. M., Mauck, R. L., & Smith, L. J. (2017). A large animal model that recapitulates the spectrum of human intervertebral disc degeneration. *Osteoarthritis and Cartilage*, *25*(1), 146–156. doi: 10.1016/j.joca.2016.08.006

Hallman, M., Driscoll, J. A., Lubbe, R., Jeong, S., Chang, K., Haleem, M., Jakus, A., Pahapill, R., Yun, C., Shah, R., Hsu, W. K., Stock, S. R., & Hsu, E. L. (2021). Influence of Geometry and Architecture on the *In Vivo* Success of 3D-Printed Scaffolds for Spinal Fusion. *Tissue Engineering Part A*, *27*(1–2), 26–36. doi: 10.1089/ten.tea.2020.0004

Hamilton. (n.d.). *Needle Gauge Chart*.

Han, B., Zhu, K., Li, F.-C., Xiao, Y.-X., Feng, J., Shi, Z.-L., Lin, M., Wang, J., & Chen, Q.-X. (2008). A Simple Disc Degeneration Model Induced by Percutaneous Needle Puncture in the Rat Tail. *Spine*, *33*(18), 1925–1934. doi: 10.1097/BRS.0b013e31817c64a9

Han, I.-B. (2020). Moving Forward: Gene Therapy for Intervertebral Disc Degeneration. *Neurospine*, *17*(1), 17–18. doi: 10.14245/ns.2040108.054

Hestbaek, L., Leboeuf-Yde, C., & Manniche, C. (2003). Low back pain: what is the long-term course? A review of studies of general patient populations. *European Spine Journal*, *12*(2), 149–165. doi: 10.1007/s00586-002-0508-5

Ho, M. M., Kelly, T.-A. N., Guo, X. E., Ateshian, G. A., & Hung, C. T. (2006). Spatially Varying Material Properties of the Rat Caudal Intervertebral Disc. *Spine*, *31*(15), E486–E493. doi: 10.1097/01.brs.0000224532.42770.c1

Holm, S., Maroudas, A., Urban, J. P. G., Selstam, G., & Nachemson, A. (1981). Nutrition of the Intervertebral Disc: Solute Transport and Metabolism. *Connective Tissue Research*, *8*(2), 101–119. doi: 10.3109/03008208109152130

Hoogendoorn, R. J., Wuisman, P. I., Smit, T. H., Everts, V. E., & Helder, M. N. (2007). Experimental Intervertebral Disc Degeneration Induced by Chondroitinase ABC in the Goat. *Spine*, *32*(17), 1816–1825. doi: 10.1097/BRS.0b013e31811ebac5

Hristova, G. I., Jarzem, P., Ouellet, J. A., Roughley, P. J., Epure, L. M., Antoniou, J., & Mwale, F. (2011). Calcification in human intervertebral disc degeneration and scoliosis. *Journal of Orthopaedic Research*, *29*(12), 1888–1895. doi: 10.1002/jor.21456

Hwang, P. Y., Chen, J., Jing, L., Hoffman, B. D., & Setton, L. A. (2014). The Role Of Extracellular Matrix Elasticity and Composition In Regulating the Nucleus Pulposus Cell Phenotype in the Intervertebral Disc: A Narrative Review. *Journal of Biomechanical Engineering*, *136*(2). doi: 10.1115/1.4026360

Iatridis, J. C., MacLean, J. J., O'Brien, M., & Stokes, I. A. F. (2007). Measurements of Proteoglycan and Water Content Distribution in Human Lumbar Intervertebral Discs. *Spine*, *32*(14), 1493–1497. doi: 10.1097/BRS.0b013e318067dd3f

Inoue, H., & Takeda, T. (1975). Three-Dimensional Observation of Collagen Framework of Lumbar Intervertebral Discs. *Acta Orthopaedica Scandinavica*, *46*(6), 949–956. doi: 10.3109/17453677508989283

James, S. L., Abate, D., Abate, K. H., Abay, S. M., Abbafati, C., Abbasi, N., Abbastabar, H., Abd-Allah, F., Abdela, J., Abdelalim, A., Abdollahpour, I., Abdulkader, R. S., Abebe, Z., Abera, S. F., Abil, O. Z., Abraha, H. N., Abu-Raddad, L. J., Abu-Rmeileh, N. M. E., Accrombessi, M. M. K., … Murray, C. J. L. (2018). Global, regional, and national incidence, prevalence, and years lived with disability for 354 diseases and injuries for 195 countries and territories, 1990–2017: a systematic analysis for the Global Burden of Disease Study 2017. *The Lancet*, *392*(10159), 1789–1858. doi: 10.1016/S0140-6736(18)32279-7

Jeong, J. H., Jin, E. S., Min, J. K., Jeon, S. R., Park, C.-S., Kim, H. S., & Choi, K. H. (2009). Human mesenchymal stem cells implantation into the degenerated coccygeal disc of the rat. *Cytotechnology*, *59*(1), 55–64. doi: 10.1007/s10616-009-9192-1

Jeong, S.-W., Lee, J.-S., & Kim, K.-W. (2014). In vitro lifespan and senescence mechanisms of human nucleus pulposus chondrocytes. *The Spine Journal*, *14*(3), 499–504. doi: 10.1016/j.spinee.2013.06.099

Kalichman, L., & Hunter, D. J. (2008). The genetics of intervertebral disc degeneration.Associated genes. *Joint Bone Spine*, *75*(4), 388–396. doi: 10.1016/j.jbspin.2007.11.002

Kasravi, M., Ahmadi, A., Babajani, A., Mazloomnejad, R., Hatamnejad, M. R., Shariatzadeh, S., Bahrami, S., & Niknejad, H. (2023). Immunogenicity of decellularized extracellular matrix scaffolds: a bottleneck in tissue engineering and regenerative medicine. *Biomaterials Research*, *27*(1). doi: 10.1186/s40824-023-00348-z

Kawecki, M., Łabuś, W., Klama-Baryla, A., Kitala, D., Kraut, M., Glik, J., Misiuga, M., Nowak, M., Bielecki, T., & Kasperczyk, A. (2018). A review of decellurization methods caused by an urgent need for quality control of cell-free extracellular matrix' scaffolds and their role in regenerative medicine. *Journal of Biomedical Materials Research Part B: Applied Biomaterials*, *106*(2), 909–923. doi: 10.1002/jbm.b.33865

Kiani, A. K., Pheby, D., Henehan, G., Brown, R., Sieving, P., Sykora, P., Marks, R., Falsini, B., Capodicasa, N., Miertus, S., Lorusso, L., Dondossola, D., Tartaglia, G. M., Ergoren, M. C., Dundar, M., Michelini, S., Malacarne, D., Bonetti, G., Dautaj, A., … International Bioethics Study Group. (2022). Ethical considerations regarding animal experimentation. *Journal of Preventive Medicine and Hygiene*, *63*(2 Suppl 3), E255–E266. doi: 10.15167/2421-4248/jpmh2022.63.2S3.2768

Kim, J., Yang, S.-J., Kim, H., Kim, Y., Park, J. B., DuBose, C., & Lim, T.-H. (2012). Effect of Shear Force on Intervertebral Disc (IVD) Degeneration: An In Vivo Rat Study. *Annals of Biomedical Engineering*, *40*(9), 1996–2004. doi: 10.1007/s10439-012-0570-z

Kim, J.-S., Kroin, J. S., Li, X., An, H. S., Buvanendran, A., Yan, D., Tuman, K. J., van Wijnen, A. J., Chen, D., & Im, H.-J. (2011). The rat intervertebral disk degeneration pain model: relationships between biological and structural alterations and pain. *Arthritis Research & Therapy*, *13*(5), R165. doi: 10.1186/ar3485

Kjaer, P., Leboeuf-Yde, C., Korsholm, L., Sorensen, J. S., & Bendix, T. (2005). Magnetic Resonance Imaging and Low Back Pain in Adults: A Diagnostic Imaging Study of 40-Year-Old Men and Women. *Spine*, *30*(10), 1173–1180. doi: 10.1097/01.brs.0000162396.97739.76

Klak, M., Łojszczyk, I., Berman, A., Tymicki, G., Adamiok-Ostrowska, A., Sierakowski, M., Olkowski, R., Szczepankiewicz, A. A., Kamiński, A., Dobrzyń, A., & Wszoła, M. (2021). Impact of Porcine Pancreas Decellularization Conditions on the Quality of Obtained dECM. *International Journal of Molecular Sciences*, *22*(13), 7005. doi: 10.3390/ijms22137005

Kroeber, M. W., Unglaub, F., Wang, H., Schmid, C., Thomsen, M., Nerlich, A., & Richter, W. (2002). New In Vivo Animal Model to Create Intervertebral Disc Degeneration and to Investigate the Effects of Therapeutic Strategies to Stimulate Disc Regeneration. *Spine*, *27*(23), 2684–2690. doi: 10.1097/00007632-200212010-00007

Krupa, K., & Bekiesińska-Figatowska, M. (2015). Artifacts in Magnetic Resonance Imaging. *Polish Journal of Radiology*, *80*, 93–106. doi: 10.12659/PJR.892628

Lai, A., Moon, A., Purmessur, D., Skovrlj, B., Winkelstein, B. A., Cho, S. K., Hecht, A. C., & Iatridis, J. C. (2015). Assessment of functional and behavioral changes sensitive to painful disc degeneration. *Journal of Orthopaedic Research*, *33*(5), 755–764. doi: 10.1002/jor.22833

Le Maitre, C., Freemont, A., & Hoyland, J. (2007). Accelerated cellular senescence in degenerate intervertebral discs: a possible role in the pathogenesis of intervertebral disc degeneration. *Arthritis Research & Therapy*, *9*(3), R45. doi: 10.1186/ar2198

Le Maitre, C., Freemont, A. J., & Hoyland, J. (2005). The role of interleukin-1 in the pathogenesis of human Intervertebral disc degeneration. *Arthritis Research & Therapy*, *7*(4), R732. doi: 10.1186/ar1732

Le Maitre, C., Hoyland, J., & Freemont, A. J. (2007). Catabolic cytokine expression in degenerate and herniated human intervertebral discs: IL-1β and TNFα expression profile. *Arthritis Research & Therapy*, *9*(4), R77. doi: 10.1186/ar2275

Lim, Y. S., Jung, K. T., Park, C. H., Wee, S. W., Sin, S. S., & Kim, J. (2015). Acute Motor Weakness of Opposite Lower Extremity after Percutaneous Epidural Neuroplasty. *The Korean Journal of Pain*, *28*(2), 144–147. doi: 10.3344/kjp.2015.28.2.144

Liu, S., Yu, J.-M., Gan, Y.-C., Qiu, X.-Z., Gao, Z.-C., Wang, H., Chen, S.-X., Xiong, Y., Liu, G.-H., Lin, S.-E., McCarthy, A., John, J. V., Wei, D.-X., & Hou, H.-H. (2023). Biomimetic natural biomaterials for tissue engineering and regenerative medicine: new biosynthesis methods, recent advances, and emerging applications. *Military Medical Research*, *10*(1), 16. doi: 10.1186/s40779-023-00448-w

Liu, X., Krishnamoorthy, D., Lin, L., Xue, P., Zhang, F., Chi, L., Linhardt, R. J., & Iatridis, J. C. (2018). A method for characterising human intervertebral disc glycosaminoglycan disaccharides using liquid chromatography-mass spectrometry with multiple reaction monitoring. *European Cells and Materials*, *35*, 117–131. doi: 10.22203/eCM.v035a09

Liu, Y., Zhao, Z., Guo, C., Huang, Z., Zhang, W., Ma, F., Wang, Z., Kong, Q., & Wang, Y. (2023). Application and development of hydrogel biomaterials for the treatment of intervertebral disc degeneration: a literature review. *Frontiers in Cell and Developmental Biology*, *11*. doi: 10.3389/fcell.2023.1286223

Liuke, M., Solovieva, S., Lamminen, A., Luoma, K., Leino-Arjas, P., Luukkonen, R., & Riihimäki, H. (2005). Disc degeneration of the lumbar spine in relation to overweight. *International Journal of Obesity*, *29*(8), 903–908. doi: 10.1038/sj.ijo.0802974

Lu, X.-Y., Ding, X.-H., Zhong, L.-J., Xia, H., Chen, X.-D., & Huang, H. (2013). Expression and significance of VEGF and p53 in degenerate intervertebral disc tissue. *Asian Pacific Journal of Tropical Medicine*, *6*(1), 79–81. doi: 10.1016/S1995-7645(12)60206-5

Lyu, F.-J., Cui, H., Pan, H., MC Cheung, K., Cao, X., Iatridis, J. C., & Zheng, Z. (2021). Painful intervertebral disc degeneration and inflammation: from laboratory evidence to clinical interventions. *Bone Research*, *9*(1), 7. doi: 10.1038/s41413-020-00125-x

Maher, C., Underwood, M., & Buchbinder, R. (2017). Non-specific low back pain. *The Lancet*, *389*(10070), 736–747. doi: 10.1016/S0140-6736(16)30970-9

Majumdar, S., Link, T. M., Steinbach, L. S., Hu, S., & Kurhanewicz, J. (2011). Diagnostic Tools and Imaging Methods in Intervertebral Disk Degeneration. *Orthopedic Clinics of North America*, *42*(4), 501–511. doi: 10.1016/j.ocl.2011.07.007

Marinelli, N. L., Haughton, V. M., & Anderson, P. A. (2010). T2 Relaxation Times Correlated with Stage of Lumbar Intervertebral Disk Degeneration and Patient Age. *American Journal of Neuroradiology*, *31*(7), 1278–1282. doi: 10.3174/ajnr.A2080

Martin, J. T., Gorth, D. J., Beattie, E. E., Harfe, B. D., Smith, L. J., & Elliott, D. M. (2013). Needle puncture injury causes acute and long-term mechanical deficiency in a mouse model of intervertebral disc degeneration. *Journal of Orthopaedic Research*, *31*(8), 1276–1282. doi: 10.1002/jor.22355

Martirosyan, N. L., Patel, A. A., Carotenuto, A., Kalani, M. Y. S., Belykh, E., Walker, C. T., Preul, M. C., & Theodore, N. (2016). Genetic Alterations in Intervertebral Disc Disease. *Frontiers in Surgery*, *3*. doi: 10.3389/fsurg.2016.00059

Masuda, K., Aota, Y., Muehleman, C., Imai, Y., Okuma, M., Thonar, E. J., Andersson, G. B., & An, H. S. (2005). A Novel Rabbit Model of Mild, Reproducible Disc Degeneration by an Anulus Needle Puncture: Correlation Between the Degree of Disc Injury and Radiological and Histological Appearances of Disc Degeneration. *Spine*, *30*(1), 5–14. doi: 10.1097/01.brs.0000148152.04401.20

Masuda, K., Oegema, T. R., & An, H. S. (2004). Growth Factors and Treatment of Intervertebral Disc Degeneration. *Spine*, *29*(23), 2757–2769. doi: 10.1097/01.brs.0000146048.14946.af

Mate, V., Smolek, T., Kazmerova, Z. V., Jadhav, S., Brezovakova, V., Jurkanin, B., Uhrinova, I., Basheer, N., Zilka, N., Katina, S., & Novak, P. (2022). Enriched environment ameliorates propagation of tau pathology and improves cognition in rat model of tauopathy. *Frontiers in Aging Neuroscience*, *14*. doi: 10.3389/fnagi.2022.935973

Mekhail, N., Mekhail, N., Saweris, Y., & Acevedo-Moreno, L.-A. (2021). Is Saline Injection a True Sham/Placebo Treatment in Randomized Controlled Trials? A Systematic Review. *Neurology and Neurobiology*, 1–7. doi: 10.31487/j.NNB.2021.02.04

Mercuri, J. J., Patnaik, S., Dion, G., Gill, S. S., Liao, J., & Simionescu, D. T. (2013). Regenerative Potential of Decellularized Porcine *Nucleus Pulposus* Hydrogel Scaffolds: Stem Cell Differentiation, Matrix Remodeling, and Biocompatibility Studies. *Tissue Engineering Part A*, *19*(7–8), 952–966. doi: 10.1089/ten.tea.2012.0088

Mern, D. S., Walsen, T., Beierfuß, A., & Thomé, C. (2021). Animal models of regenerative medicine for biological treatment approaches of degenerative disc diseases. *Experimental Biology and Medicine*, *246*(4), 483–512. doi: 10.1177/1535370220969123

Mimura, M., Panjabi, M. M., Oxland, T. R., Crisco, J. J., Yamamoto, I., & Vasavada, A. (1994). Disc Degeneration Affects the Multidirectional Flexibility of the Lumbar Spine. *Spine*, *19*(12), 1371–1380. doi: 10.1097/00007632-199406000-00011

Mitchell, P. G., Magna, H. A., Reeves, L. M., Lopresti-Morrow, L. L., Yocum, S. A., Rosner, P. J., Geoghegan, K. F., & Hambor, J. E. (1996). Cloning, expression, and type II collagenolytic activity of matrix metalloproteinase-13 from human osteoarthritic cartilage. *Journal of Clinical Investigation*, *97*(3), 761–768. doi: 10.1172/JCI118475

Miyagi, M., Millecamps, M., Danco, A. T., Ohtori, S., Takahashi, K., & Stone, L. S. (2014). ISSLS Prize Winner: Increased Innervation and Sensory Nervous System Plasticity in a Mouse Model of Low Back Pain Due to Intervertebral Disc Degeneration. *Spine*, *39*(17), 1345–1354. doi: 10.1097/BRS.0000000000000334

Mohd Isa, I. L., Abbah, S. A., Kilcoyne, M., Sakai, D., Dockery, P., Finn, D. P., & Pandit, A. (2018). Implantation of hyaluronic acid hydrogel prevents the pain phenotype in a rat model of intervertebral disc injury. *Science Advances*, *4*(4). doi: 10.1126/sciadv.aaq0597

Mohd Isa, I. L., Mokhtar, S. A., Abbah, S. A., Fauzi, M. B., Devitt, A., & Pandit, A. (2022). Intervertebral Disc Degeneration: Biomaterials and Tissue Engineering Strategies toward Precision Medicine. *Advanced Healthcare Materials*, *11*(13). doi: 10.1002/adhm.202102530

Molinos, M., Fiordalisi, M. F., Caldeira, J., Almeida, C. R., Barbosa, M. A., & Gonçalves, R. M. (2023). Alterations of bovine nucleus pulposus cells with aging. *Aging Cell*, *22*(8). doi: 10.1111/acel.13873

Mosley, G. E., Evashwick-Rogler, T. W., Lai, A., & Iatridis, J. C. (2017). Looking beyond the intervertebral disc: the need for behavioral assays in models of discogenic pain. *Annals of the New York Academy of Sciences*, *1409*(1), 51–66. doi: 10.1111/nyas.13429

Mukherjee, P., Roy, S., Ghosh, D., & Nandi, S. K. (2022). Role of animal models in biomedical research: a review. *Laboratory Animal Research*, *38*(1), 18. doi: 10.1186/s42826-022-00128-1

Murata, M., Morio, Y., & Kuranobu, K. (1994). Lumbar disc degeneration and segmental instability: a comparison of magnetic resonance images and plain radiographs of patients with low back pain. *Archives of Orthopaedic and Trauma Surgery*, *113*(6), 297–301. doi: 10.1007/BF00426175

Murphy, K., Elias, G., Steppan, J., Boxley, C., Balagurunathan, K., Victor, X., Meaders, T., & Muto, M. (2016). Percutaneous Treatment of Herniated Lumbar Discs with Ozone: Investigation of the Mechanisms of Action. *Journal of Vascular and Interventional Radiology*, *27*(8), 1242-1250.e3. doi: 10.1016/j.jvir.2016.04.012

Nauroy, P., Guiraud, A., Chlasta, J., Malbouyres, M., Gillet, B., Hughes, S., Lambert, E., & Ruggiero, F. (2019). Gene profile of zebrafish fin regeneration offers clues to kinetics, organization and biomechanics of basement membrane. *Matrix Biology*, *75–76*, 82–101. doi: 10.1016/j.matbio.2018.07.005

Nerlich, A. G., Schaaf, R., Wälchli, B., & Boos, N. (2007). Temporo-spatial distribution of blood vessels in human lumbar intervertebral discs. *European Spine Journal*, *16*(4), 547–555. doi: 10.1007/s00586-006-0213-x

Ngo, K., Patil, P., McGowan, S. J., Niedernhofer, L. J., Robbins, P. D., Kang, J., Sowa, G., & Vo, N. (2017). Senescent intervertebral disc cells exhibit perturbed matrix homeostasis phenotype. *Mechanisms of Ageing and Development*, *166*, 16–23. doi: 10.1016/j.mad.2017.08.007

Nishida, K., Kang, J. D., Suh, J.-K., Robbins, P. D., Evans, C. H., & Gilbertson, L. G. (1998). Adenovirus-Mediated Gene Transfer to Nucleus Pulposus Cells. *Spine*, *23*(22), 2437–2442. doi: 10.1097/00007632-199811150-00016

Nishida, K., Suzuki, T., Kakutani, K., Yurube, T., Maeno, K., Kurosaka, M., & Doita, M. (2008). Gene therapy approach for disc degeneration and associated spinal disorders. *European Spine Journal*, *17*(S4), 459–466. doi: 10.1007/s00586-008-0751-5

Novais, E. J., Narayanan, R., Canseco, J. A., van de Wetering, K., Kepler, C. K., Hilibrand, A. S., Vaccaro, A. R., & Risbud, M. V. (2024). A new perspective on intervertebral disc calcification—from bench to bedside. *Bone Research*, *12*(1), 3. doi: 10.1038/s41413-023-00307-3

O'Brien, F. J. (2011). Biomaterials & scaffolds for tissue engineering. *Materials Today*, *14*(3), 88–95. doi: 10.1016/S1369-7021(11)70058-X

O'Connell, G. D., Vresilovic, E. J., & Elliott, D. M. (2011). Human intervertebral disc internal strain in compression: The effect of disc region, loading position, and degeneration. *Journal of Orthopaedic Research*, *29*(4), 547–555. doi: 10.1002/jor.21232

Oda, J., Tanaka, H., & Tsuzuki, N. (1988). Intervertebral Disc Changes with Aging of Human Cervical Vertebra. *Spine*, *13*(11), 1205–1211. doi: 10.1097/00007632-198811000-00001

Ogon, I., Takebayashi, T., Takashima, H., Morita, T., Terashima, Y., Yoshimoto, M., & Yamashita, T. (2020). Imaging diagnosis for intervertebral disc. *JOR SPINE*, *3*(1). doi: 10.1002/jsp2.1066

Ohnishi, T., Novais, E. J., & Risbud, M. V. (2020). Alterations in ECM signature underscore multiple sub-phenotypes of intervertebral disc degeneration. *Matrix Biology Plus*, *6–7*, 100036. doi: 10.1016/j.mbplus.2020.100036

Oropeza, B. P., Adams, J. R., Furth, M. E., Chessa, J., & Boland, T. (2022). Bioprinting of Decellularized Porcine Cardiac Tissue for Large-Scale Aortic Models. *Frontiers in Bioengineering and Biotechnology*, *10*. doi: 10.3389/fbioe.2022.855186

Oshima, H., Ishihara, H., Urban, J. P. G., & Tsuji, H. (1993). The use of coccygeal discs to study intervertebral disc metabolism. *Journal of Orthopaedic Research*, *11*(3), 332–338. doi: 10.1002/jor.1100110304

O'Connell, G. D., Johannessen, W., Vresilovic, E. J., & Elliott, D. M. (2007). Human Internal Disc Strains in Axial Compression Measured Noninvasively Using Magnetic Resonance Imaging. *Spine*, *32*(25), 2860–2868. doi: 10.1097/BRS.0b013e31815b75fb

Pattappa, G., Li, Z., Peroglio, M., Wismer, N., Alini, M., & Grad, S. (2012). Diversity of intervertebral disc cells: phenotype and function. *Journal of Anatomy*, *221*(6), 480–496. doi: 10.1111/j.1469-7580.2012.01521.x

Pearce, R. H., Thompson, J. P. ., Bebault, G. M., & Flak, B. (1991). Magnetic resonance imaging reflects the chemical changes of aging degeneration in the human intervertebral disk. *The Journal of Rheumatology. Supplement*, *27*, 42–43.

Pellicanò, G., Martinelli, F., Tavanti, V., Bonetti, M., Leonardi, M., Muto, M., Andreula, C., & Villari, N. (2007). The Italian oxygen-ozone therapy federation (FIO) study on oxygen-ozone treatment of herniated disc. *International Journal of Ozone Therapy*, 7–15.

Peng, Y., Qing, X., Lin, H., Huang, D., Li, J., Tian, S., Liu, S., Lv, X., Ma, K., Li, R., Rao, Z., Bai, Y., Chen, S., Lei, M., Quan, D., & Shao, Z. (2021). Decellularized Disc Hydrogels for hBMSCs tissue-specific differentiation and tissue regeneration. *Bioactive Materials*, *6*(10), 3541–3556. doi: 10.1016/j.bioactmat.2021.03.014

Petetta, F., & Ciccocioppo, R. (2021). Public perception of laboratory animal testing: Historical, philosophical, and ethical view. *Addiction Biology*, *26*(6). doi: 10.1111/adb.12991

Pfirrmann, C. W. A., Metzdorf, A., Zanetti, M., Hodler, J., & Boos, N. (2001). Magnetic Resonance Classification of Lumbar Intervertebral Disc Degeneration. *Spine*, *26*(17), 1873–1878. doi: 10.1097/00007632-200109010-00011

Piening, L. M., Lillyman, D. J., Lee, F. S., Lozano, A. M., Miles, J. R., & Wachs, R. A. (2022). Injectable decellularized nucleus pulposus tissue exhibits neuroinhibitory properties. *JOR SPINE*, *5*(1). doi: 10.1002/jsp2.1187

Postacchin, F., Lami, R., & Pugliese, O. (1988). Familial Predisposition to Discogenic Low-Back Pain. *Spine*, *13*(12), 1403–1046. doi: 10.1097/00007632-198812000-00012

Prasetyono, T. O. H., & Adhistana, P. (2019). Laboratory Study on Injection Force Measurement on Syringe and Needle Combinations. *Malaysian Journal of Medical Sciences*, *26*(2), 66–76. doi: 10.21315/mjms2019.26.2.8

Qian, J., Ge, J., Yan, Q., Wu, C., Yang, H., & Zou, J. (2019). Selection of the Optimal Puncture Needle for Induction of a Rat Intervertebral Disc Degeneration Model. *Pain Physician*, *22*(4), 353–360.

Ratuski, A. S., & Weary, D. M. (2022). Environmental Enrichment for Rats and Mice Housed in Laboratories: A Metareview. *Animals*, *12*(4), 414. doi: 10.3390/ani12040414

Rayan, G. M., Gannaway, J. K., Pitha, J., & Dale, G. L. (1985). Peripheral nerve changes following epineurial injection of saline and blood in rat sciatic nerve. *Clinical Orthopaedics and Related Research*, *193*, 299–307.

Ribitsch, I., Baptista, P. M., Lange-Consiglio, A., Melotti, L., Patruno, M., Jenner, F., Schnabl-Feichter, E., Dutton, L. C., Connolly, D. J., van Steenbeek, F. G., Dudhia, J., & Penning, L. C. (2020). Large Animal Models in Regenerative Medicine and Tissue Engineering: To Do or Not to Do. *Frontiers in Bioengineering and Biotechnology*, *8*. doi: 10.3389/fbioe.2020.00972

Richardson, S. M., Purmessur, D., Baird, P., Probyn, B., Freemont, A. J., & Hoyland, J. A. (2012). Degenerate Human Nucleus Pulposus Cells Promote Neurite Outgrowth in Neural Cells. *PLoS ONE*, *7*(10), e47735. doi: 10.1371/journal.pone.0047735

Roberts, S., Menage, J., & Eisenstein, S. M. (1993). The cartilage end-plate and intervertebral disc in scoliosis: Calcification and other sequelae. *Journal of Orthopaedic Research*, *11*(5), 747–757. doi: 10.1002/jor.1100110517

Roberts, S., Menage, J., & Urban, J. P. G. (1989). Biochemical and Structural Properties of the Cartilage End-Plate and its Relation to the Intervertebral Disc. *Spine*, *14*(2), 166–174. doi: 10.1097/00007632-198902000-00005

Robinson, T. E., Hughes, E. A. B., Bose, A., Cornish, E. A., Teo, J. Y., Eisenstein, N. M., Grover, L. M., & Cox, S. C. (2020). Filling the Gap: A Correlation between Objective and Subjective Measures of Injectability. *Advanced Healthcare Materials*, *9*(5). doi: 10.1002/adhm.201901521

Rosseland, L. A., Helgesen, K. G., Breivik, H., & Stubhaug, A. (2004). Moderate-to-Severe Pain After Knee Arthroscopy Is Relieved by Intraarticular Saline: A Randomized Controlled Trial. *Anesthesia & Analgesia*, 1546–1551. doi: 10.1213/01.ANE.0000112433.71197.FA

Salo, J., Kaigle Holm, A., Indahl, A., Mackiewicz, Z., Sukura, A., Holm, S., Jämsen, E., & Konttinen, Y. T. (2008). Expression of vascular endothelial growth factor receptors coincide with blood vessel in-growth and reactive bone remodelling in experimental intervertebral disc degeneration. *Clinical and Experimental Rheumatology*, *26*(6), 1018–1026.

Samanta, A., Lufkin, T., & Kraus, P. (2023). Intervertebral disc degeneration—Current therapeutic options and challenges. *Frontiers in Public Health*, *11*. doi: 10.3389/fpubh.2023.1156749

Schneider, A. E., & Lange, J. (2018). Pen devices for self-injection: contrasting measured injection force with users' perceived ease of injection. *Expert Opinion on Drug Delivery*, *15*(2), 115–125. doi: 10.1080/17425247.2018.1415884

Segar, A. H., Fairbank, J. C. T., & Urban, J. (2019). Leptin and the intervertebral disc: a biochemical link exists between obesity, intervertebral disc degeneration and low back pain—an in vitro study in a bovine model. *European Spine Journal*, *28*(2), 214–223. doi: 10.1007/s00586-018-5778-7

Shao, J., Yu, M., Jiang, L., Wei, F., Wu, F., Liu, Z., & Liu, X. (2016). Differences in calcification and osteogenic potential of herniated discs according to the severity of degeneration based on Pfirrmann grade: a cross-sectional study. *BMC Musculoskeletal Disorders*, *17*(1), 191. doi: 10.1186/s12891-016-1015-x

Shapiro, I., & Risbud, M. (Eds.). (2014). *The Intervertebral Disc*. Vienna: Springer Vienna. doi: 10.1007/978-3-7091-1535-0

Shi, S., Kang, X.-J., Zhou, Z., He, Z.-M., Zheng, S., & He, S.-S. (2022). Excessive mechanical stress-induced intervertebral disc degeneration is related to Piezo1 overexpression triggering the imbalance of autophagy/apoptosis in human nucleus pulpous. *Arthritis Research & Therapy*, *24*(1), 119. doi: 10.1186/s13075-022-02804-y

Shiri, R., Karppinen, J., Leino-Arjas, P., Solovieva, S., & Viikari-Juntura, E. (2010a). The Association Between Obesity and Low Back Pain: A Meta-Analysis. *American Journal of Epidemiology*, *171*(2), 135–154. doi: 10.1093/aje/kwp356

Shiri, R., Karppinen, J., Leino-Arjas, P., Solovieva, S., & Viikari-Juntura, E. (2010b). The Association between Smoking and Low Back Pain: A Meta-analysis. *The American Journal of Medicine*, *123*(1), 87.e7-87.e35. doi: 10.1016/j.amjmed.2009.05.028

Showalter, B. L., Beckstein, J. C., Martin, J. T., Beattie, E. E., Espinoza Orías, A. A., Schaer, T. P., Vresilovic, E. J., & Elliott, D. M. (2012). Comparison of animal discs used in disc research to human lumbar disc: torsion mechanics and collagen content. *Spine*, *37*(15), E900-7. doi: 10.1097/BRS.0b013e31824d911c

Showalter, B. L., Beckstein, J. C., Martin, J. T., Beattie, E. E., Orías, A. A. E., Schaer, T. P., Vresilovic, E. J., & Elliott, D. M. (2012). Comparison of Animal Discs Used in Disc Research to Human Lumbar Disc. *Spine*, *37*(15), E900–E907. doi: 10.1097/BRS.0b013e31824d911c

Silagi, E. S., Shapiro, I. M., & Risbud, M. V. (2018). Glycosaminoglycan synthesis in the nucleus pulposus: Dysregulation and the pathogenesis of disc degeneration. *Matrix Biology*, *71–72*, 368–379. doi: 10.1016/j.matbio.2018.02.025

Singh, K., Masuda, K., Thonar, E. J.-M. A., An, H. S., & Cs-Szabo, G. (2009). Age-Related Changes in the Extracellular Matrix of Nucleus Pulposus and Anulus Fibrosus of Human Intervertebral Disc. *Spine*, *34*(1), 10–16. doi: 10.1097/BRS.0b013e31818e5ddd

Sivan, S. S., Tsitron, E., Wachtel, E., Roughley, P., Sakkee, N., van der Ham, F., Degroot, J., & Maroudas, A. (2006). Age-related accumulation of pentosidine in aggrecan and collagen from normal and degenerate human intervertebral discs. *Biochemical Journal*, *399*(1), 29–35. doi: 10.1042/BJ20060579

Smolders, L. A., Bergknut, N., Grinwis, G. C. M., Hagman, R., Lagerstedt, A. S., Hazewinkel, H. A. W., Tryfonidou, M. A., & Meij, B. P. (2013). Intervertebral disc degeneration in the dog. Part 2: Chondrodystrophic and non-chondrodystrophic breeds. *The Veterinary Journal*, *195*(3), 292–299. doi: 10.1016/j.tvjl.2012.10.011

Son, H.-G., Hwang, M.-H., Lee, S., Kim, A.-G., Kim, T.-W., Kim, J.-H., Choi, H., & Jeong, S. (2023). Intervertebral disc organ-on-a-chip: an innovative model to study monocyte extravasation during nucleus pulposus degeneration. *Lab on a Chip*, *23*(12), 2819–2828. doi: 10.1039/D3LC00032J

Sward, L., Hellstrom, M., Jacobsson, B. O., Nyman, R., & Peterson, L. (1991). Disc Degeneration and Associated Abnormalities of the Spine in Elite Gymnasts. *Spine*, *16*(4), 437–443. doi: 10.1097/00007632-199104000-00009

Tang, Y., Zhou, Y., & Zhang, M. (2024). A Chitosan Scaffold Supports the Enhanced and Prolonged Differentiation of HiPSCs into Nucleus Pulposus-like Cells. *ACS Applied Materials & Interfaces*, *16*(22), 28263–28275. doi: 10.1021/acsami.4c06013

Tanzli, E., Kozior, T., Hajnys, J., Mesicek, J., Brockhagen, B., Grothe, T., & Ehrmann, A. (2024). Improved cell growth on additively manufactured Ti64 substrates with varying porosity and nanofibrous coating. *Heliyon*, *10*(3), e25576. doi: 10.1016/j.heliyon.2024.e25576

Taylor, D. A., Sampaio, L. C., Ferdous, Z., Gobin, A. S., & Taite, L. J. (2018). Decellularized matrices in regenerative medicine. *Acta Biomaterialia*, *74*, 74–89. doi: 10.1016/j.actbio.2018.04.044

Taylor, J. R. (1975). Growth of human intervertebral discs and vertebral bodies. *Journal of Anatomy*, *120*(Pt 1), 49–68.

Theocharis, A. D., Manou, D., & Karamanos, N. K. (2019). The extracellular matrix as a multitasking player in disease. *The FEBS Journal*, *286*(15), 2830–2869. doi: 10.1111/febs.14818

Tomaszewski, K. A., Saganiak, K., Gładysz, T., & Walocha, J. A. (2015). The biology behind the human intervertebral disc and its endplates. *Folia Morphologica*, *74*(2), 157–168. doi: 10.5603/FM.2015.0026

Uematsu, Y., Matuzaki, H., & Iwahashi, M. (2001). Effects of nicotine on the intervertebral disc: an experimental study in rabbits. *Journal of Orthopaedic Science*, *6*(2), 177–182. doi: 10.1007/s007760100067

United Nations. (2019). *World Population Prospects 2019*.

Ura, K., Yamada, K., Tsujimoto, T., Ukeba, D., Iwasaki, N., & Sudo, H. (2021). Ultra-purified alginate gel implantation decreases inflammatory cytokine levels, prevents intervertebral disc degeneration, and reduces acute pain after discectomy. *Scientific Reports*, *11*(1), 638. doi: 10.1038/s41598-020-79958-9

Urban, J. P. G., & Maroudas, A. (1981). Swelling of the Intervertebral Disc *in Vitro*. *Connective Tissue Research*, *9*(1), 1–10. doi: 10.3109/03008208109160234

Urban, J. P. G., Smith, S., & Fairbank, J. C. T. (2004). Nutrition of the Intervertebral Disc. *Spine*, *29*(23), 2700–2709. doi: 10.1097/01.brs.0000146499.97948.52

Urits, I., Burshtein, A., Sharma, M., Testa, L., Gold, P. A., Orhurhu, V., Viswanath, O., Jones, M. R., Sidransky, M. A., Spektor, B., & Kaye, A. D. (2019). Low Back Pain, a Comprehensive Review: Pathophysiology, Diagnosis, and Treatment. *Current Pain and Headache Reports*, *23*(3), 23. doi: 10.1007/s11916-019-0757-1

van Uden, S., Silva-Correia, J., Oliveira, J. M., & Reis, R. L. (2017). Current strategies for treatment of intervertebral disc degeneration: substitution and regeneration possibilities. *Biomaterials Research*, *21*(1). doi: 10.1186/s40824-017-0106-6

Vo, N. V., Hartman, R. A., Patil, P. R., Risbud, M. V., Kletsas, D., Iatridis, J. C., Hoyland, J. A., Le Maitre, C. L., Sowa, G. A., & Kang, J. D. (2016). Molecular mechanisms of biological aging in intervertebral discs. *Journal of Orthopaedic Research*, *34*(8), 1289–1306. doi: 10.1002/jor.23195

Vo, N. V., Hartman, R. A., Yurube, T., Jacobs, L. J., Sowa, G. A., & Kang, J. D. (2013). Expression and regulation of metalloproteinases and their inhibitors in intervertebral disc aging and degeneration. *The Spine Journal*, *13*(3), 331–341. doi: 10.1016/j.spinee.2012.02.027

Wagner, W. R., Sakiyama-Elbert, S. E., Zhang, G., & Yaszemski, M. J. (Eds.). (2020). *Biomaterials Science*. Elsevier. doi: 10.1016/C2017-0-02323-6

Wang, K., Yao, D., Li, Y., Li, M., Zeng, W., Liao, Z., Chen, E., Lu, S., Su, K., Che, Z., Liang, Y., Wang, P., & Huang, L. (2023). TAK-715 alleviated IL-1β-induced apoptosis and ECM degradation in nucleus pulposus cells and attenuated intervertebral disc degeneration ex vivo and in vivo. *Arthritis Research & Therapy*, *25*(1), 45. doi: 10.1186/s13075-023-03028-4

Wang, L., Guo, X., Chen, J., Zhen, Z., Cao, B., Wan, W., Dou, Y., Pan, H., Xu, F., Zhang, Z., Wang, J., Li, D., Guo, Q., Jiang, Q., Du, Y., Yu, J., Heng, B. C., Han, Q., & Ge, Z. (2022). Key considerations on the development of biodegradable biomaterials for clinical translation of medical devices: With cartilage repair products as an example. *Bioactive Materials*, *9*, 332–342. doi: 10.1016/j.bioactmat.2021.07.031

Watt, R. P., Khatri, H., & Dibble, A. R. G. (2019). Injectability as a function of viscosity and dosing materials for subcutaneous administration. *International Journal of Pharmaceutics*, *554*, 376–386. doi: 10.1016/j.ijpharm.2018.11.012

Wehner, D., Tsarouchas, T. M., Michael, A., Haase, C., Weidinger, G., Reimer, M. M., Becker, T., & Becker, C. G. (2017). Wnt signaling controls pro-regenerative Collagen XII in functional spinal cord regeneration in zebrafish. *Nature Communications*, *8*(1), 126. doi: 10.1038/s41467-017-00143-0

Whittal, M. C., Molladavoodi, S., Zwambag, D. P., Millecamps, M., Stone, L. S., & Gregory, D. E. (2021). Mechanical Consequence of Induced Intervertebral Disc Degeneration in the SPARC-Null Mouse. *Journal of Biomechanical Engineering*, *143*(2). doi: 10.1115/1.4047995

Woods, B. I., Sowa, G., Vo, N., & Kang, J. D. (2010). A Change in Strategy: The Use of Regenerative Medicine and Tissue Engineering to Augment the Course of Intervertebral Disc Degeneration. *Operative Techniques in Orthopaedics*, *20*(2), 144–153. doi: 10.1053/j.oto.2009.10.009

Wu, P. H., Kim, H. S., & Jang, I.-T. (2020). Intervertebral Disc Diseases PART 2: A Review of the Current Diagnostic and Treatment Strategies for Intervertebral Disc Disease. *International Journal of Molecular Sciences*, *21*(6), 2135. doi: 10.3390/ijms21062135

Wu, Z., Lin, Z., Yao, A., Ye, S., Pan, H., Cui, X., & Wang, D. (2020). Influence of particle size distribution on the rheological properties and mathematical model fitting of injectable borosilicate bioactive glass bone cement. *Ceramics International*, *46*(15), 24395–24406. doi: 10.1016/j.ceramint.2020.06.222

Wuertz, K., Godburn, K., Neidlinger-Wilke, C., Urban, J., & Iatridis, J. C. (2008). Behavior of Mesenchymal Stem Cells in the Chemical Microenvironment of the Intervertebral Disc. *Spine*, *33*(17), 1843–1849. doi: 10.1097/BRS.0b013e31817b8f53

Xu, J., Liu, S., Wang, S., Qiu, P., Chen, P., Lin, X., & Fang, X. (2019). Decellularised nucleus pulposus as a potential biologic scaffold for disc tissue engineering. *Materials Science and Engineering: C*, *99*, 1213–1225. doi: 10.1016/j.msec.2019.02.045

Yao, Q., Zheng, Y.-W., Lan, Q.-H., Kou, L., Xu, H.-L., & Zhao, Y.-Z. (2019). Recent development and biomedical applications of decellularized extracellular matrix biomaterials. *Materials Science and Engineering: C*, *104*, 109942. doi: 10.1016/j.msec.2019.109942

Yee, A., Lam, M. P. Y., Tam, V., Chan, W. C. W., Chu, I. K., Cheah, K. S. E., Cheung, K. M. C., & Chan, D. (2016). Fibrotic-like changes in degenerate human intervertebral discs revealed by quantitative proteomic analysis. *Osteoarthritis and Cartilage*, *24*(3), 503–513. doi: 10.1016/j.joca.2015.09.020

Ying, Y., Cai, K., Cai, X., Zhang, K., Qiu, R., Jiang, G., & Luo, K. (2023). Recent advances in the repair of degenerative intervertebral disc for preclinical applications. *Frontiers in Bioengineering and Biotechnology*, *11*. doi: 10.3389/fbioe.2023.1259731

Zhang, K., Zhang, Y., Zhang, C., & Zhu, L. (2021). Upregulation of P53 promotes nucleus pulposus cell apoptosis in intervertebral disc degeneration through upregulating NDRG2. *Cell Biology International*, *45*(9), 1966–1975. doi: 10.1002/cbin.11650

Zhao, C., Wang, L., Jiang, L., & Dai, L. (2007). The cell biology of intervertebral disc aging and degeneration. *Ageing Research Reviews*, *6*(3), 247–261. doi: 10.1016/j.arr.2007.08.001

Zhou, X., Wang, J., Huang, X., Fang, W., Tao, Y., Zhao, T., Liang, C., Hua, J., Chen, Q., & Li, F. (2018). Injectable decellularized nucleus pulposus-based cell delivery system for differentiation of adipose-derived stem cells and nucleus pulposus regeneration. *Acta Biomaterialia*, *81*, 115–128. doi: 10.1016/j.actbio.2018.09.044

Zimmerli, W. (2011). Implanted devices: biocompatibility, infection and tissue engineering. *Seminars in Immunopathology*, *33*(3), 219–220. doi: 10.1007/s00281-011-0277-5